



Volume 1

**IV. Fluvial:
Modeling,
Hydraulic
Structures, and
Bridge Scour**



IV. FLUVIAL: MODELING, HYDRAULIC STRUCTURES, AND BRIDGE SCOUR

Page

MODIFICATION OF SEDIMENT DISCHARGE FOR THE LOWER YELLOW RIVER: Songheng Li, Binwen Lin, and Yuqian Long, Institute of Hydraulic Research, Zheng Zhou, PRC	IV - 1
APPLICATION OF CORPS SEDIMENTATION TRANSPORT COMPUTER MODELS: Jon B. Fripp, Jerry W. Webb, and Dr. Surya Bhamidipaty, COE, Huntington, WV	IV - 9
EVALUATION OF STREAM-SEDIMENTATION MODEL: Weixia Jin, Chao-Lin Chiu, University of Pittsburgh, Pittsburgh, PA; and Shou-shan Fan, FERC, Washington, DC	IV - 17
HYDRAULIC GEOMETRY FOR POLLUTANT LOADING COMPUTER MODELS USING GEOGRAPHICAL INFORMATION SYSTEMS TO DEVELOP INPUT DATA: Fred D. Theurer, NRCS, Washington, DC; Carlos V. Alonso, ARS-NSL, Oxford, MS; and Jerry M. Bernard, NRCS, Washington, DC	IV - 25
EVALUATION OF SELECTED INSTRUMENTS FOR MONITORING SCOUR AT BRIDGES IN NEW YORK: Gerard K. Butch, USGS, Albany, NY	IV - 33
SCOUR AT BRIDGES--DETAILED DATA COLLECTION DURING FLOODS: David S. Mueller, USGS, Louisville, KY	IV - 41
SCOUR AT SELECTED BRIDGE PIERS IN MISSISSIPPI: K. Van Wilson, Jr., USGS, Jackson, MS	IV - 49
MODELING ALLUVIAL-RIVER EVOLUTION BY CHARACTERISTICS METHOD: Keh-Chia Yeh, Wen-Lin Chen, Chen-Hua Chen, and Chian-Min Wu, Ministry of Economic Affairs, Taipei, Taiwan	IV - 57
GLOBAL APPROACH FOR SENSITIVITY AND UNCERTAINTY ANALYSIS OF A SEDIMENT TRANSPORT MODEL: Jinn-Chuang Yang, National Chiao Tung U., Hsinchu, Taiwan; Che-Hao Chang, Industrial Technology Research Institute, Hsinchu, Taiwan; and Chian-Ming Wu, National Chiao Tung U., Hsinchu, Taiwan	IV - 65
TIDAL MARSH SEDIMENTATION: Guang-dou Hu, Northwest Hydraulic Consultants, Sacramento, CA	IV - 73
NUMERICAL MODELING OF STORM-INDUCED BEACH EROSION: S. Jarrell Smith and Randall A. Wise, COE, Vicksburg, MS	IV - 81
AN INQUIRY OF METHOD CALCULATING MEAN SEDIMENT DISCHARGE: Zhan Niu and Qingyun Ma, Yellow River Conservancy Commission, Zheng Zhou City, Henan, PRC	IV - 89
SEDIMENT TRANSPORT MODELING FOR THE GLEN-COLUSA IRRIGATION DISTRICT FISH SCREEN MODIFICATIONS: Cassie Klumpp, Mark Sailer, and Brent Mefford, USBR, Denver, CO	IV - 92
GENERALIZED STREAM TUBE MODEL FOR ALLUVIAL RIVER SIMULATION (GSTARS-2): Chih Ted Yang, USBR, Denver, CO	IV - 100

- SEDIMENT RESUSPENSION DUE TO WIND GENERATED WAVES IN THE
SHALLOW NAVIGATION POOLS OF THE UPPER MISSISSIPPI RIVER: Ferris
W. Chamberlin, COE, St. Paul, MN IV - 106
- THE K-E TURBULENCE MODEL FOR PREDICTING SECONDARY CURRENTS IN
OPEN CHANNELS: Youssef Ismail Hafez, Nile Research Institute, Egypt IV - 114

MODIFICATION OF SEDIMENT DISCHARGE FOR THE YELLOW RIVER

By Li Songheng, Engineer, IHR, YRCC; Lin Binwen, Senior Engineer, Dept. of Science & Technology, YRCC;
Long Yuqian, Senior Engineer, IHR, YRCC, Zheng Zhou, China

Abstract: In this paper, the coefficient of modification for sediment discharge (K) is defined as the ratio of Q_{SmeP} to Q_{Sm} , in which, Q_{SmeP} is the total sediment discharge calculated by using the modified version of MEP, and Q_{Sm} is the measured sediment discharge. The coefficient K is correlated with sediment concentration (C). In the relation, the K is regarded as a grey number which means K varies within a certain scope defined by a upper and lower limit, and can be calculated by using the whitening function. The measured daily sediment discharge may be corrected by using the relation between K and C . This method is applied to calculate the amount of sedimentation in the Sanmenxia reservoir and the lower Yellow River. It is found that the agreement between the calculated difference of sediment load at two terminal sections, taking proper account of input or output from intermediate area, and that obtained by repetitive range surveys is reasonably well and greatly improved than that using the computed difference of sediment load without corrections. The relation between K and C has some theoretical basis. The modification procedure is simple and the daily measured value can be corrected, which could be used to provide a more reasonable database for further analysis.

INTRODUCTION

Comparison of the computed difference of sediment load at two terminal sections, taking proper account of input and output from intermediate area, and that obtained by repetitive range surveys in the Sanmenxia reservoir and the lower Yellow River showed that a systematic error of measured daily sediment discharge existed [Lin & Liang 1987, Xiong et al. 1983, Long et al. 1982]. The Sanmenxia gauging station is located at a gorge section downstream the dam site, where the flow is fully turbulent. The river bed is composed of pebble, water and sediment flushing from the outlets mixed completely, and the distribution of sediment concentration at the vertical and in the cross section is quite uniform, therefore, no correction is deemed necessary. Xiong [Xiong et al. 1983] reported that the measured sediment discharge at Xiaolangdi, Huayuankou, Lijin gauging stations, located 129, 259, 923 km far downstream from Sanmenxia, was less by 2.0%, 8.2%, 3.6% respectively by sediment budget using the measured data from 1961 to 1980. Long [Long et al. 1982] obtained that the difference of the amount of sedimentation between measured and calculated value was about 6.7% of the oncoming sediment load in the Sanmenxia reservoir, 8.8% for the upper reaches, and 4.4% for the lower reaches of the lower Yellow River.

The error involved in the range survey is random in nature and no appreciable systematic error can be found [Lin, 1982]. The error involved in the measured sediment discharge is the main source which causes the systematic deviation between the result calculated by difference of sediment load at two terminal sections and that obtained by repetitive range surveys. The amount of bed load is less than 1% of the total sediment load in the lower Yellow River by statistics of 118 sets data of bed load [Lin & Liang 1987], so the error involved in the measured suspended sediment discharge is the major source of error of the measured sediment discharge in the Yellow River. Research

findings might be misleading if the error were not corrected properly when the measured data is directly used for analysis.

In 1950's, Colby & Hembree [Colby & Hembree 1955] presented the method of Modified Einstein Procedure (MEP) for computation of total sediment load by using the measured data. In 1987, Lin introduced the MEP to the Yellow River, after a lot of deep studies according to the actual characteristics of the Yellow River, the original MEP was further modified [program MODEIN-L], and applied to the Yellow River [Lin & Liang, 1987].

COEFFICIENT OF MODIFICATION FOR SEDIMENT DISCHARGE

Theoretical Formulae for Coefficient of Modification for Sediment Discharge: Total sediment discharge may be obtained by integration of multiple of flow velocity and sediment concentration along whole water depth [Einstein]:

$$i_t q_t = i_B q_B \cdot (1 + P \cdot I_1 + I_2) \quad (1)$$

in which, q_t is the total sediment discharge per unit width, i_t is the percentage of a certain size gradation to the bed material load, $i_B q_B$ is the bed load of a certain size gradation sediment per unit width, P is a parameter correlated with water depth and bed roughness, I_1, I_2 are the function of A, Z , which A is the ratio of height of bed layer to water depth, and Z is the suspension index.

Einstein evaluated Colby & Hembree's MEP [Einstein], and indicated that MEP took the same procedure with Einstein's computation of total sediment discharge, but modifications were taken. Einstein defined the coefficient of modification for sediment discharge as follows

$$\frac{i_t q_t}{i_{Sm} q_{Sm}} = \left(\frac{E}{A}\right)^{Z-1} \cdot \left(\frac{1-A}{1-E}\right)^Z \cdot \frac{(1+P \cdot I_1 + I_2)_A}{(P \cdot I_1 + I_2)_E} \quad (2)$$

in which, $i_{Sm} q_{Sm}$ is the suspended sediment discharge within the measured zone of depth-integration, E is the ratio of unmeasured height to water depth. Here, the coefficient of modification for sediment discharge is the ratio of theoretical calculated value of total sediment discharge to suspended sediment discharge within measured zone. It is obvious that the coefficient is the function of P, A, Z, E .

For sampling by points, the ratio of calculated total sediment discharge to the measured suspended sediment discharge within a certain size gradation may be expressed as follows:

$$\frac{i_t q_t}{i_{Sm} q_{Sm}} = \frac{1}{\theta} = \frac{(1-A)^Z}{A^{Z-1}} \cdot \frac{4.648 \cdot (1+P \cdot I_1 + I_2)}{\sum_{i=1}^N W_i \cdot \left(\frac{1-X_i}{X_i}\right)^Z \cdot (P + \ln X_i)} \quad (3)$$

in which, N is the number of measuring point, X_i, W_i is the relative depth and weight of each measuring point respectively. Coefficient of modification is the function of P, A, Z when X_i and W_i are determined (for instance three-point method or five-point method of streamgaging).

Definition of coefficient of modification for sediment discharge: MEP is not the general formula derived for evaluation of sediment transport capacity. The modification procedure is based on the measured data. Corrected value of total sediment discharge is obtained by the multiple of measured sediment discharge and the coefficient of modification, which is the ratio of sediment discharge calculated in whole water depth to the computed value within the measured zone. In this paper, the definition of coefficient of modification for sediment discharge follows:

$$K = \frac{Q_{SmeP}}{Q_{Sm}} \quad (4)$$

here, Q_{SmeP} is the total sediment discharge computed by program MODEIN-L provided by Lin [Lin & Liang 1987], Q_{Sm} is the measured sediment discharge.

Influencing Factors of Coefficient of Modification for Sediment Discharge: It can be seen from Equ.(2). (3) that coefficient of modification for sediment discharge is the function of P , A , Z etc.. According to the measured data in the lower Yellow River, P generally varies from 10 to 16, averaged 13, A from 10^{-5} to 10^{-3} , the difference of θ (see Equ. (3)) is quite small when $A=10^{-5}$ or $A=10^{-3}$ [Long etc. 1982], therefore, Z is a major influencing factor. The mean sediment concentration is correlated with sediment concentration at the reference point, by the function of P , A , Z etc.. The author [Li 1993] analyzed the relation between K and flow Reynolds Number, discharge, sediment concentration, and ratio of percentage of coarse sediment to fine. The approach in this paper is to establish the relation between K and C (sediment concentration) instead of the relationship between K and P , A , Z etc., in this manner, modification procedure can be more simple. General speaking, the daily sediment concentration can be obtained conveniently, therefore, not only has the modification method some theoretical basis, but also the modification procedure itself becomes more simple and available to be used.

Figure 1(1)-(2) show the K - C relation, it can be seen, the smaller the C , the greater the K , the greater the C , the smaller the K , the lower limit of K is 1.0. The relation between K and C of all gauging stations in the Yellow River is similar. The data points composing in the relationship of K and C are scattered within a band, because there are other factors influencing K besides C .

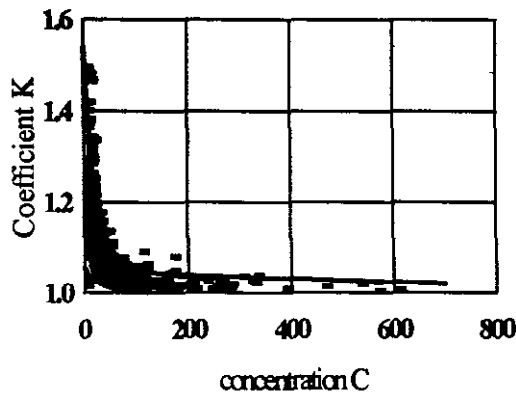


Fig. 1(1) K - C Relation of Tongguan Station

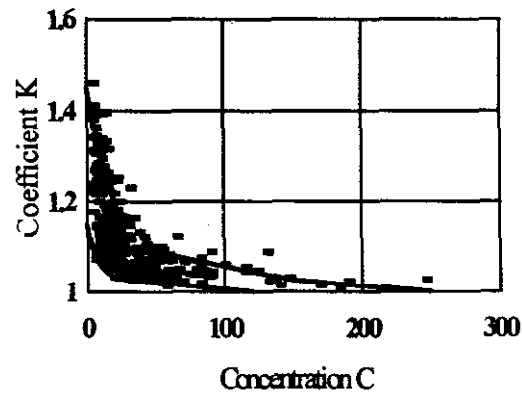


Fig. 1(2) K - C Relation of Huanyuankou Station

GREY RELATION BETWEEN THE COEFFICIENT OF MODIFICATION FOR SEDIMENT DISCHARGE AND SEDIMENT CONCENTRATION

The so-called grey indicates that the information of a certain system is not complete. Grey system is a system in which the information is not complete, similarly, grey number is a number without complete information. Grey phenomena exists universally in the nature. General speaking, the grey system emphasizes the study of problems with clearly defined objects, and their internal relationship is fuzzy, for instance, the relationship between rainfall and runoff is to be studied, it is the relationship of rainfall and runoff that will be studied, not any other relations to be studied, so the objects are definite, but the relationship between rainfall and runoff is not quite clear, it is necessary to be further studied, therefore, the internal relationship is still fuzzy [Deng, 1988].

In this paper, the concept of grey is applied to the study of the relation between K and C , K is regarded as a grey number, and the K - C relation as a grey relation. In fact, it is the relation of K and C that will be analyzed, not any other relations, so the problem of study is clearly defined, the relation of K and C shows that K varies within a certain scope under a same value of C , the exact value of K is not definite, in other words, the intention of the problem is not clear, therefore, the relation between K and C is a grey relation and can be solved by using the method of grey system.

K is regarded as a grey number varying within a certain scope with a upper limit α and lower limit β . The upper and lower limit may be defined according to the relation of K and C . The grey number is changeable and should be a definite value so that it can be used to deal with the relative problems. The processing of being a definite value is called whitening. K is whitened by taking advantage of the whitening function as follows

$$K = \rho \cdot \alpha + (1 - \rho) \cdot \beta \quad (5)$$

in which, ρ is called the whitening weight varying between 0 and 1. On the basis of the defined upper and lower limit, taking a initial value of ρ , C is known, α and β can be obtained by the K - C relationship under a certain C , so K can be obtained and sediment discharge can be easily corrected. ρ should be appropriately defined by trial calculation. By the way, value of α , β and ρ may not be the same for different person, but the modified results should show no difference.

The approach of modification is based on the following three aspects: ① absorbing and adopting completely the concepts and measurements dealing with problems of the grey system theory; ② the results of application of MEP to the Yellow River is reasonable and reliable as indicated by Lin [Lin & Liang, 1987]; ③ the amount of erosion and deposition in a long term and long reach obtained by repetitive range surveys is reasonable and reliable through measured data analysis, modified sediment discharge must be verified by comparison of calculated amount of erosion and deposition by sediment load difference method and measured value by repetitive range surveys.

MODIFICATION OF SEDIMENT DISCHARGE

The Sanmenxia reservoir may be divided into upper and lower reaches named LHHZ-Tonggua(LHHZ-TG) and Tongguan-Sanmenxia(TG-SMX) respectively. The lower Yellow River may be divided into four reaches by the name

of Sanmenxia-Huayuankou(SMX-HYK), Huayuankou-Gaocun(HYK-GC), Gaocun-Aishan(GC-AS), Aishan-Iijin(AS-LJ). Basic data for MODEIN-L of each gauging station are summarized in Table 1, which include date, discharge(Q), water surface width(W), water depth(d), water surface slope(J), water temperature(T), sediment concentration(C), size gradation of bed material(BM), and size gradation of suspended sediment(SS).

Table 1 Basic data for MODEIN-L computation

station	LM	TG	HYK	GC	AS	LJ
L (km)	-242	-115	+259	+447	+641	+923
date	1970-1987	1960-1988	1958-1988	1963-1988	1959-1988	1963-1988
sets of data	250	703	278	266	350	328
Q (m ³ /s)	107-8930	113-9180	118-12400	61-7300	25-7470	30-7470
W (m)	74-376	79-984	132-3190	144-2240	75-417	73-555
d (m)	0.84-6.1	0.5-6.8	0.55-3.42	0.57-5.3	1.02-7.0	0.67-6.1
T (°C)	0-29.5	0-30.3	0.5-31.1	0-31.7	0-30.4	0-32
C (kg/m ³)	1.21-630	0.08-605	1.82-244	0.71-201	0.46-217	0.16-164
J	Both the measured J and the calculated J may be used in MEP					
BM, SS	Both BM and SS are divided into 9 classes: <0.025 <0.01 <0.025 <0.05 <0.1 <0.25 <0.5 <1.0 <2.0 (mm)					

Notation: "L" is the distance from SMX, "-" upstream SMX, "+" downstream SMX

The coefficient of modification K can be obtained by Q_{Smp} over Q_{Sm} , On the basis of the relationship between K and C , the upper limit α and the lower limit β can be determined, when the whitening weight is given, K is obtained under a certain C . The whitening weight most likely should be determined by trial. When the upper and lower limit are determined, the only restriction for determining suitable ρ is that the amount and accumulative process of erosion and deposition by the difference of modified sediment load at two terminal sections should accord with that obtained by repetitive range surveys. The details of determining the upper limit, the lower limit, and the whitening weight are not mentioned in this paper.

VERIFICATION FOR MODIFICATION OF SEDIMENT DISCHARGE

Comparison between calculated and measured accumulative erosion and deposition in different reaches is summarized in Table 2.

Figure 2(1-6) show the accumulative erosion and deposition process of each reach. From Table 2 and figures, it can be seen that there will be a quite difference between the calculated and measured erosion and deposition without modification of sediment discharge at the terminal stations, and the agreement is reasonably well and greatly improved after modification.

Table 2 Comparison of calculated and measured accumulative deposition

reach	date (y.m-y.m)	accumulative erosion and deposition (* in 10 ⁸ ton, others in10 ⁸ m ³)		
		measured	with modification	without modification
LHHZ-TG	60.04-90.09	42.75*	44.91*	31.96*
TG-SMX	60.07-90.10	33.06*	34.11*	15.06*
SMX-HYK	60.04-90.09	-2.13	-1.84	17.43
HYK-GC	60.04-90.09	9.34	9.99	8.19
GC-AS	60.04-90.09	8.06	7.99	5.84
AS-LJ	60.04-90.09	2.89	2.97	6.18

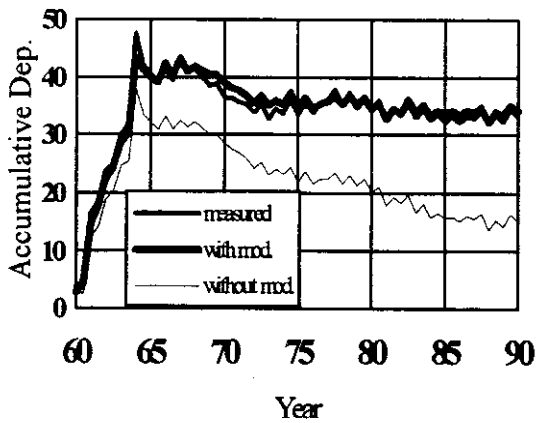


Fig. 2(1) Comparison of Calculated & Measured Deposition in LHHZ-TG Reach

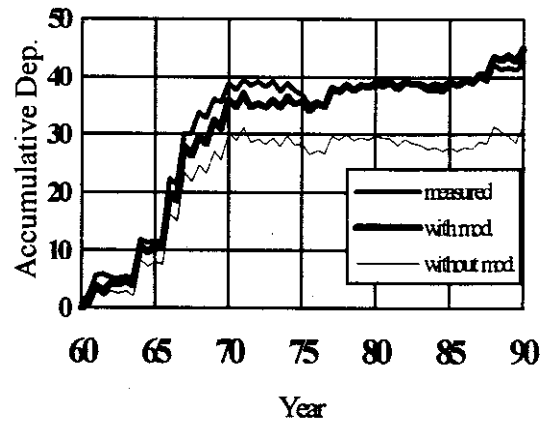


Fig. 2(2) Comparison of Calculated & Measured Deposition in TG-SMX Reach

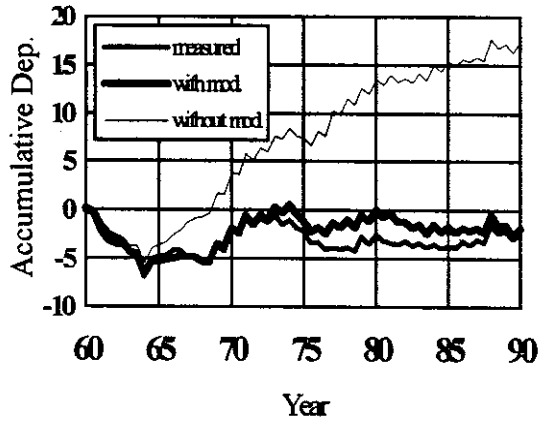


Fig. 2(3) Comparison of Calculated & Measured Deposition in SMX-HYK Reach

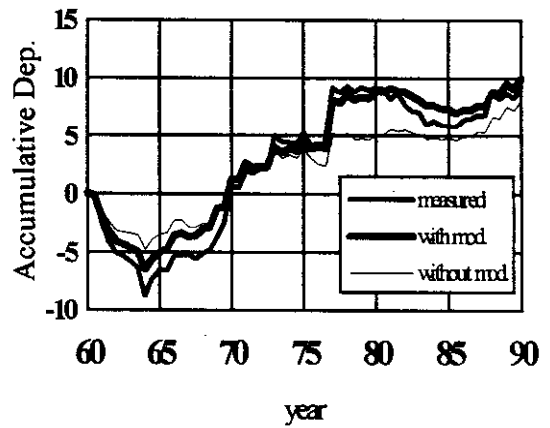


Fig. 2(4) Comparison of Calculated & Measured Deposition in HYK-GC Reach

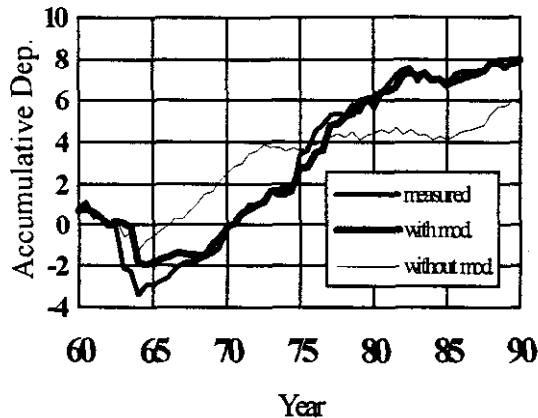


Fig. 2(5) Comparison of Calculated & Measured Deposition in GC-AS Reach

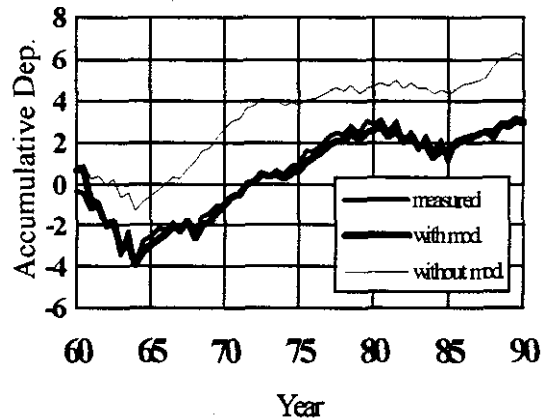


Fig. 2(6) Comparison of Calculated & Measured Deposition in AS-LJ Reach

CONCLUSIONS

A systematic error of sediment discharge exists at gauging stations in the Yellow River, the measured daily sediment discharge is less than that it should be. The modification of sediment discharge is deemed necessary.

There are many factors which influence the coefficient of modification for sediment discharge. The theoretical coefficient (K) of modification for sediment discharge can be denoted as the function of P , A , Z , E etc., the cross sectional mean sediment concentration (C) is correlated with P , A , Z and the sediment concentration of the reference point. Both P and A may be considered as constants in the Yellow River. The approach is to establish the relation between K and C instead of that between K and P , A , Z , E , etc.. In this manner, the procedure of modification will be more simple and available to be used.

The coefficient of modification for sediment discharge (K) is defined as the ratio of Q_{Smep} to Q_{Sm} , in which, Q_{Smep} is the total sediment discharge calculated by using the Program MODEIN-L and Q_{Sm} is the measured value.

K is regarded as a grey number which means K varies within a certain scope defined by a upper and a lower limit. Similary, the relationship of K and C is considered the grey relation. The smaller the C , the greater the K , the greater the C , the smaller the K , and the minimum of K is 1.0. The upper limit, the lower limit, and the whitening weight may most likely not be the same value for different person, but the modified results should show no difference, in other words, the modified sediment discharge should be verified by comparison between the calculated and measured accumulative amount and process of erosion and deposition.

The procedure to modify sediment discharge by utilizing the relation between K and C is simple. The K - C relation itself has some theoretical basis. The daily measured sediment discharge may be corrected conveniently. The study makes clear that the modification of sediment discharge for the Yellow River is reasonable and available to be used.

REFERENCES

- Lin Binwen & Liang Guoting, 1987, Application and Modification of The Total Sediment Discharge Computation (in Chinese), Technical Report of Institute of Hydraulic Research(IHR) No. 87021, Yellow River Conservancy Commission(YRCC).
- Xiong Guishu, Sun Tongxian & Zhu Qingxue, 1983, An Analysis of Errors In Sediment Measurement in The Lower Yellow River, Proceedings of The Second International Conference on River Sedimentation, 986-995.
- Long Yuqian, Lin Binwen & Xiong Guishu, 1982, Preliminary Analysis of Measurement Error of Sediment Discharge (in Chinese), Journal of Sediment Research No. 4, 52-58.
- Lin Binwen, 1982, Major Reasons Causing The Deviation Between Deposition computed by Difference of Sediment Load at Two Terminal Sections and That by Repetitive Range Surveys (in Chinese), Technical Report of IHR ,YRCC.
- Colby, B.R. & Hembree, C.H., 1955, Computation of Total Sediment Discharge, Niobrara River Near Cody, Nebraska,USGS Water-Supply Paper 1357.
- Einstein, H.A., River Sedimentation, Handbook of Applied Hydrology, A Compendium of Water-resources Technology, chapter 17 pp35-37.
- Li Songheng, 1993, Application and Modification of Sediment Discharge for The Lower Yellow River (in Chinese), Technical Report of IHR No. 93029, YRCC.
- Deng Julong et al., 1988, Grey System, p1-12 & 117-127.

APPLICATION OF CORPS SEDIMENTATION TRANSPORT COMPUTER MODELS

Jon B. Fripp¹, Jerry W. Webb and Dr. Surya Bhamidipaty²

Abstract The two major sediment analysis programs in use by the U.S. Army Corps of Engineers are HEC-6 and SAM. The current paper illustrates the strengths and weaknesses of these two computer programs through a recent study conducted by the Huntington District of the U.S. Army Corps of Engineers. The Athens, Ohio channel improvement project is estimated to have prevented over 68 million dollars in damages since its completion in 1971 but has incurred increasing maintenance costs due to sedimentation. At the request of the local sponsor, the Huntington District of the U.S. Army Corps of Engineers has investigated several possible alternatives to the continued dredging using HEC-6, a Corps of Engineers computer model. The development of an HEC-6 computer model often requires more time than many studies allow. Where time or funding is limited, the Corps program SAM is often used to assess sedimentation. The current paper presents an overview of the Athens, Ohio study results as well as a comparison to the results which could have been obtained through the use of SAM.

INTRODUCTION

Cities and towns which are located along streams and rivers often have economic areas which are located in the floodplain. Channel improvements are a common means of providing flood protection for the flood prone areas of these communities. The channel improvement discussed in the current paper is located on the Hocking River in Athens, Ohio. Since its completion in 1971, the project is estimated to have prevented over 68 million dollars in flood damages. As is common in many older channel improvement projects, this project enlarged the existing channel cross sections in order to increase the conveyance of the natural channel.

The Athens, Ohio flood protection project begins at the remains of White's Mill Dam and extends downstream for approximately five miles. The existing project as well as the original river is shown in Figure 1. The channel improvement project consisted of straightening and increasing the width of the original channel to 215 feet. The Hocking

¹Hydraulic Engineers, Hydrology and Hydraulics Branch, Corps of Engineers, 502 Eighth St, Huntington, WV 25701-2070

²Supervisory Hydraulic Engineers, Hydrology and Hydraulics Branch, Corps of Engineers, 502 Eighth St, Huntington, WV 25701-2070

River through the local protection project is now almost twice as wide and 1,400 feet shorter than it was originally. As evidenced by the prevented flood damages, this project design is effective in reducing flood water surface profiles. However, the dramatic change in the river's geometry has caused this project to be susceptible to sediment deposition. As a result, maintenance dredging has been undertaken to maintain the design conveyance in the Athens, Ohio project area. Since project completion, approximately 95,000 yd³ of material has been removed from the channel at a cost in excess of \$325,000. Figure 2 provides photographs of the Hocking River above and within the local protection project. These photographs show the change in the river geometry between the project and the natural river conditions.

The Huntington District of the U.S. Army Corps of Engineers has investigated possible alternatives to the continuation of the current dredging requirements. These alternatives include structural modifications to the channel that would either reduce sediment deposition, or localize it within easily maintainable areas. The Corps computer programs, HEC-2 and HEC-6, as well as site reconnaissance and engineering judgement, have been applied to predict the behavior of the river under the various alternative scenarios that were studied. Since deposition occurs in the approximate same areas of the project soon after maintenance dredging, the current study has also examined the possibility that the Hocking River has reached a quasi stable condition with the current deposition. Another possibility that has been addressed is that significant flood events would flush the deposited sediment through the system.

HEC-6 SEDIMENTATION STUDY

Existing Conditions The Corps computer model HEC-2 has been used to assess the impact of the current deposition in the project. An HEC-2 model was developed for a 12.6 mile reach of the Hocking River using cross section data from a 1992 field survey. A second HEC-2 model was developed for the original, design geometry of the project. The two models have identical Manning's "n" values, therefore the calibration of the two models are comparable. Both models also use the same downstream rating curve so that the only difference between the two models reflects the results of sedimentation in the project.

By comparing the results of the two models for several large flood events, it was determined that the reduction in conveyance, due to sediment deposition, induces an increase in flood profiles from 0.5 to 1 foot. While approximately 95,000 yd³ of material has been removed from the channel since project construction, comparisons of design and current cross sections show that the original channel cross sectional shape has been reduced. To regain the original conveyance of the project, either dredging efforts must be increased, the sediment transport capacity of the channel must be increased, or the amount of sediment that enters the channel must be reduced.

Development of the HEC-6 Model The Corps computer program, HEC-6, has been used to model the erosion and depositional trends in the project. This program simulates the sediment transport capacity of a river by mathematically modeling the interaction between sediment inflow and the hydraulic characteristics of the study reach. It is important to note that high water surface profiles calculated with HEC-6 and HEC-2 are not necessarily directly comparable. As a rule, HEC-6 is used to predict changes in flood profiles over time while HEC-2 is used to calculate flood profile elevations. The required input into HEC-6 includes such site specific information as geometry, inflow hydrology, sediment inflow, and sediment transport capacity.

The geometry for the HEC-6 model was obtained from the first HEC-2 model. Sediment samples were taken from the bed of the study reach and used to develop the bed gradation of the model. Forty years of streamflow records were obtained from several USGS gages for the hydrologic input in the HEC-6 model. The Corps's Sediment Weighted Histogram Generator (SWHG) program was used to reduce the 365 mean daily records into blocked histograms of thirty events per year. The sediment yield of the watershed is required as input into the HEC-6 model. Since historical records of sediment inflow do not exist, Toffaleti's (1948) computational technique was used to determine total sediment load, as well as the sediment distribution by size fraction for various discharges. Results of this technique were adjusted to reflect local conditions by using a regression relation between mean annual sediment discharge and mean annual water discharge that is provided in the USGS report titled "Summary of Fluvial-Sediment Studies in Ohio, Through 1987".

Madden's (1985) modification of Laursen's (1958) relationship was selected for the sand transport equation in the HEC-6 model. Many of the other sediment transport methods available in HEC-6 were tested but they produced thalweg elevations which became progressively unstable with time. In HEC-6, the basis for simulating vertical movement of the bed in response to scour or deposition is the Exner equation for continuity of material. It was determined that five iterations of the Exner equation produced the most stable results in the current model. Long term depositional trends indicated by the model compared favorably to historic dredge records.

The results of the HEC-6 computations are very dependent upon the accuracy of the data used to calibrate the model as well as the assumptions made concerning the equations used to model the interaction of sediment and flow. Where possible, each step taken in the development of the HEC-6 model was checked with available information. Therefore, it is necessary to conduct a sensitivity analysis to assess the impacts of possible errors. It is very labor intensive to develop and calibrate an HEC-6 model. Depending upon the skill of the modeler and the available information, the development of an HEC-6 model to this point can take up to three months. In many situations, not all of the information is readily available thus the creation of the HEC-6 model can take even longer.

Alternatives Several channel maintenance options were analyzed in the current study. These include allowing the current conditions to continue without maintenance, a compound channel through the project with a dry floodway on the right bank, channel improvements downstream of the project, construction of an upstream sediment trap, the use of flood walls and/or levees, reconstructing White's Mill Dam, reconstructing White's Mill Dam with an upstream sediment trap, and reconstructing White's Mill Dam with channel improvements downstream of the project. The performance of each alternative was measured by pulsing the peak discharges of test floods through the HEC-6 model at short time increments, both at the beginning and the end of the 40 years of record. This provides "before" and "after" water surface profiles. The effect that the alternative under consideration has upon the sedimentation in the project is reflected in the relative elevation difference of these water surface profiles. The analyses of some of these alternatives are summarized below. Of these alternatives, only those that involve a sediment trap provide a cost effective and practical solution.

Current Conditions Allowing current conditions to continue without maintenance dredging was modeled by simply allowing the HEC-6 model to run over the available 40 years of flow records. The model indicates that a steady state condition will not be achieved in this time frame and that deposition will continue in the project. The results of a 100 year flood was also modeled using HEC-6. The model indicated that the rising limb of the hydrograph would deposit more material in the project and that the peak discharge would not erode a significant amount of material.

Compound Channel with a Floodway The main objective of a compound channel with a floodway was to create a self maintaining pilot channel to carry the normal river flow with a floodway to pass the flood flows. The pilot channel was designed using regime theory approximated the original channel dimensions of the Hocking River through Athens before construction of the project. The pilot channel meander was configured in the model to coincide with the current sand bar deposition. The HEC-6 model indicated that deposition in the pilot channel would be significantly reduced. Unfortunately, the size of the floodway is limited by existing bridges and roads. As a result, the overall conveyance in the project would be reduced and the flood profiles would be raised.

Downstream Channel Improvement An HEC-2 analysis indicates that, by improving the channel below the project, flood profiles are lowered in the project. However, an HEC-6 analysis indicates that this downstream channel improvement does not improve the sediment deposition problems in the project. While the proposed channel improvement remains relatively clear and stable, material continues to deposit in the existing project. Eventually, without continued dredging efforts, the advantage of the channel improvement would begin to diminish.

Sediment Trap In the current study, alternatives that involve an upstream sediment trap

were the most successful with respect to providing long term reductions in water surface profiles, and in reducing much of the maintenance required in the project. The concept of a sediment trap, a dredged hole in the stream bed, is to provide a local sink for inflowing sediment so that deposition is confined to one area where it can be periodically removed. This alternative confines the maintenance of the project to monitoring and periodically removing material from a single location rather than over the length of the project. HEC-6 has the capability to directly model this option. The model indicates that the sediment trap reduces much of the sediment transport into the project and that flood water surface profiles would be lowered over time.

SAM SEDIMENTATION STUDY

The Corps computer program, SAM can be used to calculate sediment-discharge rating curves for given hydraulic parameters. These sediment rating curves can be integrated with flow-duration measurements to calculate average annual sediment yield for a reach of river. Sediment yield is often calculated as part of a sediment impact assessment. While a sediment impact assessment was not utilized in the Athens, Ohio study, it has been conducted for the current paper to provide a comparison of results with the more involved HEC-6 analysis.

A sediment impact assessment study uses a sediment budget analysis to assess the potential for degradation or aggradation of sediment. With this procedure, the estimated average annual sediment load entering the project is compared to the average annual sediment load that the project is capable of transporting. If there is more material entering the project than the project is capable of passing, the difference will most likely be deposited in the project. If the project can transport more material than is entering the area, then erosion can be anticipated. A sediment budget analysis using the Corps computer program SAM is significantly less time consuming than a full HEC-6 study. However, when used for a sediment budget analysis, SAM typically provides results that are more qualitative than quantitative in nature. The capability of SAM to quantify erosion or deposition at specific locations is limited. Since the goal of the Athens, Ohio sedimentation study was to investigate several options to continued dredging, the sole use of a sediment budget analysis was not appropriate.

To determine average annual sediment yield, it is necessary to calculate hydraulic characteristics of the stream under flows of known exceedence durations. These flows have been obtained from the USGS water data report number OH-94-1 for 90%, 50%, and 10% exceedence. The required hydraulic properties are velocity, depth, stream width, and energy slope. These values have been obtained from the HEC-2 model for the reach of the Hocking River above the project and for the reach of the Hocking River in the project reach. While it is not necessary to conduct the extensive sediment sampling required in the HEC-6 study, a characteristic bed gradation for the study reach is used in the SAM model.

All of the input used in the SAM model are reach-characteristic values. They do not reflect the localized changes which are characteristic of the alternatives that were investigated in the current study.

SAM contains a feature which provides guidance in the selection of sediment transport functions given the hydraulic parameters of the study reach. Both Yang's and Madden's modification of Laursen's equations were recommended by SAM for the hydraulic parameters which are characteristic of the Hocking River in the project area. Since there is little evidence of armoring in the project reach, it is assumed that the entire sediment transport capacity is utilized. Both of these transport functions indicate that approximately 80% more material will be transported by the reach of the Hocking River that is above the project than can be transported by the Hocking River within the project. This result agrees with the HEC-6 model insofar as that the project reach will continue to experience significant sediment deposition. However, even if all of this excess material is assumed to deposit within the project, the SAM results slightly underestimates the deposition indicated by the dredge records and the HEC-6 model. Nevertheless, as an order of magnitude approximation, SAM provides satisfactory results. The conclusion of the sediment budget analysis is that the current Athens, Ohio project is a depositional reach that will require significant dredging to maintain design conveyance. The most significant advantages that a SAM study has over HEC-6 study is cost and time. Depending upon the skill of the modeler and the available information, a sediment budget analysis could be completed in two to three weeks.

SUMMARY

The Corps sediment transport models, HEC-6 and SAM indicate that the Hocking River, through the Athens, Ohio local protection project, is a depositional reach and will continue to be so as long as current conditions persist. A sediment impact level of analysis using SAM can be used to arrive at this conclusion a lot faster than an HEC-6 study. However, an HEC-6 study is necessary to quantify the deposition and to assess the relative merit of different options to continued dredging.

Figure 1

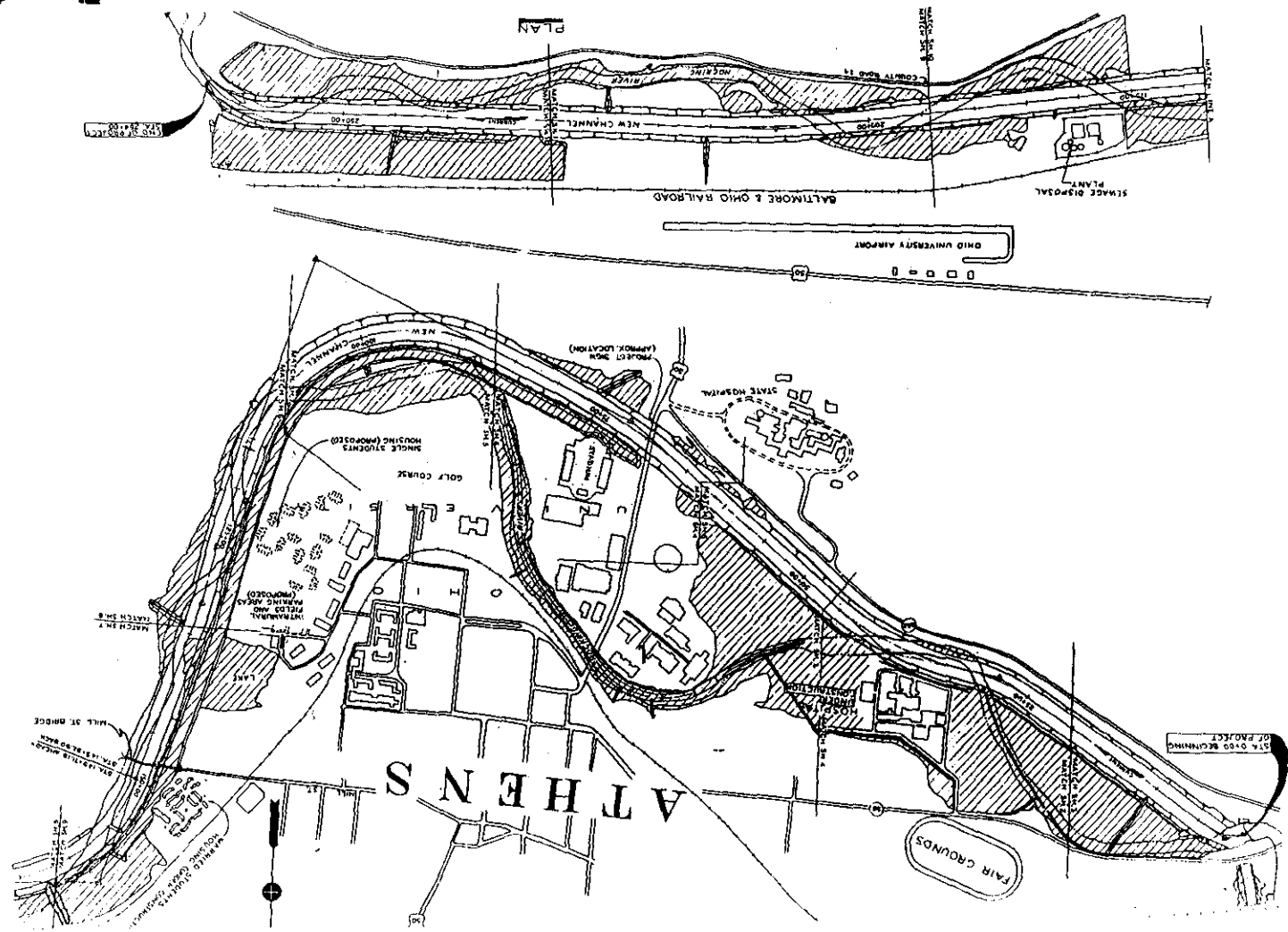




Figure 2a. Hocking River above the Athens Ohio channel improvement project.



Figure 2b. Hocking River in the Athens Ohio channel improvement project.

EVALUATION OF STREAM-SEDIMENTATION MODEL

By Weixia Jin, Graduate Student; Chao-Lin Chiu, Professor, Department of Civil & Environmental Engineering, University of Pittsburgh, Pittsburgh, PA 15261; Shou-shan Fan, Federal Energy Regulation Commission, Washington, D.C. 20426.

Abstract: Four test elements have been identified that tend to affect the flow properties computed with a sedimentation model. The orthogonal test design has been found capable of representing efficiently the possible combinations of individual factors at all levels of variation in evaluation of stream-sedimentation model. Sensitivity of sediment discharge should be tested with respect to individual factors at different values at different locations. Sediment discharge computed by HEC-6 has been found to be most sensitive to water discharge.

INTRODUCTION

There are a number of test elements to be considered in determining the sensitivity of a flow property computed by a sedimentation model. They include (a) test design, (b) factor to be tested for its effect on the flow property, (c) value of the factor within its possible range of variation, and (d) location of the river section at which the sensitivity tests are to be conducted. In this paper the three river-flow properties considered are the water-surface elevation, bed elevation and sediment discharge. The six factors considered to be affecting the flow properties are Manning's n , water discharge, channel slope, bed-material size, sediment inflow and time interval of computation. For illustration, HEC-6 was tested by using the data (EX3.DAT) from a river channel of movable boundaries provided by the developer of HEC-6 model (U.S. Army Corps of Engineers 1993). Fig. 1 gives a schematic plan of the river channel that includes a lake (reservoir) and indicates the river sections where the sensitivity tests were conducted.

EFFECT OF TEST DESIGN

Within the possible ranges of variation of the factors to be considered, a test design to be selected should satisfy the requirement that the test points are uniformly distributed in the multidimensional space formed by the factors, so that all possible combinations of the factors at different values may be represented in the test. The "Orthogonal Experimental Design" or "Taguchi design" (Taguchi 1987) is a technique developed to satisfy this uniformity requirement in an efficient manner by minimizing the number of tests required. It allows testing the sensitivity of a computed flow property to a factor at a certain value or "level," under possible combinations of the other factors at various possible values that can be represented by levels 1, 2, 3 et al. In practical applications of orthogonal design, selection of tests will depend on the actual numbers of factors and levels of these factors to be considered, and has been worked out in easy tabular forms by Taguchi (1987). For example, for the present case with the six factors (Fan 1988) and three levels of these factors defined in Table 1, there are eighteen tests shown in Table 2 to be conducted under the orthogonal design. The elements of Table 2 are 1, 2 or 3 that represents a level of an individual factor, above, at or below the norm. For example, if the upper and lower limits of a factor are plus and minus 5% of the norm, the levels 1, 2 and 3 of the factor are 1.05, 1.00 and 0.95 times the norm, respectively, as shown in Table 1.

Figs. 2 and 3 show the effect of the difference in test design on the sensitivity of computed water surface elevation (H) or bed elevation (BH) to each of the six factors is expressed in terms of the deviation of the water surface elevation or bed elevation, in percentage of local water depth, from that computed with all factors fixed at their norms. In the orthogonal tests the "norm" shown in the figures means that the particular factor being considered is at its norm (level 2) but the other five factors are at all possible levels (levels 1,

2, 3), whereas in the single-factor tests, the norm situation means that all six factors are at their norms. This explains why the test results at the norm situations under the two test designs are different. Fig. 4 compares the sensitivity of computed sediment discharge (Q_s) to each of the six factors, in which plotted on the vertical axis is the deviation (in percentage) of sediment discharge from Q_{s0} or the sediment discharge computed with all factors fixed at their norms.

These figures show that the effect of test design on the sensitivity of flow properties to each of the six factors is appreciable mainly at channel sections upstream from the dam in which the backwater effect exists. In general, a higher level of sensitivity of a computed flow property to each factor can be detected under the orthogonal test design.

EFFECT OF INDIVIDUAL FACTORS

The sensitivity analysis revealed that the three flow properties are relatively sensitive to the channel slope, water discharge, and Manning's n . These three factors can be ranked 1, 2 and 3, respectively, in the sensitivity of water surface elevation and bed elevation; and ranked 2, 1 and 3, respectively, in the sensitivity of sediment discharge. The particular importance of water discharge to computation of sediment discharge should be noted. Flow properties are generally more sensitive to the factors in sections upstream from the lake that are under the backwater effects; however, the computed sediment discharge downstream from the lake is also sensitive to the three factors, especially to the water discharge.

EFFECT OF LEVELS OF INDIVIDUAL FACTORS AND LOCATIONS OF CHANNEL SECTIONS

The sensitivity of a flow property to an individual factor also tends to vary with the value of the factor within a possible range of variation as well as the location of the channel section. At a given channel section, a flow property may not be appreciably sensitive to a factor when the factor is within a certain range but the sensitivity may increase dramatically beyond the range. Figs.5-7 show the variations of flow properties along the river, when the range of water discharge is varied. The response of a flow property to each factor was obtained by averaging the results from the six orthogonal tests, in which the range of the factor considered was varied while the ranges of the other factors were kept constant at $\pm 5\%$ about the norms, since it is reasonable to consider that a $\pm 5\%$ fluctuation or error in any factor is practically negligible. Physically, the norm of a factor may be considered as an estimated value while the actual value may be a certain percent ($\pm 5\%$, $\pm 10\%$ or $\pm 20\%$) lower or higher than the estimated. The variations of flow properties from those computed at the norms represent the errors in estimation. In reality a plus or minus 20 percent errors in estimation of Manning's n in a river flow commonly occur (Chow 1959). Errors in estimated values of some of the other factors may be even greater and vary from factor to factor. Generally, the variation or uncertainty of computed flow properties increases with the distance from the boundary from which the computation begins due to the accumulation of numerical errors. The sediment discharge is most sensitive to the water discharge although it is also very sensitive to the bed slope and Manning's n . The sensitivity is great in and in the vicinity of the lake. This implies that, in estimating the sediment inflow to a reservoir the accuracies of these three factors, the waters discharge in particular, are important and should be carefully estimated.

SUMMARY AND CONCLUSION

Flow properties computed with a model tend to vary with the test elements that have been identified. The orthogonal test design is capable of representing efficiently and uniformly the possible combinations of individual factors at all levels of variation. This is important since the sensitivity of a computed flow property tends to depend on the value of the factor within its possible range of variation. Furthermore, the

sensitivity of a computed flow property to a factor also varies with the location of the river section. Therefore, the sensitivity of sediment discharge computed by a model should be tested and analyzed with respect to individual factors at different values at different locations. The sensitivity of sediment discharge to a factor indicates the importance of the factor and the accuracy of the estimated value of the factor required by a model. For example, the sediment discharge computed by HEC-6 has been found to be most sensitive to the water discharge, especially in a region upstream from a dam where the backwater effect exists. Therefore, the estimated water discharge must be sufficiently accurate in order to assure the accuracy of sediment inflow to a reservoir computed by HEC-6 or any other model.

REFERENCES

Chow, V. T. (1959). Open channel hydraulics. McGraw-Hill Book Co., New York.

Fan, Shou-Shan (1988). Twelve selected computer stream sedimentation models developed in the United States. A report published by Federal Energy Regulatory Commission, Washington, D.C.

Taguchi, Genichi (1987). System of experimental design, Quality Resources, A Division of the Kraus Organization Limited, White Plains, New York. Vol. One and Two.

U. S. Army Corps of Engineers (1993). HEC-6 Scour and deposition in rivers and reservoirs. User's Manual. Hydrologic Engineering Center, 609 Second Street, Davis, CA 95616-4687.

ACKNOWLEDGMENT

This paper is based on work partially supported by the U. S. Federal Energy Regulatory Commission (FERC), under Cooperative Agreement No. FERC94-CHL-01567.

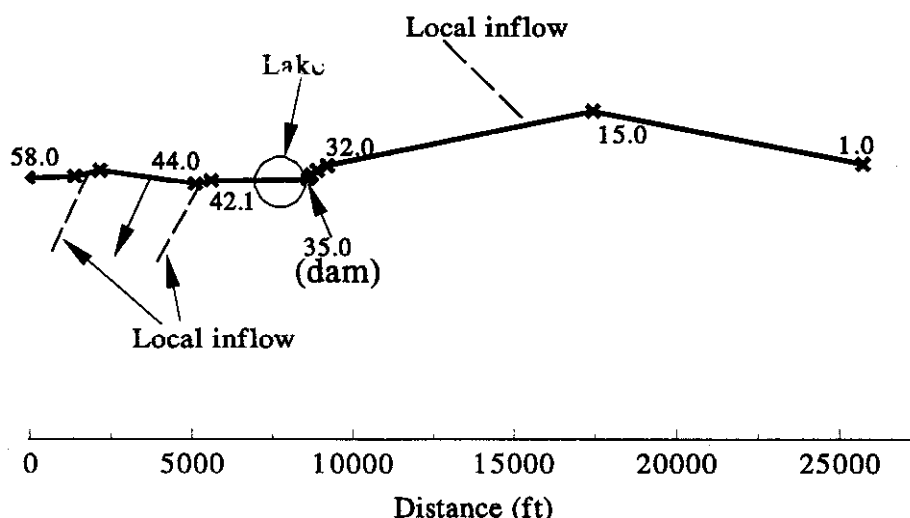


Fig. 1 Description of River Channel (Schematic Plan)

Table 1 Test Factors and Three Levels of Variation

Levels of variation	Manning's n	Water discharge Q_w (cfs)	Bed slope s_o	Bed material size D_{50} (mm)	Inflow sediment Q_{SI} (cfs)	Time interval (day)
	(A)	(B)	(C)	(D)	(E)	(F)
1	1.05n	1.05 Q_w	1.05s	1.05 D_{50}	1.05 Q_{SI}	1.5 Δt
2	1.0n	1.0 Q_w	1.0s	1.0 D_{50}	1.0 Q_{SI}	1.0 Δt
3	0.95n	0.95 Q_w	0.95s	0.95 D_{50}	0.95 Q_{SI}	0.5 Δt

Table 2 Orthogonal Tests with Six Factors and Three Levels

Tests No. (1)	Factors					
	A (2)	B (3)	C (4)	D (5)	E (6)	F (7)
1	1	1	1	1	1	1
2	2	2	2	2	2	2
3	3	3	3	3	3	3
4	1	1	2	2	3	3
5	2	2	3	3	1	1
6	3	3	1	1	2	2
7	1	2	1	3	2	3
8	2	3	2	1	3	1
9	3	1	3	2	1	2
10	1	3	3	2	2	1
11	2	1	1	3	3	2
12	3	2	2	1	1	3
13	1	2	3	1	3	2
14	2	3	1	2	1	3
15	3	1	2	3	2	1
16	1	3	2	3	1	2
17	2	1	3	1	2	3
18	3	2	1	2	3	1

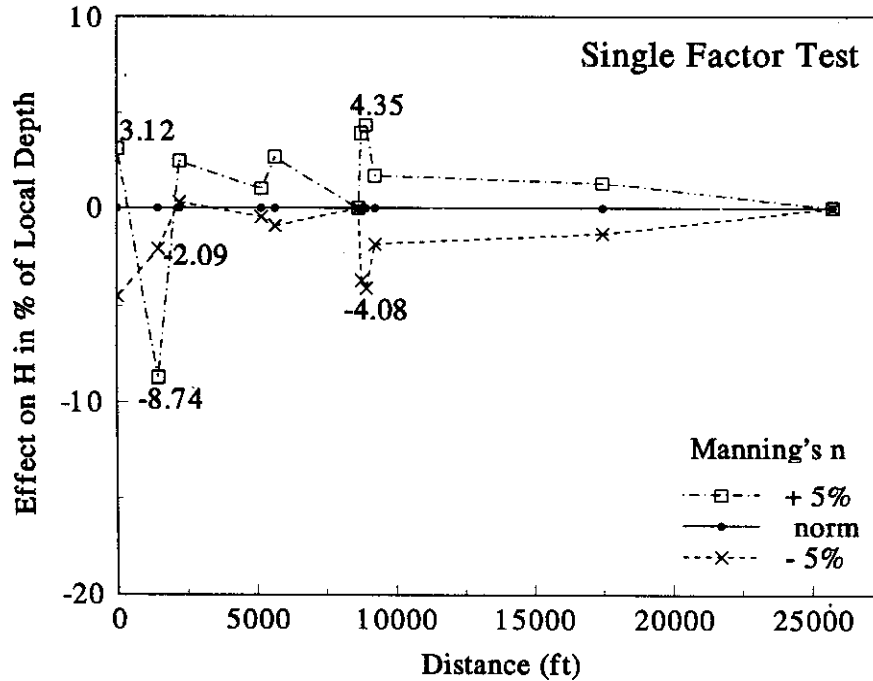
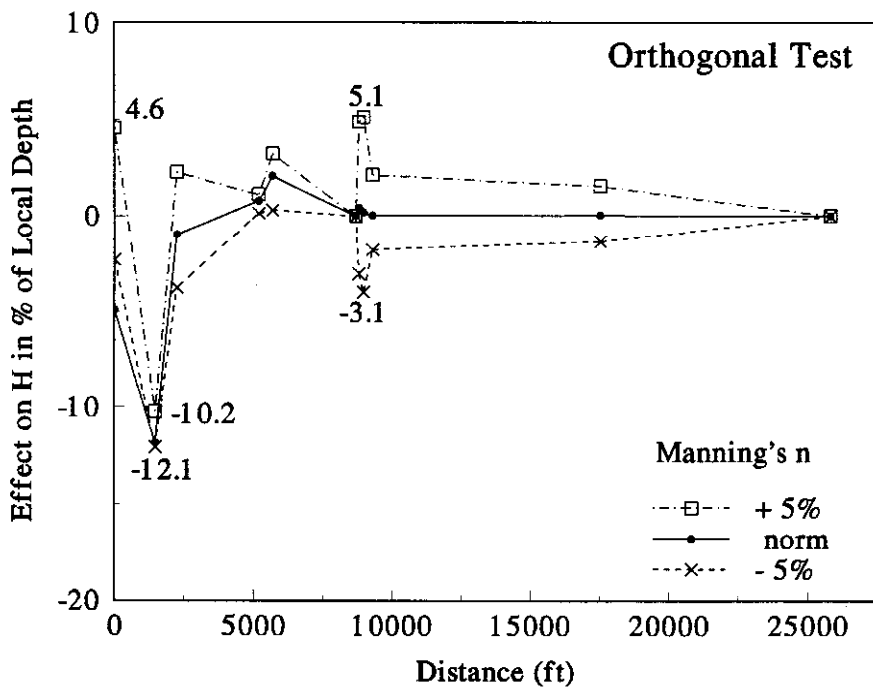


Fig. 2 Sensitivity of Water Surface Elevation to Manning's n

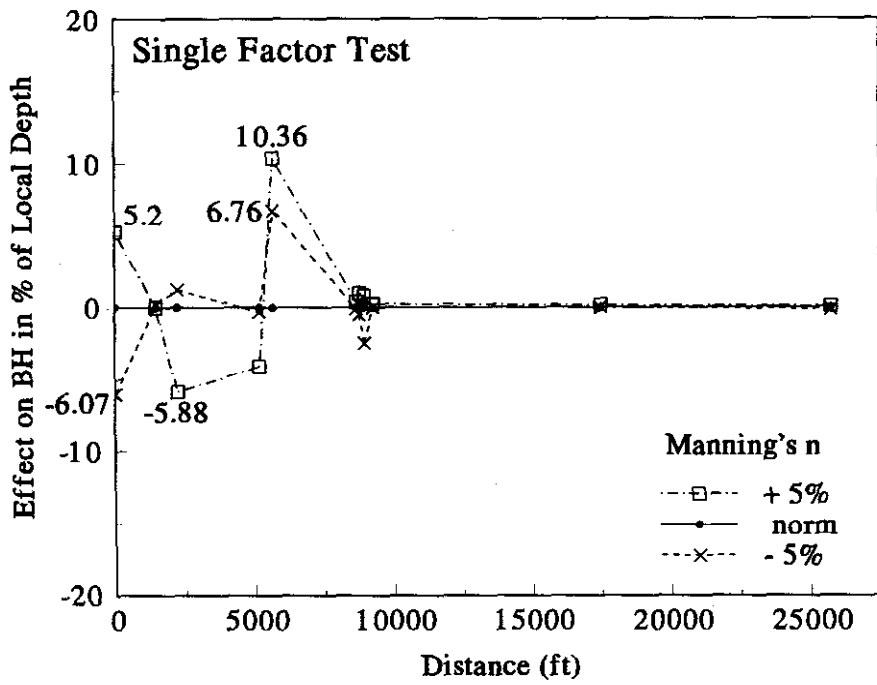
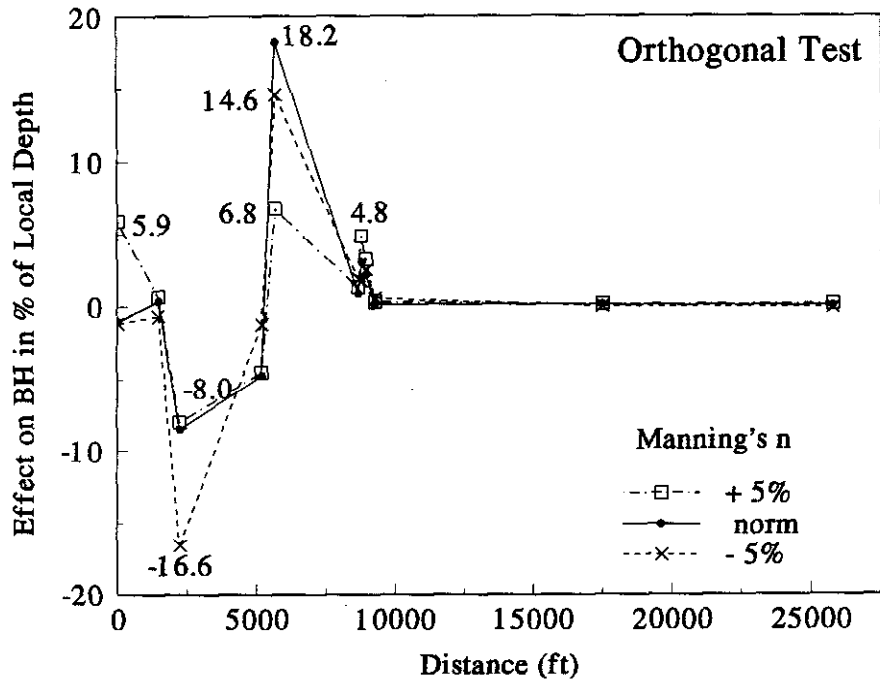


Fig. 3 Sensitivity of Bed Elevation to Manning's n

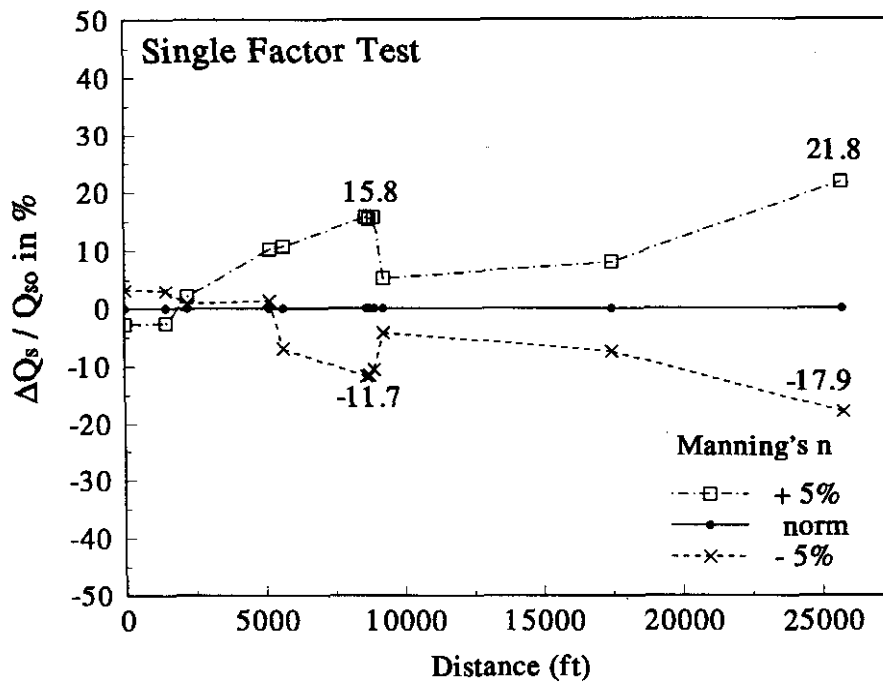
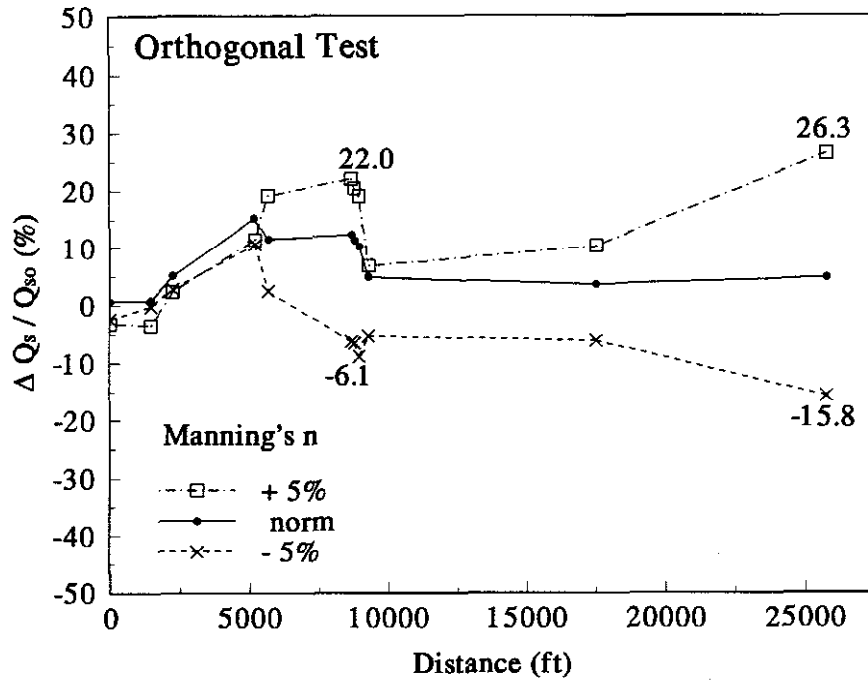


Fig. 4 Sensitivity of Sediment Discharge to Manning's n

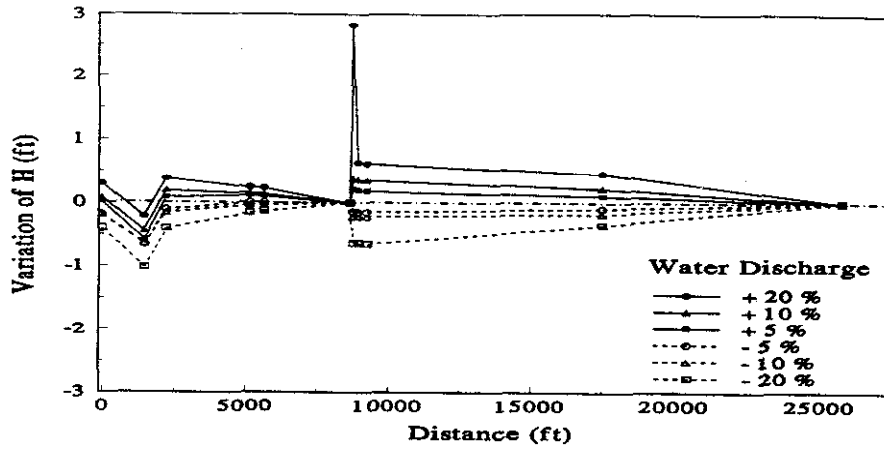


Fig. 5 Effects of Variation of Water Discharge and Location of Channel Section on Water Surface Elevation

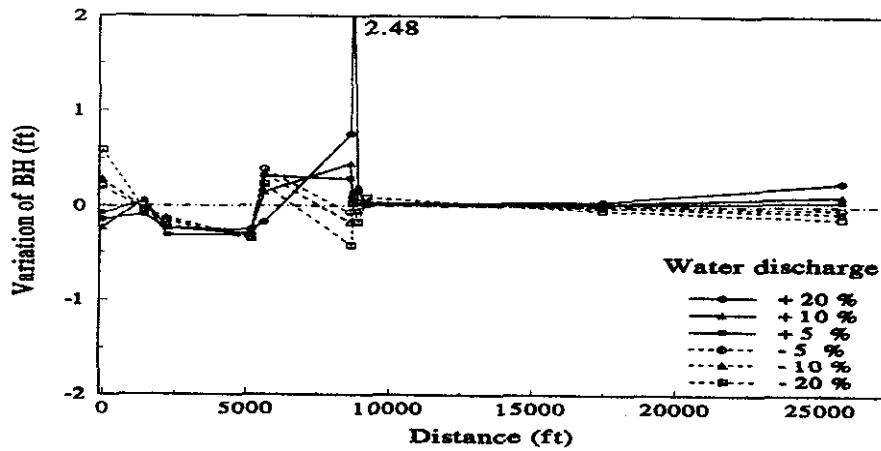


Fig. 6 Effects of Variation of Water Discharge and Location of Channel Section on Bed Elevation

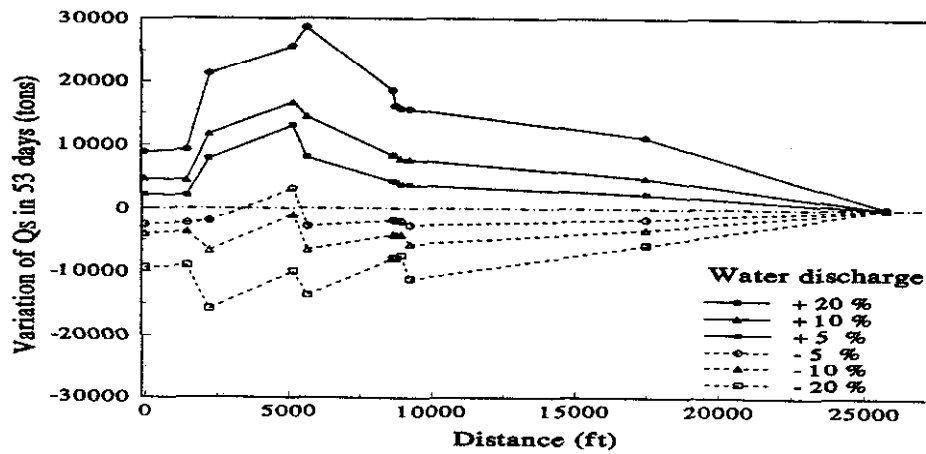


Fig. 7 Effects of Variation of Water Discharge and Location of Channel Section on Sediment Discharge in 53 Days

HYDRAULIC GEOMETRY FOR POLLUTANT LOADING COMPUTER MODELS USING GEOGRAPHICAL INFORMATION SYSTEMS TO DEVELOP INPUT DATA

By: Fred D. Theurer, Agricultural Engineer, Natural Resources Conservation Service, USDA, Washington, DC; Carlos V. Alonso, Research Hydraulic Engineer, National Sedimentation Laboratory, USDA, Oxford, MS; and Jerry M. Bernard, National Geologist, Natural Resources Conservation Service, USDA, Washington, DC.

Abstract: Stream channel field data (bankfull flow area, top width at bankfull, drainage areas, channel lengths, elevation, and Manning's roughness) were collected in three different basins that have widely divergent geomorphology. The advantages of using hydraulic geometry as a function of drainage area for geographic information system based pollutant loading computer models are explained. Power-law functions of top width & flow area at bankfull versus drainage areas were developed. Error analyses were performed. Comparisons were made to published regionalized power functions. One of the hydrologic modeling uses (T_c) was tested and comparisons made.

INTRODUCTION

The purpose of this paper is to:

1. Demonstrate the efficiency and efficacy of using hydraulic geometry equations derived from geomorphic relationships.
2. Compare results using hydraulic geometry relationships derived from field data collected in each HUA (Theurer & Bernard 1992; Iivari & Theurer 1993) to regionalized relationships (Dunne & Leopold 1978; Leopold 1994).

As a part of the USDA's water quality initiative, eight hydrologic unit areas (HUA) were selected to beta test USDA Natural Resources Conservation Service's (NRCS) pollutant loading (PL) computer model/geographic information system (GIS) interface. This paper reports on three of these HUA's. The PL computer models that are being used are the NRCS versions of the Agricultural Research Service's (ARS) Agricultural Non-Point Source pollution (AGNPS) (Young et al. 1987) and Simulator for Water Resources in Rural Basins—Water Quality (SWRRBWQ) (Arnold et al. 1990) watershed-scale computer models.

The three HUA's selected were:

- (1) Seco Creek Demonstration Project—Seco Creek (total drainage area of 39,471 acres & 6 cross-sections) & Little Seco Creek (total drainage area of 12,467 acres & 6 cross-sections), is a source of recharge water for Edwards Aquifer, Texas.
- (2) Greenbriar Water Quality Project—Davis Hollow Basin (total drainage area of 2700 acres & 39 cross-sections), Hole Basin I (total drainage area of 193 acres & 4 cross-sections), and Hole Basin II (total drainage area of 205 acres & 7 cross-sections), are tributaries to the Greenbriar River, West Virginia.
- (3) New York City Water Supply Project—Wrights Brook (2 subwatersheds with maximum drainage areas of 1931 acres with 4 cross-sections & 1807 acres with 8 cross-sections) and Kiff Brook (2 subwatersheds with maximum drainage areas of 3986 acres with 7 cross-sections & 1750 acres with 7 cross-sections). Both are upstream basins in the West Branch of the Delaware River Basin, New York.

Below the confluence of Seco & Little Seco Creeks, nearly all of the low flow discharge recharges groundwater. Davis Hollow & the Hole Basins are in a karst geologic area. Each Hole Basin terminates as a sinkhole. All of the Davis Hollow surface runoff for the upper third of the drainage area flows into a cavern at a single known sinkhole. The underground flow reappears at an outlet for the cavern at a single known location in the stream near the lower end of the watershed. The surface runoff for Wrights Brook & Kiff Brook remains as surface flow in the stream. There are no sinks or caverns in the stream system.

The authors collected the field data for the Seco & Greenbriar projects using a cloth tape, hand level, & rod. Horizontal control was done by locating the cross-sections on USGS 7.5 minute quadrangle sheets. Drainage areas, stream channel lengths, & slopes were calculated by means of measurements from the quadrangle sheets. Manning's "n" values (channel roughness) were estimated by visual inspection in the field. The field data for Wrights Brook & Kiff Brook were provided by the NRCS New York staff.

THE POWER FUNCTION

Equations: Watershed-scale hydrologic modeling requires stream channel hydraulic geometry. NRCS's PL computer models assume rectangular channel cross-sections. All NRCS versions of PL computer models for surface runoff involve the development of hydrographs using unit hydrograph methods. They also involve the use of sediment transport models based on unit discharge models (flow per foot of top width). NRCS unit hydrograph generation uses a time of concentration based upon bankfull depth of flow, and unit discharges are based on top widths at bankfull.

An important practical necessity for GIS-based hydrologic modeling is that the input data for computer models be related to spatial data as much as possible; i.e., hydraulic geometry should be related to drainage area rather than to dominant or reference discharge. For one thing, discharge is not readily available in ungaged watersheds. For another, grid-based computer models require bankfull top width & associated hydraulic depth for each grid cell. Several thousand cells may be needed for large watersheds. It is not practical to manually input the hydraulic geometry for such applications, necessitating simple geomorphic relationships.

It is a widely accepted empirical fact that bankfull hydraulic geometry is related to drainage area (Dunne & Leopold 1978). Accordingly, Equation 1 & Equation 2 are the two hydraulic geometry equations that were determined by regression analysis. They are:

$$A_b = a \cdot D_a^b \quad \text{Equation 1}$$

Where:

- A_b = flow area at bankfull flow, ft²;
- a = hydraulic geometry coefficient for the flow area at bankfull flow;
- b = hydraulic geometry exponent for the flow area at bankfull flow; and
- D_a = drainage area, acres.

$$W_b = c \cdot D_a^d \quad \text{Equation 2}$$

Where:

- c = hydraulic geometry coefficient for the top width at bankfull flow;
- D_a = drainage area, acres;
- d = hydraulic geometry exponent for the top width at bankfull flow; and
- W_b = top width at bankfull flow, ft.

Equation 3 is the third hydraulic geometry equation and is defined by the definition for hydraulic depth ($D_b = A_b / W_b$). It is:

$$D_b = e \cdot D_a^f \quad \text{Equation 3}$$

Where:

- D_b = hydraulic depth at bankfull flow, ft;
- e = hydraulic geometry coefficient for the hydraulic depth at bankfull flow; and
- f = hydraulic geometry exponent for the hydraulic depth at bankfull flow.

The definition for the hydraulic depth determines the coefficient & exponent in Equation 3. Equation 4 & Equation 5 can be derived by dividing Equation 1 by Equation 2. This leads to:

$$e = a / c \quad \text{Equation 4}$$

Where:

- a = hydraulic geometry coefficient for the flow area at bankfull flow;

- c = hydraulic geometry coefficient for the top width at bankfull flow; and
- e = hydraulic geometry coefficient for the hydraulic depth at bankfull flow.

and:

$$f = b - d$$

Equation 5

Where:

- b = hydraulic geometry exponent for the flow area at bankfull flow;
- d = hydraulic geometry exponent for the top width at bankfull flow; and
- f = hydraulic geometry exponent for the hydraulic depth at bankfull flow.

Coefficients & Exponents: The regionalized power law coefficients & exponents shown in Table 1 were taken from Figure 8.5, Leopold (1994) and corrected for units (drainage area from square miles to acres). Leopold states that the data used to develop these curves were taken from basins in:

- Curve A—Mediterranean climates of winter rainfall such as the San Francisco region at 30 inches annual precipitation.
- Curve B—high-rainfall areas such as Pennsylvania, with average annual precipitation of 45 inches.
- Curve C—mountain areas in the Upper Green River, Wyoming.
- Curve D—mountain areas in the Upper Salmon River, Idaho.

**Table 1: Regionalized Power Law Coefficients & Exponents
(after Leopold 1994)**

Leopold's Curve	Flow Area (ft ²)		Top Width (ft)		Hydraulic Depth (ft)	
	a	b	c	d	e	f
A	0.384	0.64	1.37	0.38	0.280	0.26
B	0.290	0.67	1.13	0.39	0.257	0.28
C	0.135	0.65	0.410	0.45	0.330	0.20
D	0.101	0.63	0.587	0.39	0.172	0.24

To determine the HUA field data power law coefficients & exponents, standard least squares regression of the log transforms of the flow area, top widths, and drainage areas for all the cross-sections in each watershed were done. The coefficients were adjusted to generate a mean error (ft) of zero for the field data set. An alternative could be to generate a mean error (%) of zero.

Table 2 shows the HUA field data coefficients & exponents calculated for each of the three HUA's. The regionalized values were selected from Table 1. Seco Creek was assumed to be similar to the Mediterranean climate (curve A) because of its limited average annual precipitation. The Greenbriar HUA was assumed to be most like the high-rainfall areas such as Pennsylvania (curve B).

Initially, the New York HUA was assumed to be most like Curve B because it is also in a high-rainfall area. However, the errors were so great that curves C & D were investigated. Curves C & D each gave a much better fit than curve B. Curve D gave the best fit.

Does this mean the upstream watersheds of the West Branch of the Delaware River in New York are hydrogeomorphically similar to the mountain areas of the Upper Salmon River in Idaho?

The regionalized top width power function fits the field data reasonably well (see Table 4). The regionalized flow area power function does not (see Table 3). The upstream watersheds in the Rocky Mountains run much deeper than the upstream watersheds in the West Branch of the Delaware River (see Table 5).

Does this mean that more hydro-geomorphic regions for hydraulic geometry should be done with better descriptions?

**Table 2: Power Law Coefficients & Exponents
(regionalized values after Leopold 1994)**

HUA	Hydraulic Parameter	HUA Field Data		Regionalized	
		Coef.	Exp.	Coef.	Exp.
Seco	Flow Area (ft ²)	1.624	0.534	0.384	0.64
	Top Width (ft)	3.682	0.315	1.370	0.38
	Hydraulic Depth (ft)	0.441	0.219	0.280	0.26
Greenbriar	Flow Area (ft ²)	0.208	0.711	0.290	0.67
	Top Width (ft)	1.085	0.419	1.13	0.39
	Hydraulic Depth (ft)	0.192	0.291	0.257	0.28
New York W/S	Flow Area (ft ²)	0.0210	0.8033	0.101	0.63
	Top Width (ft)	0.4051	0.4429	0.587	0.39
	Hydraulic Depth (ft)	0.0518	0.3604	0.172	0.24

Error Analysis: Table 3 shows the mean (ϵ) & standard deviation (σ) for the flow areas and associated errors. The predicted HUA field data calculations were based upon the respective HUA's field data coefficients & exponents. The regionalized calculations were based upon the respective HUA's regionalized coefficients & exponents. The statistics (ϵ & σ) are for all field data cross-sections for the respective HUA's. The error statistics in feet are defined to be the difference between the predicted and the observed. The error statistics in percent are defined to be the difference between the predicted and the observed divided by the observed times 100.

Table 3: Flow Area Statistics

HUA		HUA Field Data				Regionalized		
		Observed	Predicted	Error		Predicted	Error	
		(ft ²)	(ft ²)	(ft ²)	(%)	(ft ²)	(ft ²)	(%)
Seco	ϵ	235.23	235.23	0.00	15.4	158.33	-76.90	-25.6
	σ	158.25	158.95	135.01	53.2	117.12	129.04	41.3
Greenbriar	ϵ	9.98	9.98	0.00	23.0	10.91	0.93	37.2
	σ	9.00	10.04	6.71	81.4	10.31	6.82	91.4
New York W/S	ϵ	5.21	5.21	0.00	35.4	7.32	2.11	108.5
	σ	4.49	3.61	2.21	99.0	4.10	2.36	166.4

Table 4 shows the mean (ϵ) & standard deviations (σ) for the top widths and associated errors. The calculations were done in the same manner as Table 3.

Table 4: Top Width Statistics

HUA		HUA Field Data				Regionalized		
		Observed	Predicted	Error		Predicted	Error	
		(ft)	(ft)	(ft)	(%)	(ft)	(ft)	(%)
Seco	\bar{x}	63.00	63.00	0.00	16.0	43.88	-19.12	-20.0
	σ	40.43	33.18	33.37	45.5	25.19	33.25	35.2
Greenbriar	\bar{x}	9.47	9.47	0.00	7.3	8.36	-1.11	-3.2
	σ	5.37	5.81	3.85	40.7	4.84	3.49	35.5
New York W/S	\bar{x}	7.91	7.91	0.00	7.6	7.95	0.03	9.9
	σ	3.93	3.33	1.90	30.3	3.05	1.97	32.4

Comparisons: A definition of an average hydraulic geometry parameter for a specific watershed is the definite integral of the power function whose lower limit is 1 acre and upper limit is the maximum drainage area, and then divided by the difference between limits. Table 5 shows the ratio of the regionalized to the HUA field data averages for upper limit drainage areas of 1 acre and the maximum drainage areas for each of the two subbasins in each HUA.

Table 5: Ratio of Regionalized to HUA Field Data Power Law Average Hydraulic Parameters

Hydraulic Geometry	Seco Creek			Greenbriar			New York W/S		
	at 1 acre	main	Little	at 1 acre	Davis	Hole II	at 1 acre	Wrights	Kiff
Flow Area	0.24	0.66	0.58	1.39	1.05	1.17	4.81	1.57	1.38
Top Width	0.37	0.70	0.64	1.04	0.85	0.92	1.45	1.03	0.99
Hydraulic Depth	0.63	0.94	0.90	1.34	1.24	1.28	3.32	1.52	1.39

Figure 1 shows a graph of all of the Seco Creek's data for the flow area versus drainage area. The observed points are the actual field data and the line plots are the two predicted curves—HUA Field Data & Leopold (Curve A). Figure 2 does the same for the top widths.

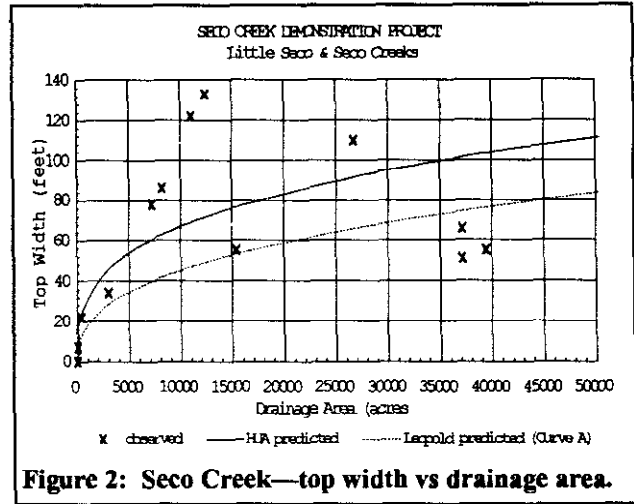
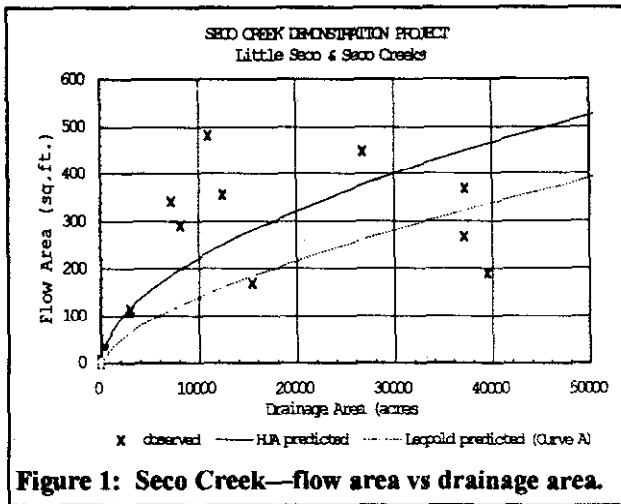


Figure 3 shows a graph of all of the Greenbriar's data for the flow area versus drainage area. The observed points are the actual field data and the line plots are the two predicted curves—HUA Field Data & Leopold (Curve B). Figure 4 does the same for the top widths.

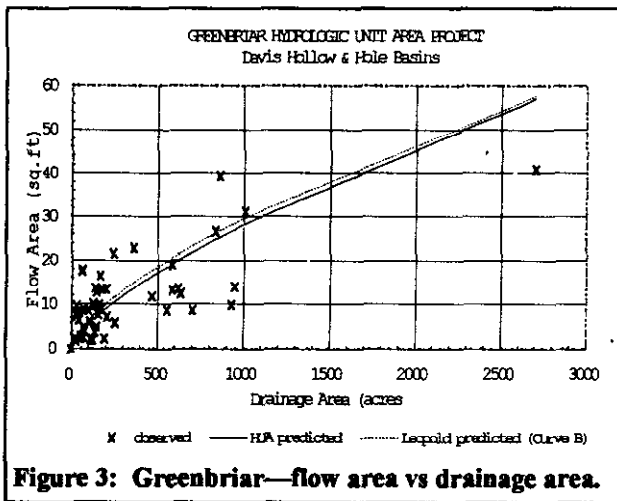


Figure 3: Greenbriar—flow area vs drainage area.

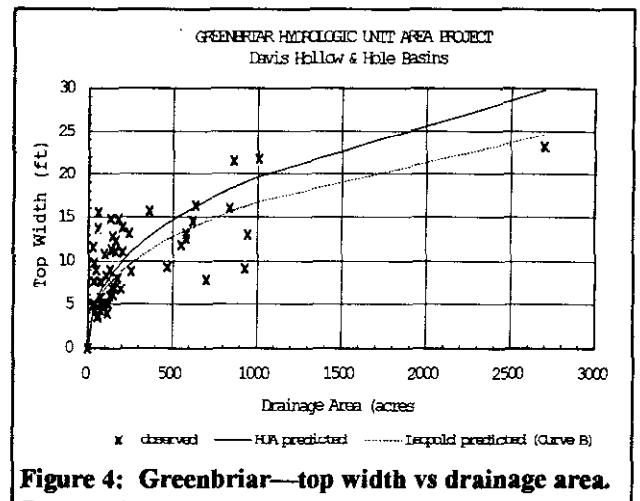


Figure 4: Greenbriar—top width vs drainage area.

Figure 5 shows a graph of all of the New York City's data for the flow area versus drainage area. The observed points are the actual field data and the line plots are the two predicted curves—HUA Field Data & Leopold (Curve D). Figure 6 does the same for the top widths.

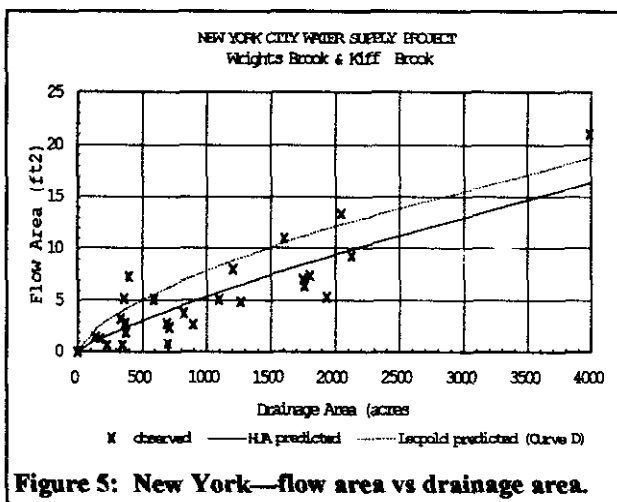


Figure 5: New York—flow area vs drainage area.

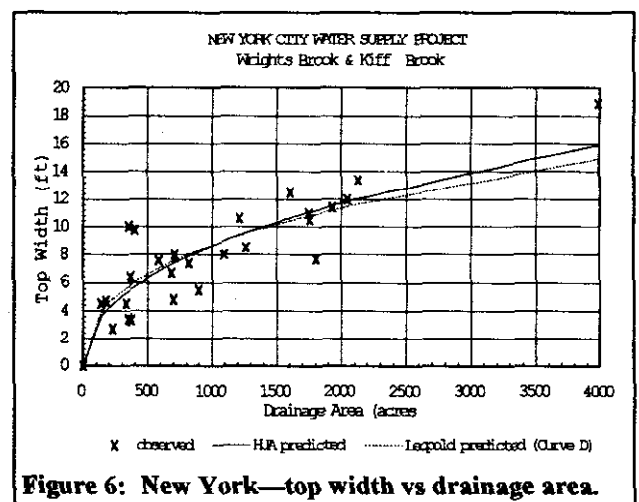


Figure 6: New York—top width vs drainage area.

Time of Concentrations: One of the major uses of the hydraulic geometry in hydrologic modeling is to compute the time of concentration (T_c) in order to generate hydrographs. Differences between T_c 's calculated using the field data (observed) and the two power function predictions (HUA Field Data & Leopold's curves) are shown.

Travel times (T_t) for each stream reach was calculated based upon the velocity at bankfull. T_t is defined to be the channel length divided by the harmonic mean of the velocities of the up & downstream cross-sections for the reach. Upstream T_t 's were summed to determine the T_c for the respective cross-section's drainage area. The channel lengths, elevations, Manning's roughness provided with the field data were used with the respective hydraulic geometry's method (observed, HUA field data, & Leopold) for the calculations.

Figure 7 shows a graph of the time of concentration versus drainage area for the main stem of Seco Creek. The observed points are the actual field data and the line plots are the two predicted curves—HUA Field Data & Leopold (Curve A). Figure 8 is the same but for Little Seco Creek. The two predicted line plots in Figure 7 are nearly identical.

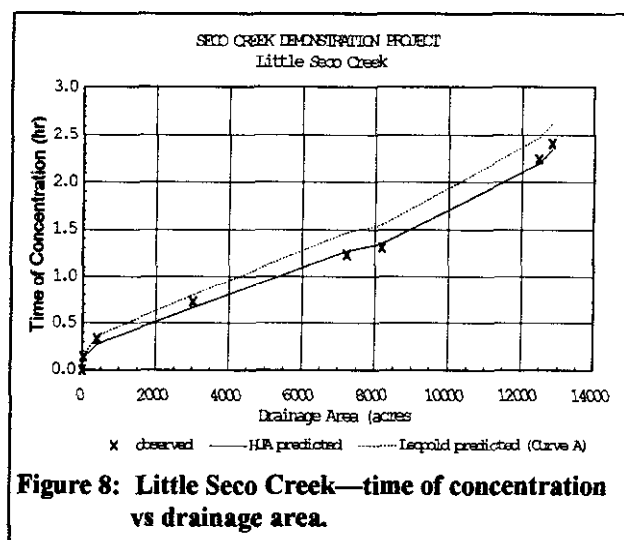
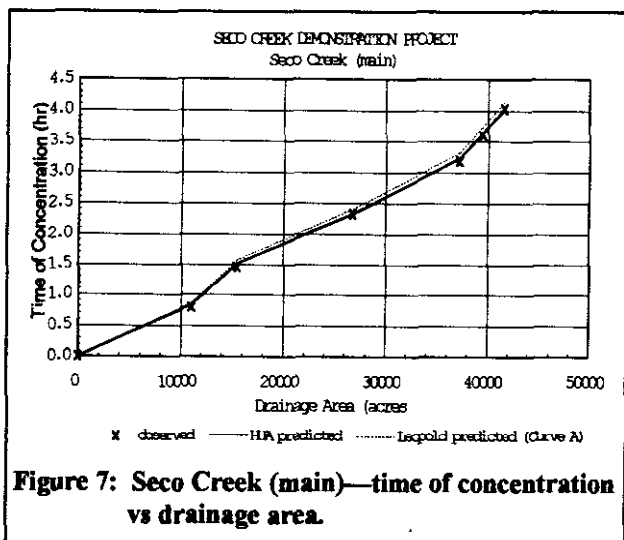


Figure 9 shows a graph of the time of concentration versus drainage area for the upper portion of Davis Hollow Basin before it is captured by the sink. The observed points are the field data and the line plots are the two predicted curves—HUA Field Data & Leopold (Curve B). Figure 10 is the same but for the lower portion of Davis Hollow after the sink.

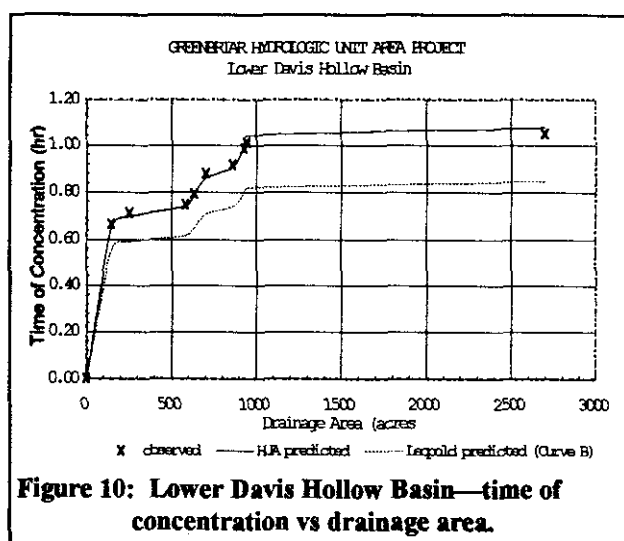
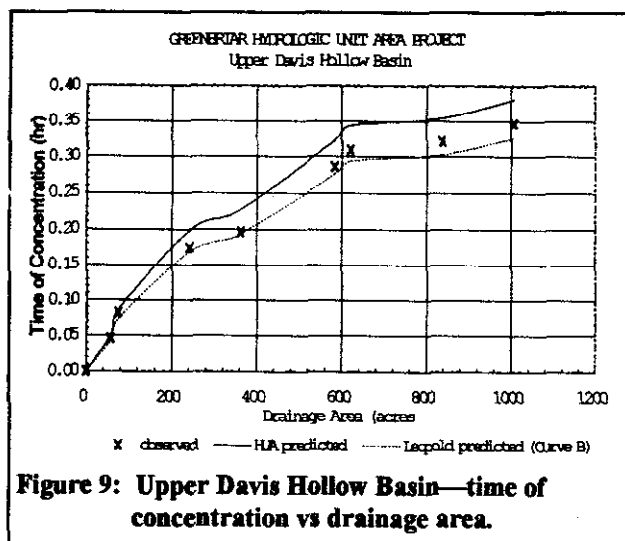


Figure 11 shows a graph of the time of concentration versus drainage area for Wrights Brook. The observed points are the field data and the line plots are the two predicted curves—HUA Field Data & Leopold (Curve D). Figure 12 is the same but for Kiff Brook.

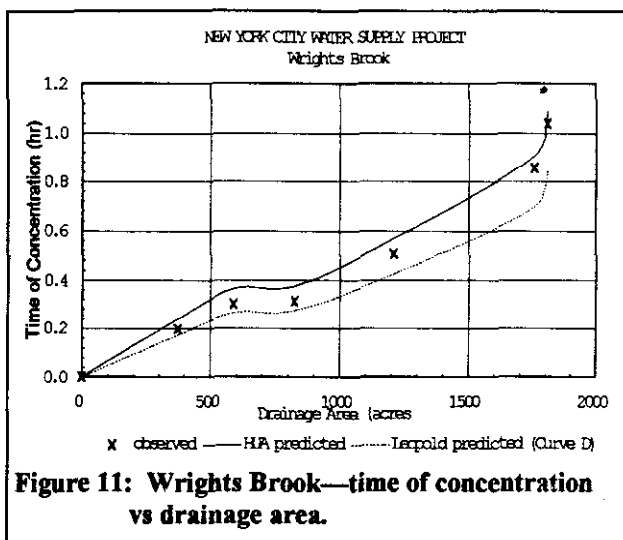


Figure 11: Wrights Brook—time of concentration vs drainage area.

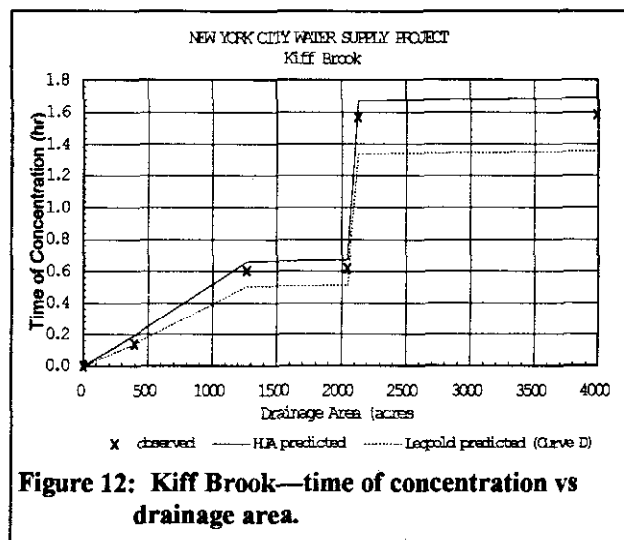


Figure 12: Kiff Brook—time of concentration vs drainage area.

Interpretations & Conclusions

Table 5 indicates that there can be significant differences between power functions based upon specific watershed field data and the limited regionalized power functions. Furthermore, the difficulty in determining the best set of regionalized power function parameters suggests that additional development of regionalized hydraulic geometry should be done in conjunction with better definitions for the hydro-geomorphic regions.

The authors reached the following conclusions:

- Power functions for the hydraulic geometry as a function of drainage area are powerful tools when used in conjunction with hydrologic models; and may be necessary for those computer models requiring large volumes of varying hydraulic geometry.
- Power functions can not be expected to predict the hydraulic geometry at a specific location but does predict the downstream trend and can be calibrated to reproduce some selected hydraulic geometry statistics.
- Power functions can be used with some assurance that they will perform reasonably well with hydrologic models (as was demonstrated by the T_c comparisons); however, further error analysis should be done with respect to sediment transport.
- Until formal hydro-geomorphic regions are defined and their hydraulic geometry parameters are developed, field data collection is recommended either to calibrate a set of hydraulic geometry parameters for a specific watershed or to aid in choosing a regionalized set of values (as was demonstrated for the New York HUA's).

References

- Arnold, J.G., J.R. Williams, A.D. Nicks, & N.B. Sammons. 1990. *SWRRB*, a basin scale simulation model for soil and water resources management. Texas A&M University Press, College Station, Texas, 1990.
- Dunne, T. & L.B. Leopold. 1978. *Water in Environmental Engineering*. W.H. Freeman & Co. San Fran., CA
- Leopold, L.B. 1994. *A view of the river*. Harvard University Press, Cambridge, Massachusetts.
- Theurer, F.D. & J.M. Bernard. 1994. *Seco Creek: hydraulic geometry*. 28 Nov. 1994. USDA-NRCS. 10 pg.
- Iivari, T. & F.D. Theurer. 1993. *WQ computer model-GRASS interface: hydraulic geometry report*, Greenbriar Hydrologic Unit Area, WV. February 1993. USDA-NRCS. 23 pg.
- Young, R.A., C.A. Onstad, D.D. Bosch, & W.P. Anderson 1987. *AGNPS*, Agricultural Non-Point-Source Pollution Model. A Watershed Analysis Tool. U.S. Dept. of Agr., Conservation Research Report 35, 80 pp.

EVALUATION OF SELECTED INSTRUMENTS FOR MONITORING SCOUR AT BRIDGES IN NEW YORK

Gerard K. Butch, Hydrologist, U.S. Geological Survey, Troy, N.Y.

Abstract: Reliable methods to monitor scour at bridges are needed to ensure public safety and minimize the cost to repair or replace vulnerable bridges. The U.S. Geological Survey, in cooperation with the New York State Department of Transportation, is evaluating four instruments for the Federal Highway Administration's Demonstration Project 97, "Scour Monitoring and Instrumentation." The instruments include (1) a magnetic sliding collar developed in the National Cooperative Highway Research Program (NCHRP), (2) an NCHRP sonar system, (3) a commercial sonar and satellite telemetry (SST) system, and (4) a commercial multichannel sonar and telephone telemetry (MSTT) system.

The instruments were installed between August 1994 and February 1995 and were not damaged by ice or debris during the first year of operation. The reliability of the equipment requires further evaluation because the 1995 peak discharges were less than 50 percent of the mean-annual peak discharges at the study sites. Minor errors in the sliding-collar measurements resulted from accumulation of excess sensor cable at bends in the pipe. The errors between median sonar depths and field-measured depths ranged from 0.2 to 0.4 feet. Sonar data were adversely affected whenever a transducer was exposed to air, ice, or debris, or located less than the minimum distance from the streambed (1-2 feet). The MSTT system measured 0.4 feet of scour that developed during a 12-hour period beginning about 6 hours before the 1995 peak discharge.

INTRODUCTION

Bridge failures in California during March 1995 reemphasize the dangers of scour noted in the 1987 collapse of the New York State Thruway bridge over Schoharie Creek. Streambeds at about 85,000 bridges in the United States are vulnerable to scour, and an additional 100,000 bridges have unknown foundations that must be monitored (Lagasse and others, 1995). The Federal government spent about \$200 million to repair bridges damaged by floods during the 1980's. Repair costs in New York were about \$7 million, and indirect costs to business and industry in New York were about \$36 million (Rhodes and Trent, 1993). Reliable methods to monitor scour at bridges are needed to ensure public safety and minimize the cost to repair or replace vulnerable bridges.

The National Cooperative Highway Research Program (NCHRP) in 1989 began project 21-3, "Instrumentation for Measuring Scour at Bridge Piers and Abutments," to develop, test, and evaluate scour-monitoring instruments. Subsequently, the Federal Highway Administration (FHWA) developed Demonstration Project 97 (DP-97), "Scour Monitoring and Instrumentation," to promote new and innovative equipment that State and local highway departments can use to measure and monitor scour.

The U.S. Geological Survey (USGS), in cooperation with New York State Department of Transportation (NYSDOT), is evaluating four scour monitors for FHWA DP-97: (1) an NCHRP sliding collar, (2) an NCHRP sonar system, (3) a commercial sonar and satellite telemetry (SST) system, and (4) a commercial multichannel sonar and telephone telemetry (MSTT) system. Scour holes that were present before installation of the sliding collar, SST system, and MSTT system were backfilled with bed material by NYSDOT. Data collected from the instruments are being compared with field observations to verify spatial and temporal changes in streambed elevations.

This report describes the installation procedures and principles of operation for each instrument; it also describes the performance and accuracy of the equipment during the first year of monitoring.

SCOUR-MONITORING INSTRUMENTS

The reliability of a sliding collar and three sonars in New York's harsh stream environment is being evaluated in a 2-year study. The instruments were installed between August 1994 and February 1995, and methods to protect the equipment from ice and debris are also being evaluated. Further information on the design and operation of sonar systems are described by Mueller and Landers (1995), Hayes and Drummond (1995), and Crumrine (1992).

NCHRP Sliding Collar: The NCHRP magnetic sliding collar (fig. 1) is a simple device that rests on the streambed and slides down a 2-in i.d. vertical stainless-steel pipe as the streambed is scoured beneath the collar. The sliding collar at State Route 30/145 over Schoharie Creek at Middleburg, N.Y. was installed in September 1994. Before installation, NYSDOT backfilled with sand, gravel, and cobbles a scour hole that partly exposed the footing. The collar (fig. 1) was mounted near the top of the stainless-steel pipe, about 25 ft below the bridge deck and 0.5 ft below the streambed. Schedule-40 galvanized pipe was attached to the stainless-steel pipe and was supported by a steel bracket at the base of the pier. Schedule-80 galvanized pipe was mounted to the upstream side of the pier from the steel bracket to the bridge deck. Rubber O-rings and a waterproof compound prevented seepage into the pipe. The distance from the top of the pipe to the collar was measured from the bridge deck by a sensor attached to the end of a 40-ft-long graduated cable. The cable was inserted into the pipe until the sensor was adjacent to the magnetic collar and activated a buzzer.

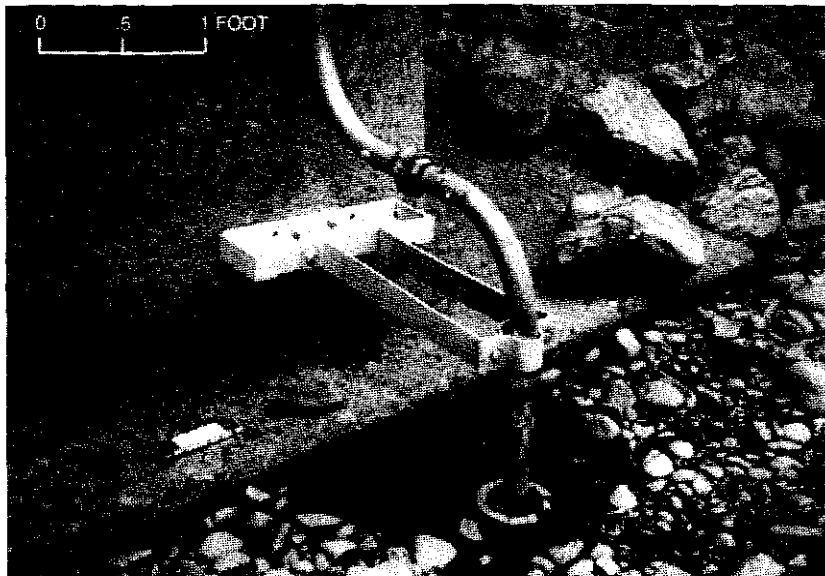


Figure 1. Sliding collar installed upstream of bridge pier at State Route 30/145 over Schoharie Creek at Middleburg, N.Y.

NCHRP Sonar: An NCHRP sonar device was installed at State Route 418 over the Hudson River near Warrensburg, N.Y. in October 1994 to monitor the stability of rock installed by NYSDOT at the base of the pier. The device measures the time required for an 8°, 192-kHz acoustic pulse to travel from the transducer to the streambed and back. The range of the sonar signal is 2 to 100 ft, and the resolution is 0.1 ft. The traveltime of the reflected signal is converted into distance from the velocity of sound in freshwater at 60°F. The maximum distance that can be measured without exceeding an error of 1.0 ft ranges from 30 ft at 32°F to 40 ft at 80°F (Schall and others, 1994).

A permanent shield was installed around the transducer by NYSDOT to protect the transducer and cable from ice and debris (fig. 2). The transducer was mounted 3 ft from the streambed in a 4-in i.d. schedule-80 galvanized pipe angled 10° upstream from the pier. The pipe was angled upstream so that the signal path between the transducer and the streambed would be unobstructed by the pier footing. The transducer cable extended 270 ft to an instrument shelter and was installed in a groove cut into the pier for added protection. A data logger activates the sonar at 1-hour intervals, processes the signal, and can store about 2 years of data. A portable computer and software provided by the manufacturer were used to program the data logger and retrieve data. The sonar and data logger are powered by a 12-V battery and solar panel. An internal battery maintains data storage if power is interrupted.

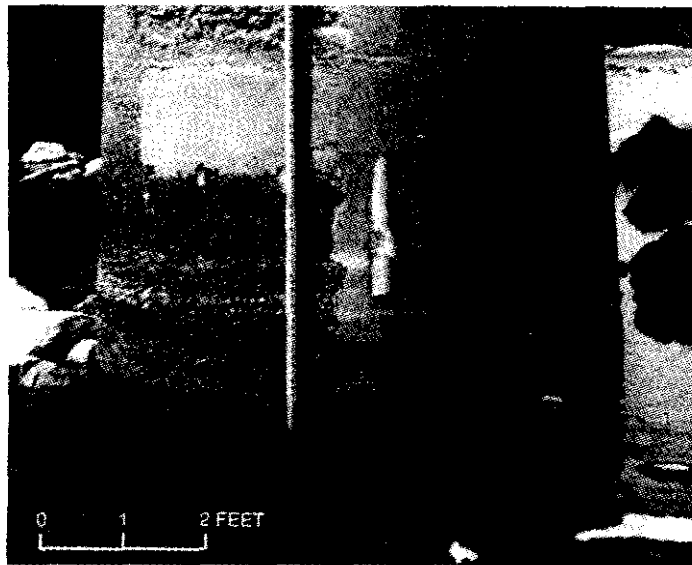


Figure 2. Protective shield for transducer mounted in bridge pier at State Route 418 over Hudson River near Warrensburg, N.Y.

Sonar and Satellite Telemetry System: A commercial SST system was installed at State Route 41 over the Susquehanna River at Afton, N.Y. in August 1994. The unit transmits an 8°, 200-kHz acoustic signal that is corrected by a microprocessor for variations in water temperature, false echoes, and ambient noise. The unit is a modified version of a sonar system that was installed at another bridge during 1989-93 (Butch, 1991). The range is 1.0 to 10.0 ft, and the resolution is less than 0.1 ft.

The transducer was mounted in a 5-in i.d. pipe angled 22° upstream from the pier so that the signal path between the transducer and the streambed would be unobstructed by the pier footing (fig. 3). The transducer cable was protected from ice and debris by 2-in i.d. schedule-80 galvanized pipe and extended 300 ft to an instrument shelter. A data-collection platform (DCP) activates the sonar at 1-hour intervals when the transducer is submerged, and at 24-hour intervals when the transducer is above the water surface. A portable computer was used to program the DCP, which transmitted data to the USGS by satellite telemetry every 4 hours. A scour hole at the upstream side of the pier was backfilled with bed material by NYSDOT in June 1995. The SST system is powered by a 24-V battery and a regulator charger.

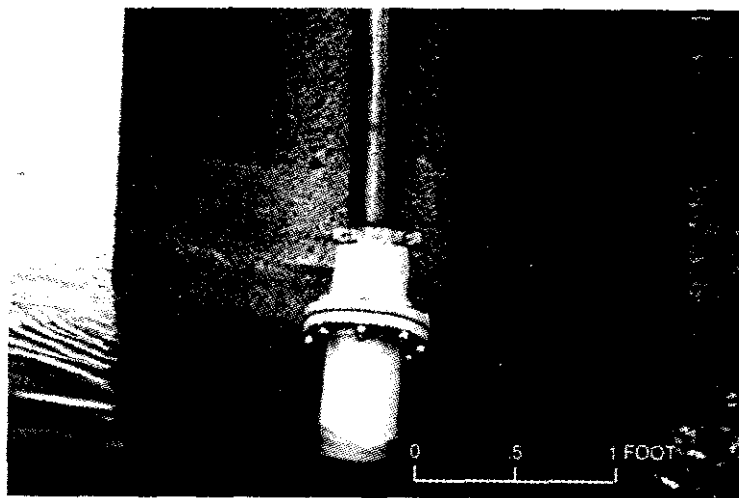


Figure 3. Protective shield for transducer mounted onto bridge pier at State Route 41, over Susquehanna River at Afton, N.Y.

Multichannel Sonar and Telephone Telemetry System: A commercial MSTT system was installed at State Route 23 over the Otselic River at Cincinnatus, N.Y. in February 1995 (fig. 4). The unit transmits an 8°, 200-kHz acoustic signal at 15-minute intervals. The range is 1.0 to 32.8 ft, and the resolution is less than 0.1 ft. The streambed was monitored at four locations around the pier because (1) high flows lowered the streambed about 8 ft at the upstream (northern) side of the pier during 1981-94, (2) a 30° angle between the flow and the pier extended the scour hole along the western side of the pier, and (3) a mobile gravel bar was observed at the eastern and southern sides of the pier (Butch, 1993, 1994).

NYSDOT graded the streambed and backfilled the scour holes with sand and gravel before installation of the MSTT system in 1994. Four transducers were installed around the pier to measure the distance from the footing to the streambed; a fifth transducer was inverted at the western side of the pier to measure the distance from the footing to the water surface. Shields and 2-in i.d. schedule-40 galvanized pipe were installed to protect the transducers and cables from ice and debris. The cables extended 200 ft to an instrument shelter, where the MSTT system can store about 3 months of data. A portable computer and software provided by the manufacturer were used to program the unit and retrieve data. A modem was used for remote interrogation. The unit is powered by a 24-V battery and a regulator charger. An internal battery maintains data storage for about 90 days if power is interrupted.

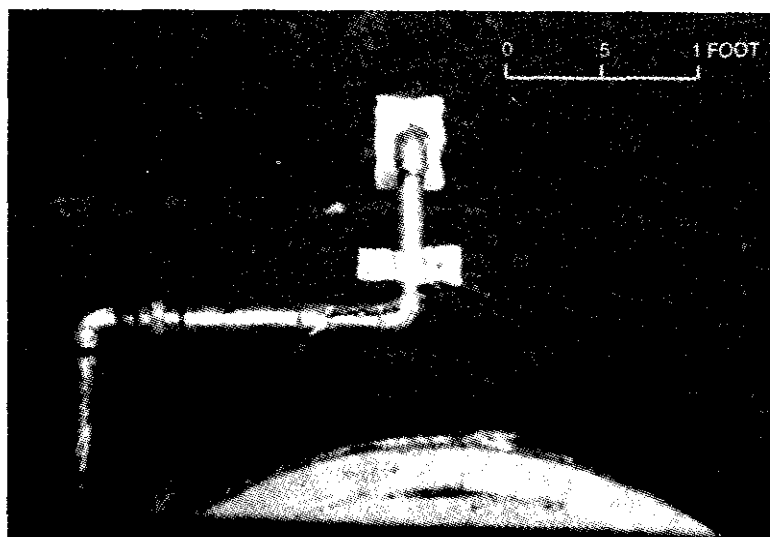


Figure 4. Protective shield for transducer mounted onto pier footing at State Route 23, over Otselic River at Cincinnatus, N.Y. (viewed from above).

INSTRUMENT PERFORMANCE

None of the scour monitors were damaged by ice or debris during the first year of operation. The reliability of the equipment needs further evaluation, however, because the 1995 peak discharges were less than 50 percent of the mean-annual peak discharges at the study sites.

NCHRP Sliding Collar: The distance from the top of the pipe to the collar ranged from 28.8 to 29.0 ft during the four inspections at State Route 30/145 over Schoharie Creek in the 1995 water year. The range between measurements resulted from accumulation of excess cable at two bends in the pipe as the sensor was lowered to the magnetic collar. The July inspection found the collar to be uncovered but not undermined; this could have occurred during peak stages in January or March, as indicated by gage-height data 7 mi upstream at Breakabeen (USGS station 01350355) (fig. 5).

The cable used to position the collar broke during shipment and was cumbersome to store; also, it stiffened in cold temperatures. A newer version of the sliding collar does not use a graduated cable and can be connected to a data logger; it also may be less vulnerable to ice and debris than the model tested because the sensor cable can be mounted to the downstream side of the pier.

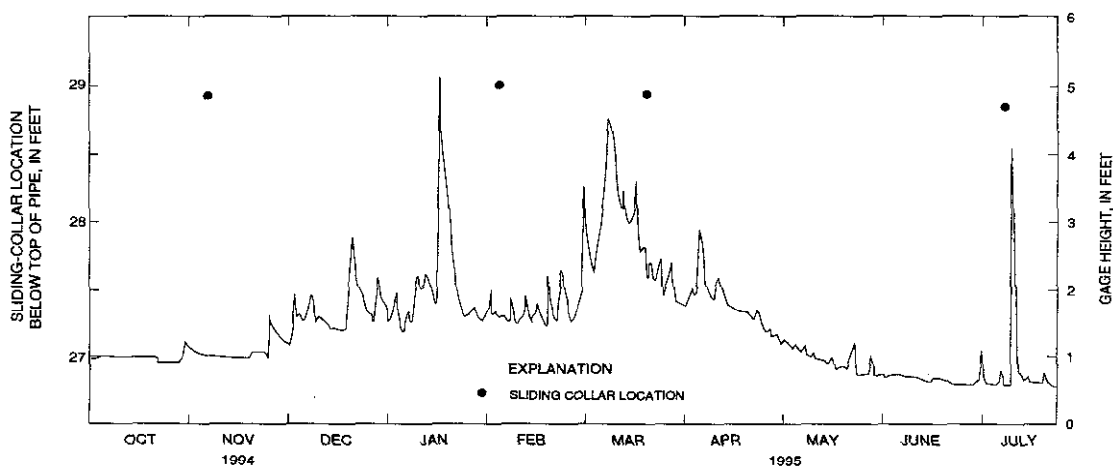


Figure 5. NCHRP sliding-collar measurements at State Route 30/145, and gage height at Schoharie Creek at Breakabeen, N.Y. (01350355), October 1994 through July 1995.

NCHRP Sonar: The NCHRP sonar at State Route 418 over the Hudson River performed well after the measurement time was increased from 20 seconds to 45 seconds in March 1995. The site was inspected nine times during the 1995 water year, and no scour was observed. The field-measured distance between the transducer and the streambed ranged from 2.8 to 3.0 ft, and the median sonar depth ranged from 3.0 to 3.2 ft (fig. 6). The transducer is submerged whenever the gage height at Hadley, 13 mi downstream (USGS station 01318500), exceeds about 4 feet (fig. 6). No data were recorded when the transducer was above the water surface or surrounded by ice.

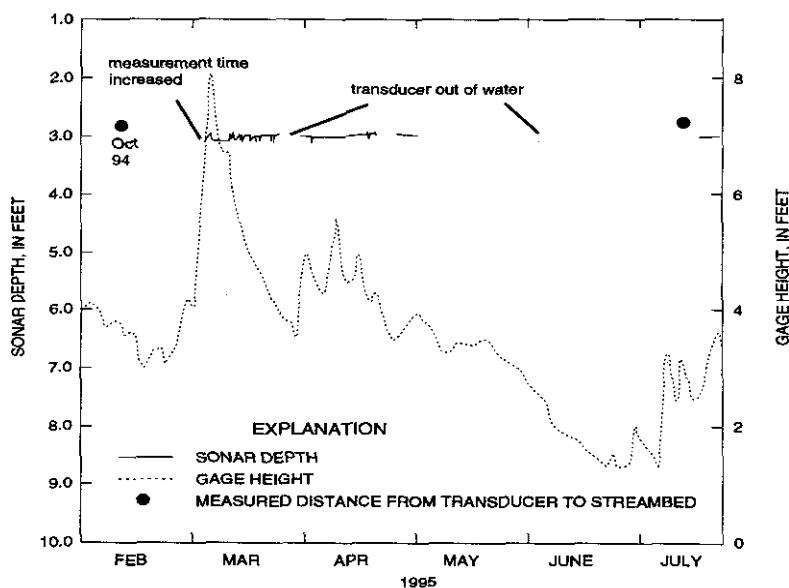


Figure 6. Sample NCHRP sonar depth and measured distance at State Route 418, and gage height at Hudson River at Hadley, N.Y. (01318500), February through July 1995.

No sonar data were collected from October 1994 through March 1995 because the 20-second measurement time that was programmed in the data logger was too short to activate the sonar and compute an average depth. A 45-second measurement time was ample to process the signal; it also improved streambed detection when floating ice momentarily obstructed the signal path. The other processing routines in the data logger include (1) activation of the sonar at 1-hour intervals, (2) computation of an average depth if the difference between three depth readings is 0.3 ft or less, (3) the recording of a "no lock" condition when an echo is not received, and (4) the recording of an "outside limits" condition if an average depth cannot be computed within the programmed measurement time. The 270-ft-long transducer cable and the 10° transducer angle did not adversely affect the signal because the shallow depth and solid streambed minimize signal attenuation. Despite a malfunctioning relay, the solar panel provided adequate power at -20°F to maintain continuous operation of the sonar.

Sonar and Satellite Telemetry System: The commercial SST system at State Route 41 over the Susquehanna River operated with few problems. The site was inspected five times during the 1995 water year, and no scour was observed. NYSDOT backfilled the scour hole with bed material in June 1995; as a result, the field-measured distance between the transducer and the streambed decreased from 3.8 ft to 1.7 ft, and the median sonar depth decreased from 4.2 ft to 2.1 ft. (fig. 7). The transducer gave inaccurate data when exposed to air or ice and became submerged whenever the gage height 50 ft downstream at Afton (USGS station 01502701) exceeded about 2 ft. Debris attached to a submerged log resulted in occasional spikes in the data until the log was removed in June 1995 (fig. 7). Minor signal scatter is attributed to wide reflections from cobbles. The 22° transducer angle and the 300-ft length of the cable did not adversely affect the data, although the cable length increased signal noise.

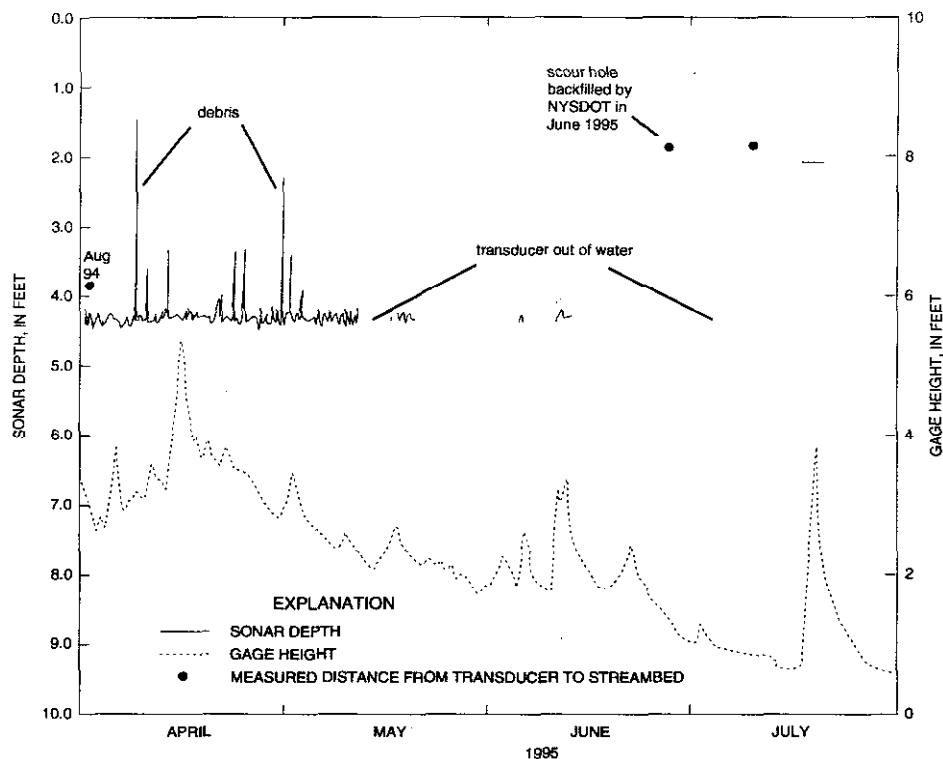


Figure 7. Example Sonar and Satellite Telemetry System sonar depth and measured distance at State Route 41, and gage height at Susquehanna River at Afton, N.Y. (01502701), April through July 1995.

Multichannel Sonar and Telephone Telemetry System: The commercial MTT system at State Route 23 over the Otselic River performed well, except when the distance between the transducer and the streambed was less than about 1 ft (the minimum range of the sonar). The site was inspected three times during the 1995 water year. The field-measured distance between the streambed and the transducer at the upstream (northern) side of the pier in February 1995 was 1.3 ft, and the median sonar depth was 1.0 ft. The median sonar depth increased to 1.4 ft during the 1995 peak discharge in March (fig. 8), and the field-measured distance increased to 1.6 ft. Scour began about 6 hours before the peak and continued for about 12 hours (fig. 9). Median sonar depth and field-measured distance had decreased about 0.4 ft by July, possibly the result of low flows and (or) adjustment of the graded streambed to an equilibrium elevation. Signal scatter increased in March as the scour hole deepened and the local slope of the streambed increased. Scour may have occurred April 4 or April 13 but debris degraded the signal from the transducer. New software corrected a modem problem that resulted in loss of data for 3 days during March. The number of multiple echoes increased during June and July as the distance between the transducer and streambed decreased.

The sonar depths measured by the transducers mounted on the western and southern sides of the pier are unreliable because the distance to the streambed is less than 1.0 ft. The transducer mounted on the eastern side of the pier was found buried by a gravel bar in April. The two transducers mounted on the western side of the pier were shifted by ice or debris. Gage-height data less than 1 mi upstream at Cincinnati (USGS station 01510000) were used to supplement the sonar data because turbulence and debris had degraded the signal from the transducer aimed upward at the water surface.

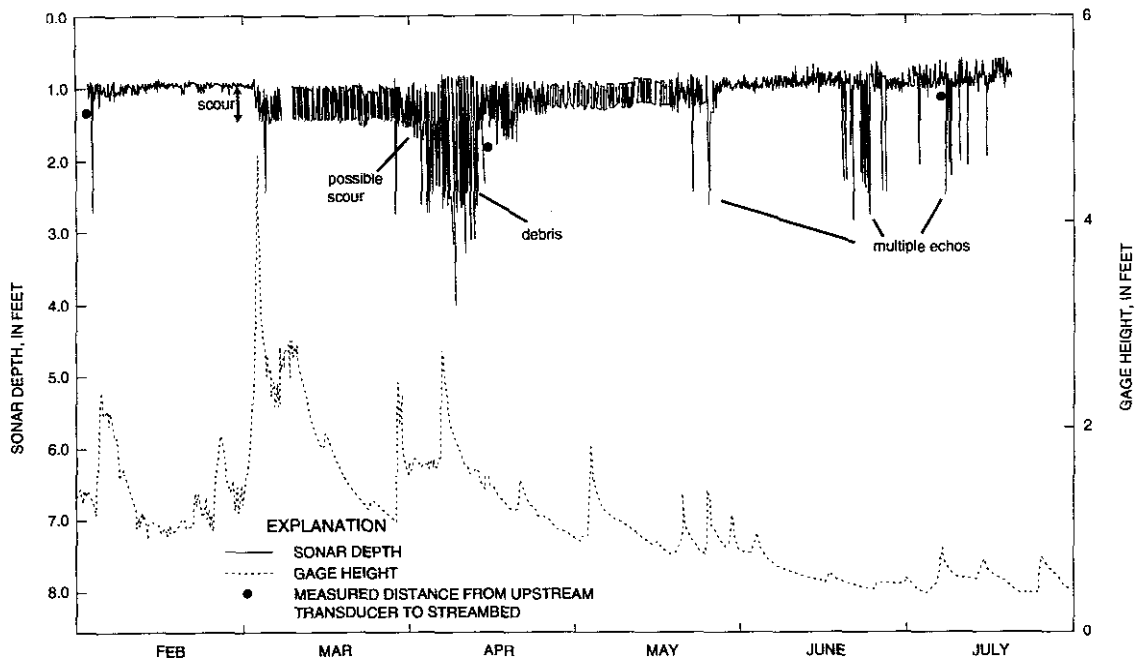


Figure 8. Multichannel Sonar and Telephone Telemetry System sonar depth and measured distance at State Route 23, and gage height at Otselic River at Cincinnatus, N.Y. (01510000), February 1995 through July 1995.

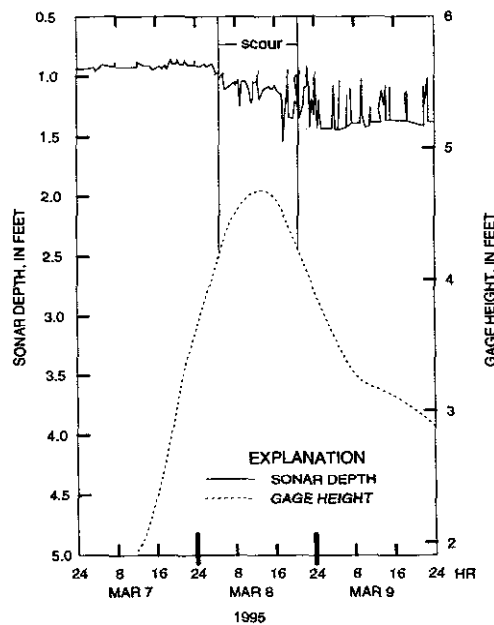


Figure 9. Multichannel Sonar and Telephone Telemetry System sonar depth at State Route 23 and gage height at Otselic River at Cincinnatus, N.Y. (01510000), March 7-9, 1995.

SUMMARY

Four types of scour-monitoring instruments are being evaluated for FHWA Demonstration Project 97, "Scour Monitoring and Instrumentation": (1) an NCHRP sliding collar, (2) an NCHRP sonar system, (3) a commercial sonar and satellite telemetry (SST) system, and (4) a commercial multichannel sonar and telephone telemetry (MSTT) system. The instruments were installed between August 1994 and February 1995 and were not damaged by ice or debris during the first year of operation. The reliability of the equipment needs to be evaluated during flows higher than 1995 peak flows, which were less than 50 percent of the mean-annual peak discharges at the study sites. Scour holes that were present before the study began were

backfilled with bed material by NYSDOT. Sonar data were adversely affected whenever a transducer was exposed to air, ice, or debris, or located less than the minimum distance from the streambed (1-2 ft).

The NCHRP sliding collar was installed in September 1994 and did not indicate any scour. Minor measurement errors resulted from accumulation of excess sensor cable at bends in the pipe. A newer version of the collar does not require a graduated cable and can be connected to a data logger; it also may be less vulnerable to ice and debris than the model tested.

The NCHRP sonar system performed well after the measurement time was increased from 20 seconds to 45 seconds in March 1995. Median sonar depths were within 0.2 ft of measured distances. The processing routines identified inaccurate data that resulted from the transducer's exposure to air or ice, but other errors were occasionally recorded when the transducer was partly submerged. A portable computer is needed to program the data logger and retrieve data.

The commercial SST system has performed well since the unit was installed in August 1994, although it has indicated no scour. Median sonar depths were within 0.4 ft of measured distances. Inaccurate data were collected whenever the transducer was exposed to air, ice, or debris. A DCP activates the sonar at 1-hour intervals when the transducer is submerged and at 24 hour intervals when the transducer is above the water surface. Data are transmitted to the USGS by satellite telemetry every 4 hours.

The commercial MSTT system has operated with no major problems. The median sonar depths were within 0.3 ft of the measured distances at the upstream side of the pier. The unit measured 0.4 ft of scour during the 1995 peak discharge. The scour started about 6 hours before the peak and continued for about 12 hours. Sonar depths from three other transducers mounted around the pier are unreliable because the distance between each transducer and the streambed is less than 1.0 ft, the minimum range of the unit. Turbulence and debris affected a fifth transducer that measures the distance from the pier footing to the water surface. A portable computer and modem were used to program the unit and retrieve data.

REFERENCES

Butch, G.K., 1991, Measurement of bridge scour at selected sites in New York, excluding Long Island: U.S. Geological Survey Water Resources Investigations Report 91-4083, 17 p.

, 1993, Estimating bridge scour in New York from historical U.S. Geological Survey streamflow measurements, *in* Hydraulic Engineering '93--Proceedings of the 1993 Conference, Shen, H.W., Su, S.T., and Wen, Feng, eds., American Society of Civil Engineers, New York, New York, v. 2, p. 1866-1871.

, 1994, Effects of flow duration on local scour at bridge piers in New York, *in* Hydraulic Engineering '94--Proceedings of the 1994 Conference, Cotroneo, G.V., and Rumer, R.R., eds., American Society of Civil Engineers, New York, New York, v. 1, p. 46-50.

Crumrine, M. D., 1992, Bridge-scour data for the highway 101 bridge over Alsea river estuary at Waldport, Oregon--1988-90: U.S. Geological Survey Open-file Report 91-531, 48 p.

Hayes, D.C., Drummond, F. E., 1995, Use of fathometers and electrical-conductivity probes to monitor riverbed scour at bridge piers: U.S. Geological Survey Water-Resources Investigations Report 94-4164, 17 p.

Lagasse, P.F., Thompson, P.L., and Sabol, S.A., 1995, Guarding against scour: *Civil Engineering*, v. 65, no. 6, p. 56-57.

Mueller, D.S., Landers, M.N., (*in press*), Evaluation, development, and performance of portable instrumentation and deployment systems for real-time measurement of scour at bridges: Federal Highway Administration publication FHWA-IP-95-xxx.

Rhodes, Jennifer, Trent, R.E., 1993, Economics of floods, scour, and bridge failures, *in* Hydraulic Engineering '93--Proceedings of the 1993 conference, Shen, H.W., Su, S.T., and Wen, Feng, eds., American Society of Civil Engineers, New York, New York, v. 1, p. 928-933.

Schall, J.D., Richardson, J.R., and Price, G.R., 1994, Low-cost bridge scour measurements, *in* Fundamentals and Advancements in Hydraulic Measurements and Experimentation--Proceedings of the Symposium, Pugh, C.A., ed., American Society of Civil Engineers, New York, New York, p. 114-118.

SCOUR AT BRIDGES — DETAILED DATA COLLECTION DURING FLOODS

David S. Mueller
Hydrologist, U.S. Geological Survey, Water Resources Division
2301 Bradley Avenue, Louisville, KY 40217

Abstract: The U.S. Geological Survey, in cooperation with the Federal Highway Administration, has recently developed equipment and techniques for collecting detailed bathymetric and hydraulic data needed to characterize and study the processes associated with scour at bridges. A cooperative study is underway to collect detailed data during floods. Detailed data were collected on the Mississippi River in 1993, on the Brazos River in 1994, on the Sacramento River in 1995, and on several small streams in Missouri in 1995. Bathymetric data were collected using a digital echo sounder. Broadband Acoustic Doppler Current Profilers were used to measure three-dimensional velocities. The locations of all data collected were obtained using either a range-azimuth tracking system or a global positioning system. All of the instruments performed well, within their limitations. A remote-control boat has proved useful for instrument deployment on small streams where a manned vessel cannot be used safely. Future developments will likely result in improved data accuracy, increased data coverage, and more efficient data collection procedures.

INTRODUCTION

Scour of the streambed at bridge piers and abutments during floods has resulted in more bridge failures than all other causes in recent history (Murillo, 1987). A complete understanding of processes causing scour at bridges has been restricted by the complexity of the processes and by the lack of detailed field data. Most of the research on scour at bridges has been conducted in the laboratory with almost no validation by field data. The U.S. Geological Survey (USGS), in cooperation with the Federal Highway Administration (FHWA), has collected and compiled more than 300 field measurements of scour at bridges (Landers and Mueller, in press). These data can be used to evaluate equation performance; however, most of the data collected in this initial effort provide only limited characterization of the complex scour processes. These data do not have the spatial extent necessary to characterize scour hole shape or to study contraction and abutment scour. In order to obtain more detailed data to study these scour phenomena, the USGS, in cooperation with the FHWA, have developed and used equipment and techniques for collecting detailed bathymetric and hydraulic data associated with scour at bridges.

Collecting hydraulic and sediment transport data during floods in sufficient detail to study scour processes and to improve design and evaluation methods is difficult. A complete data set should include three-dimensional velocity measurements, channel bathymetry, bed-material load, bed material samples, water-surface elevation, water-surface slope, water temperature, and discharge. Ideally, these data should be collected during the rising limb, at the peak, and during the recession limb of the flood hydrograph in the reaches upstream, at, and downstream from the bridge with increased detail around bridge piers and abutments. Although the methods for accurately measuring bed-material load are still lacking, recently introduced technology, improvements in existing technology, and application of instruments used in hydrographic surveying and oceanographic research have made the collection of the bathymetric and hydraulic data feasible. This paper will describe the equipment used to collect detailed scour data during floods and present examples of the data.

DATA COLLECTION EQUIPMENT AND TECHNIQUES

A system for making detailed scour measurements must be portable, operate reliably in the flood environment, and able to measure the required data with sufficient accuracy. Because the location and magnitude of floods are difficult to predict in advance, and the duration of floods on small streams is commonly short, scour measuring equipment must be of a size and weight to allow quick and easy transport by vehicle and overnight air freight. Once the equipment is on site, the time required to setup and begin data collection should be less than two hours, in order to minimize lost opportunities for collecting data. In addition, the equipment must be rugged to prevent damage during frequent transport and use in severe flood conditions. Because elevation and horizontal positioning are critical in understanding scour processes, the equipment must be able to measure these data to an acceptable degree of accuracy. The initial design accuracy for streambed elevation measurements and horizontal positioning was 15 cm. This goal was determined to be

unrealistic within the size, weight, and cost constraints of the project. However, accuracies of 30 cm for streambed elevation measurements and 60 cm for horizontal positioning have been achieved. Portable scour-measuring systems consist of the following four components: (1) the instrument(s) for making streambed elevation and water velocity measurements, (2) a deployment system, (3) a method to measure the horizontal position of the data collected, and (4) a data storage device.

Streambed Elevation Measurement: The distance from the water-surface to the streambed is commonly measured with an echo sounder. The accuracy of a streambed elevation measurement is dependent on the echo sounder and the stability of the deployment platform. Transducers are characterized by their frequency and beamwidth. Higher frequency signals (> 200 kHz) provide better resolution but poorer penetration of deep or sediment-laden waters (Landers and others, 1993). The acoustic footprint of the echo sounder is a function of the beamwidth of the transducer. A wide beamwidth (>8°) results in a large footprint and less accurate measurements of steep slopes or rapidly changing bottom. Peak value detection analyzes all reflected acoustic energy and computes the distance associated with the peak of the return signal. The peak value detection method is less sensitive to acoustic reflectors in the water column (sediment, fish, debris, etc.) and tends to measure to the approximate center of the acoustic footprint. The echo sounder selected uses a 3° beamwidth transducer operating at 200 kHz, digitizes the depth using peak value detection, and provides both RS-232 compatible digital output and an analog paper chart. The value of the analog paper chart was realized during data collection on the Mississippi River. The paper chart records the vertical location of all objects causing acoustic reflection, while the digital processing produces only a single value. Figure 1 shows a situation with the transducer near a bridge pier where the riverbed had scoured below the top of the footing. Portions of the acoustic signal reflected off the pedestal, footing, and seal of the pier before reflecting off the bed. The reflection off the pier was strong enough to cause the signal processor to digitize a depth shallower than the actual depth to the riverbed. Using only digital data, the actual depth and extent of the scour hole would not have been measured; however, the depth and extent of the scour hole are clearly shown on the paper chart. Therefore, it is important that the paper chart be used to verify the digital data and that any necessary corrections to the digital data are made.

Without vessel motion compensation, the accuracy of the riverbed elevation measurements is a function of the dynamic motion of the boat and slope of the water surface. Heave of the boat, the change in vertical position of the boat caused by wave action, causes rapid vertical change in the distance from the transducer to a known datum. In addition, pitch and roll of the boat moves the transducer out of its vertical orientation; therefore, the distance measured may not be a true vertical distance. The

instruments designed to measure vessel attitude accurately in dynamic conditions are very expensive and were beyond the financial constraints of this project. Therefore, streambed elevation is determined by assuming the transducer remains vertical and at fixed distance below the average water surface. Near the bridge, the water surface is assumed constant; and in the approach and exit reaches, the water-surface elevation is adjusted for the average water-surface slope in the area estimated from upstream and downstream gages and concurrent water-surface surveys. The estimated accuracy of the riverbed elevation data is about 30 cm.

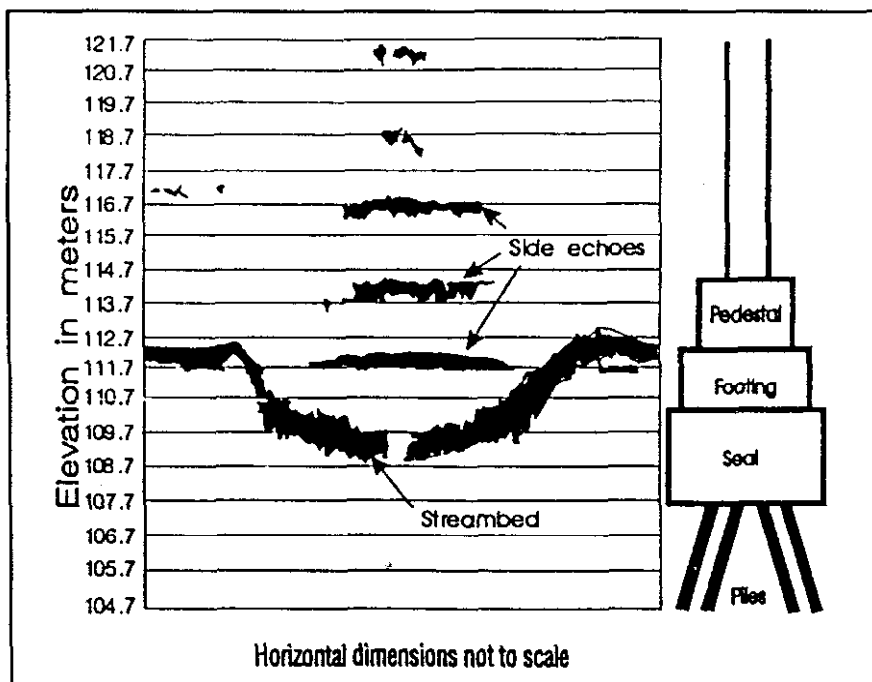


Figure 1. Example of side echoes from bridge pier.

Velocity Measurement: Traditional river velocity measurements made with horizontal or vertical axis meters contained only velocity magnitude. The inclusion of a flux gate compass in the weight deployed with the meters allows the horizontal direction of the velocity to be measured. However, these techniques measure only one point at a time and do not measure vertical velocities. Acoustic Doppler Current Profilers (ADCP) have been used for more than 10 years in the study of ocean currents and estuaries. The development of the Broadband Acoustic Doppler Current Profiler (BB-ADCP)¹ allows three-dimensional velocity profiles and discharge to be measured in rivers and canals with an acceptable accuracy.

The BB-ADCP measures velocity magnitude and direction by use of the Doppler shift associated with the reflection of acoustic waves off moving objects (acoustic reflectors). The BB-ADCP transmits pairs of short, phase-encoded acoustic pulses along four narrow beams (figure 2) at a known, fixed frequency (from 300-1,200 kHz for rivers). The reflected signal is discretized by time differences into individual segments representing specific depth cells within the water column. The time-lag change and difference in frequency (shift) between successive echoes are proportional to the relative velocity of the acoustic reflectors referenced to the BB-ADCP. This frequency shift is known as the Doppler effect. The BB-ADCP uses this technique to compute a water-velocity component along each beam. By use of trigonometric relations and the geometric arrangement of the beams, three-dimensional velocity vectors are computed for each depth cell. For the trigonometric relations to be valid, water velocities must be horizontally homogeneous in all four beams. Although, theoretically, only three beams are needed, the fourth beam provides a quality check of the measurement (RD Instruments, 1993).

To use the BB-ADCP on a moving boat, the speed and direction of the boat must be measured and used to correct the water velocity measured by the BB-ADCP. Under most conditions, the BB-ADCP measures its velocity by bottom-tracking. The BB-ADCP sends bottom-track acoustic pulses and analyzes the Doppler shift of the backscattered energy reflected from the streambed. If the streambed is stationary, this technique measures the velocity and direction of the boat accurately. However, if the streambed is actively transporting sediment, this technique may not accurately measure the speed and direction of the boat. Problems associated with sediment transport along the streambed have been frequently encountered during flood measurements. Sometimes use of a lower frequency BB-ADCP (using a 300-kHz instrument instead of a 1200-kHz instrument) will allow penetration through the mobile sediment and result in a stable bottom reference where a higher frequency instrument detects a moving bottom (Oberg and Mueller, 1994). During floods the accuracy of the bottom tracking should be verified by anchoring the boat in the main flow and checking the vessel speed determined by bottom tracking. An alternate method for measuring the boat speed and direction is to use real-time kinematic differential global positioning systems (DGPS), however, the accuracy of using DGPS as the velocity reference has not been defined.

The BB-ADCP's allowed very detailed velocity data to be collected in the approach and exit reaches and near the bridge. However, the BB-ADCP's cannot

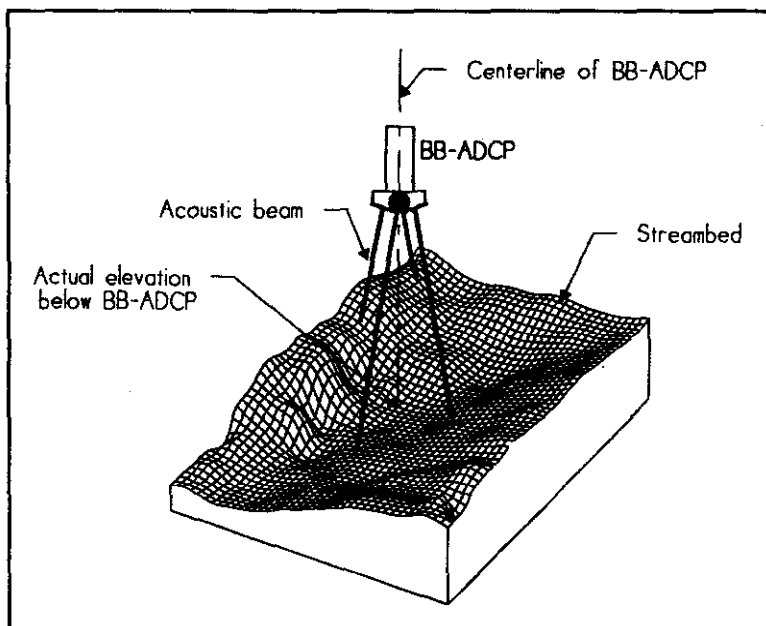


Figure 2. Illustration of acoustic beams and depths measured by Broadband Acoustic Doppler Current Profiler.

¹Any use of trade, product, or firm names is for descriptive purposes only and does not imply endorsement by the U.S. Government.

measure velocity in two locations that are very critical to scour — near and adjacent to the streambed and in the vortices at the bridge piers. Acoustic energy from the side lobes reflects off the streambed and interferes with the acoustic energy from the main beams reflecting off acoustic reflectors near the streambed. This interference prevents measurement of velocities in the lower 6 percent of the water column for BB-ADCPs commonly used in streams. The vortices near bridge piers are often smaller than the area bounded by the four acoustic beams. Therefore, the flow measured by one beam may not be continuous with flow measured by another beam. Although the instruments can compute the velocities parallel to the beams, they are unable to resolve the velocity vectors into horizontal and vertical components due to the lack of flow uniformity between the beams (Mueller and Landers, 1994).

Horizontal Positioning: The value of the streambed elevations and three-dimensional velocity profiles is dependent on knowing the horizontal position for each data point. Technology related to horizontal position determination has improved dramatically during the past several years. Previous technology developed for hydrographic surveying could not typically provide real-time position measurements with an accuracy of less than 1 m and often required time-consuming presurveying of setup locations. Current technology provides better than 1 m accuracy and fast setup with no presurveying requirements. Both a range-azimuth system and DGPS have been used to measure the horizontal position of the data collected.

Range-azimuth tracking systems are similar to total stations used for land surveying. The position of the target is determined by measuring the range using a laser and the corresponding azimuth and vertical angle with an electronic theodolite. Tracking systems can update readings every 0.5 second and the laser automatically resumes measuring the distance to the target even after the target is lost for a period of time. The tracking system must be setup in a location where the operator can manually track a target mounted on the boat. The system selected for this project has a distance accuracy of 0.1 m and a horizontal and vertical angle accuracy of 5 seconds. Although these numbers suggest accuracy in the order of 20 cm, in practice, keeping the instrument pointed directly at a moving target is difficult. During the data collection on the Mississippi River, it is believed that an accuracy of approximately 70 cm was achieved when tracking the target mounted on the moving survey vessel. On smaller streams accuracies better than 50 cm are typical.

Setup of the range-azimuth system is quick once a suitable location is identified. During floods, locations for instrument setup that provide an adequate view of the bridge, approach, or exit sections are often difficult to find, especially at sites with very wide flood plains and (or) dense vegetation. The power of the laser allows setup points to be referenced to the bridge quickly and often without the need of a prism. Many setups were referenced to the centerlines of several piers by pointing the instrument at the centerline of each pier and reflecting the laser directly off the concrete pier. Plotting of the pier and setup point locations showed that an accuracy of about 30 cm was achieved when using the instrument to survey setup points in the manner described.

Real-time, kinematic, DGPS used for positioning allows rapid collection of velocity and bathymetric data in the approach and exit reaches of the river. GPS measures the position of an antenna using triangulation from three or more satellites. Differential corrections from a GPS base station located over a known point are transmitted to the mobile GPS unit and used to obtain real-time positions with accuracies better than 1 m. Because DGPS requires no setups at the site and no personnel to track the boat, data can be collected very rapidly and over a much longer reach of river than is feasible with the range-azimuth tracking system. However, data collection near tree lines and bridges is hampered by loss of adequate satellite coverage caused by blockage of the sky by trees and bridge structure.

Deployment Platforms: Deployment of instruments from the water surface is necessary to obtain the spatial coverage required for detailed data sets. The use of manned boats during floods can be hazardous in many situations, particularly when there is insufficient clearance for the boat beneath the bridge. The clearance requirements for a manned boat severely limit data collection on smaller rivers where clearance under bridges is commonly less than 1.5 m during floods. Launching boats in a flood can be difficult because boat ramps are flooded and velocities can be high even near the shore. Flooded local streets with sufficient slope and the river side of levees are often used to launch a manned survey vessel. The support and cooperation of local citizens and government agencies are valuable in finding adequate launch facilities at all sites. The reliability and handling characteristics of the vessel are important for safety and are required when maneuvering the vessel near and around the bridge piers.



Figure 3. Photograph of remote-control boat.

The safety, launching, and clearance restrictions of a manned boat may be eliminated with a properly designed unmanned or remote-control boat. Development of unmanned vessels has been accomplished for other applications, although most of that effort has been on remotely operated vessels (ROVs) for oceanographic research. Two commercially available remote-control boats were evaluated but neither met the requirements and cost constraints of this application. Development of a remote-control boat specifically for collecting scour data around bridges was initiated in 1992 (Landers and others, 1993). The design goals for the remote-control boat were to minimize size and weight while maintaining stability and operability in a flood environment. Although the Small Waterplane Area, Twin-Hull (SWATH) design theoretically should provide a stable deployment platform (Landers and others, 1993), tests showed that the lack of active stabilization severely degraded the stability of the SWATH design. Subsequently, V-hull, twin-hull, and flat-bottom boats were tested to determine their suitability as deployment platforms. The flat-bottom boat provided the best stability, availability, durability, and ease of modification for deployment of instruments (figure 3).

The design of the engine and remote controls required a balance between power requirements, weight, and reliability. Electric motors, although preferred for their greater reliability, were not selected because they could not sustain the speeds needed to operate in floods without exceeding overall weight constraints. The boat is powered by an 8-horsepower gasoline outboard motor with a remotely controlled electric start. Modifications to the motor were minimized and consisted of removing the tiller and throttle assembly, the rope start and associated brackets. Radio control was achieved using standard off-the-shelf recreational remote-control radios and accessories. The radio receiver, voltage regulator, relays, and servos were mounted beneath the engine cover or on the transom mount allowing the engine to be used on any suitable boat. Risk of losing the boat due to loss of radio contact is a potential problem. Although a fail-safe anchor system is under development, current testing and use of the boat has been restricted to situations where a manned boat can be used to retrieve the remote-control boat in case of radio failure or where the remote-boat can be tethered with a nylon rope.

Data Recording: Detailed data sets consist primarily of digital data recorded on a field computer. Although survey information and observations are recorded in a notebook, the data collected using the instruments described is primarily digital. Typically, data measured by the instrument deployed on the boat (BB-ADCP or digital echo sounder) are

transmitted to the shore using data radios. These data are recorded on a field computer simultaneously with position data from the range-azimuth tracking system. When a manned boat is used with the range-azimuth positioning system, the data radios can transmit data from the positioning system on the shore to a field computer on the boat. If DGPS is used with a manned boat the position and depth are recorded by the field computer on the boat and no equipment on the shore is required. Modifications to the data radios by the manufacturer were made to allow the radios to communicate with the BB-ADCP, which requires bidirectional communication and a break to initiate communication. This method of data recording has been used successfully on both large and small streams and in extreme environmental conditions.

DISCUSSION OF DATA COLLECTED

The equipment and techniques described herein have been used successfully to collect detailed data on scour processes at bridges. This equipment was used with a manned boat on the Mississippi River in 1993, on the Brazos River near Lake Jackson, Texas in 1994, and on the Sacramento River near Hamilton City, California in 1995. The first detailed data sets were collected in 1993 at Interstate 255 over the Mississippi River near St. Louis and at State Route 51/150 over the Mississippi River at Chester, Illinois. The bathymetry mapping equipment worked very well and allowed detailed mapping of scour holes (figure 4). Collection of detailed bathymetric data to delineate the maximum depth and shape of local scour holes requires measurement of many cross sections and longitudinal sections to be measured. A highly skilled boat operator is required to collect these data near the pier. Problems were encountered with the 1200 kHz BB-ADCP due to sediment movement along the streambed. A 300-kHz BB-ADCP was successful at penetrating the moving sediment and was used to collect velocity data several times during the flood. A 300-kHz BB-ADCP was also used successfully at Farm-Market 2004 over the Brazos River near Lake Jackson, Texas to collect detailed velocity. This site represents a detailed study site with a significant debris accumulation on the pier in the main flow. A 1200 kHz BB-ADCP was used to measure both the channel bathymetry and velocity profiles at U.S. highway 32 over the Sacramento River near Hamilton City. Figure 5 shows a velocity profile collected downstream from the bridge.

The remote-control boat was first used to collect scour data during flooding in Missouri in May 1995. The remote-control boat allowed data to be collected on small streams with low bridges where use of a manned boat was not feasible. Use of the remote-control boat near piers was difficult due to the inability of the operator to visually resolve distances of less than 1 m from a distance of about 50 m. Data collection on small streams is more difficult than on larger streams due to the proximity of vegetation and the shallow depths in the flood plains. Although minor problems with the remote-control boat were identified, it proved to be an efficient and viable tool for data collection on small streams.

FUTURE DEVELOPMENTS

Advancements in technology have greatly improved our ability to collect detailed data and subsequent improvements will improve the accuracy and detail of scour measurements even more. The use of scanning or phased-array sonar allows a wide area of the stream bed to be surveyed rapidly and in greater detail than is possible with traditional echo sounders. These instruments require stable deployment platforms or vessel attitude compensation and can be very expensive. However, as the technology matures, scanning and phased-array sonar will likely become feasible for detailed scour measurements. The BB-ADCP measures the depth along each beam. With the development of postprocessing software, the BB-ADCP can be operated as a multi-transducer mapping systems, measuring four depths simultaneously. This technique was used on the Sacramento River but efficient software to process the data is still in development. Three-dimensional velocities in the vortices immediately adjacent to bridge piers and abutments may be measurable if acoustic correlation current profilers currently being used for oceanographic work can be adapted to work in depths typical of inland waterways. DGPS is a rapidly developing technology. The accuracy of DGPS has increased significantly during the last three years. Inertial navigation systems can be used for positioning during DGPS outages of 30-60 sec, such as when the survey vessel is under the bridge. This technology is commonly used on large ocean vessels but is too large, requires too much power, and is too expensive for use in scour data collection. The FHWA has funded a contract to develop a small lightweight system. This development could remove the problems associated with using a land based positioning system, such as the range-azimuth system. Development of these instruments will allow scour processes to be studied in the field at a level of detail that was previously only available in the laboratory.

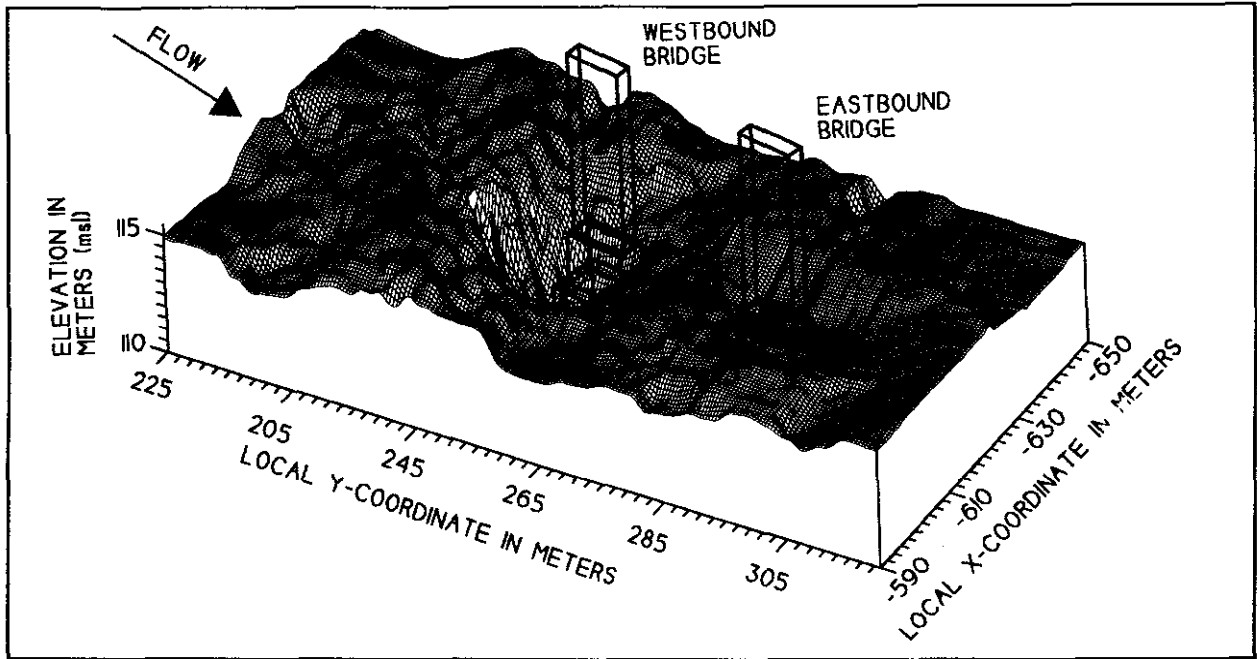


Figure 4. Three-dimensional mesh of streambed near pier eight of I-255 over the Mississippi River near St. Louis, Missouri.

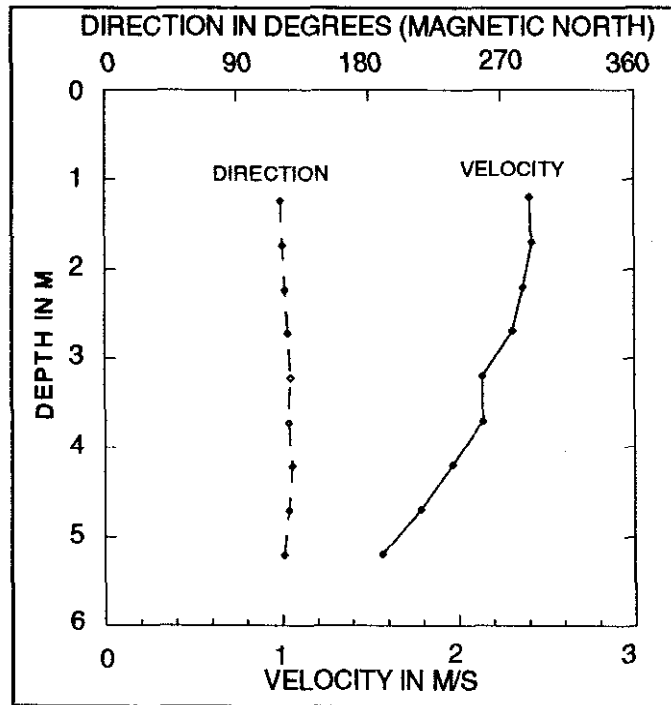


Figure 5. Velocity profile downstream from U.S. highway 32 over the Sacramento River near Hamilton City, California.

REFERENCES

- Oberg, K.A., and Mueller, D.S., 1994, Recent Applications of Acoustic Doppler Current Profilers. Fundamentals and Advancements in Hydraulic Measurements and Experimentation, Pugh, C.A., ed., American Society of Civil Engineers, New York, p. 341-350.
- Landers, M.N., and Mueller, D.S., in press, Channel Scour at Bridges in the United States. Federal Highway Administration Research Report.
- Landers, M.N., Mueller, D.S., and Trent, R.E., 1993, Instrumentation for Detailed Bridge-Scour Measurements. Hydraulic Engineering '93 — Proceedings of the 1993 Conference, Shen, H.W., Su, S.T., and Wen, Feng, eds., American Society of Civil Engineers, New York, p. 2063-2068.
- Mueller, D.S., and Landers, M.N., 1994, Real-Time Data Collection of Scour at Bridges. Fundamentals and Advancements in Hydraulic Measurements and Experimentation, Pugh, C.A., ed., American Society of Civil Engineers, New York, p. 104-113.
- Murillo, J.A., 1987, The Scourge of Scour. Civil Engineering, American Society of Civil Engineers, Vol. 57, No. 7, p. 66-69.
- RD Instruments, 1993, Direct-Reading Broadband Acoustic Doppler Current Profiler Technical Manual. RD Instruments, San Diego, Calif., 224 p.

SCOUR AT SELECTED BRIDGE PIERS IN MISSISSIPPI

by K. Van Wilson, Jr., Hydrologist, U.S. Geological Survey, Jackson, MS

INTRODUCTION

Exposure or undermining of bridge pier and bridge abutment foundations by the erosive action of flowing water, including tidal currents, can result in structural failure of a bridge. Bridge failure results in large capital expenditures for repair or replacement and may cause loss of life. Erosion (scour) of the ground in the vicinity of bridge piers and abutments during floods has resulted in more bridge failures than all other causes in recent history (Murillo, 1987). Many bridges in Mississippi are at risk of failure due to scour. The design and maintenance of bridge foundations require consideration of the maximum depth of scour that could occur during an extreme flood. Bridge pier and abutment foundations need to extend below the anticipated maximum scour depths to provide support for bridges if scour does occur.

The term "scour," as used here, is defined as the lowering of the ground by erosion below an assumed natural level or other appropriate datum. "Scour depth" is the depth to which material is removed below the stated datum. Scour is a natural phenomenon that is of primary concern in alluvial streams. However, scour can be a problem in any waterway having erodible bed materials. Scour around bridges can be the result of any one of, or combination of, three interrelated components.

- Local scour - erosion caused by local disturbances in the flow, such as vortices and eddies near piers, abutments, and debris piles.
- Constriction scour - erosion caused by increased flow velocities through a bridge opening due to the decreased flow area formed by the bridge, the approach embankments, the piers, and any debris piles.
- General scour - progressive degradation caused by natural processes or by changes in channel controls that occur over a long channel reach and, possibly, over many years. General scour could be part of a temporary fluctuation about some mean bed level. This is the scour that occurs in a channel even if no bridge is present.

Although these components of scour are not completely independent, general practice in bridge design is to estimate each component of scour separately and to combine the predicted scour depths to estimate the total scour depth at a bridge site.

Many empirical equations have been developed to compute local scour and constriction scour at bridges. These equations can provide a large range of scour depths for the same set of conditions. Most of the equations are based on scale-model laboratory experiments and have not been field verified due to the lack of onsite high-flow data. Bridge designers and bridge inspectors need more onsite high-flow data to validate computed scour depths for the varying conditions that occur in Mississippi and throughout the United States.

Adequate definition of potential scour at bridge sites is essential to proper bridge design, construction, and maintenance. Accurate estimates of scour depths for varying conditions are a prerequisite for safe, cost-effective bridge design. Underestimating scour depths puts bridges and human life at risk. Overestimating scour depths results in overdesign, which translates into an economic loss in the form of higher construction costs. Collection of onsite scour data is recognized as one way, and perhaps the only convincing way, to improve bridge design procedures (Highway Research Board, 1970; Hopkins and others, 1980; Jones, 1984; Laursen, 1984; Murillo, 1987).

The U.S. Geological Survey (USGS), in cooperation with the Mississippi Department of Transportation (MDOT), began a study of bridge scour in Mississippi in 1989. The objectives of this study were to: (1) perform onsite high-flow scour measurements at selected bridge sites, (2) evaluate the usefulness of available scour equations for estimating local pier scour, (3) develop a scour-prediction equation that could be used to better estimate local pier scour for Mississippi streams, and (4) analyze available discharge measurement soundings for an indication of total scour.

Purpose and Scope

This paper briefly summarizes pier-scour data collected during 1942-94 at 22 selected bridge sites in Mississippi (fig. 1). These data and additional bridge-scour data collected during 1938-94 are described in more detail by Wilson (1995). The methods used to measure scour and selected characteristics at each site are described. Selected hydraulic and bridge-geometry characteristics are presented. An envelope-curve equation for the Mississippi pier-scour data was developed by relating measured pier-scour depth divided by normal pier width to measured approach-flow depth divided by normal pier width. The measured pier-scour depths were compared to the envelope curve and to the pier-scour prediction equation recommended in the Federal Highway Administration (FHWA) Hydraulic Engineering Circular No. 18 (HEC-18) by Richardson and others (1993).

Methods of Study

The scour data-collection sites presented in this paper were selected from a list of sites known by the MDOT to be susceptible to scour. Data were also obtained at a few additional sites if, during the study, high flow occurred at a site, and the USGS and the MDOT considered the data useful for bridge maintenance. Scour data were collected as near the peak discharge as possible. If the high flow was of sufficient duration, additional measurements were obtained during the rising and falling limbs of the flood hydrograph.

Measurements of water depth and velocity to determine discharge were obtained using standard streamflow-gaging procedures as described by Rantz and others (1982). Depth, vertical position, and velocity were measured by suspending a 100-, 150-, or 200-pound Columbus-type sounding weight and Price AA-type current meter in the water.

Soundings to the channel bed to measure channel geometry were obtained either by sounding with a weight or with an Eagle Model Mach 1 Graph (the use of trade of product names in this report is for identification purposes only and does not constitute endorsement by the USGS) recording fathometer. Transducers used with the fathometer produced an 8-degree beam width, allowing close access to bridge piers without creating echoes off the sides of the pier. Use of the fathometer made soundings possible at a large number of points across a cross section. During high flows, the transducer was attached to the bottom of the sounding weight, which was lowered into the water from a truck-mounted boom and winch assembly and was then towed through the water as the truck was driven across the bridge at a slow, nearly constant speed. Where piers were inset from the upstream side of the bridge, a flotation device was used to allow the flow to drag the transducer close to the upstream side of the pier. During low to medium flows, the transducer was attached at or near the bow of a boat, which traversed the cross section or longitudinal profile.

Bed samples were collected to characterize the streambed composition. They were collected primarily during low-flow conditions and are assumed to be representative of high-flow conditions. Sites generally were sampled at three cross sections through a channel reach of at least one bridge length upstream of the site. For some sites, bed-sample information was obtained from MDOT soils reports or from nearby sampled sites on the same stream, where bed conditions were considered to be similar.

Description of Bridge-Scour Sites

Scour data presented in this paper were collected at 22 selected bridge sites in Mississippi (fig. 1). The drainage area of the bridge-scour sites ranged from 60.8 to 5,720 mi², and the slope in the vicinity of each site ranged from 0.00011 to 0.00163 ft/ft. The bed material at most sites consisted of sand or gravel. In some cases, the sand or gravel was underlain by a clay stratum, which was thought to affect the measured scour depths.

PIER-SCOUR DATA

Measurements of pier-scour depths obtained during this study by fathometer and sounding weight were combined with soundings from concurrent and historical discharge measurements, which had soundings near the bridge piers. This information provided an approximation of pier-scour depth for 190 pier-scour measurements at 21 of the 22

sites. Of the 121 pier-scour measurements obtained since 1990, 112 were obtained with a fathometer, and 9 were obtained with a sounding weight. Of the 69 pier-scour measurements obtained prior to 1990, all but 5 were determined from selected discharge measurements. Three of the five were pier-scour measurements obtained in 1989 at site 21, where upstream and downstream sides of the bridge were sounded. The remaining two pier-scour measurements were obtained in 1972 and 1973 by a scour-monitoring device installed at site 17 by Hopkins and others (1975, 1980) for the FHWA.

Both upstream and downstream sides of the bridge were usually sounded with the fathometer. The upstream and downstream pier-scour depths were compared for each pier, and the maximum pier-scour depth was used in this paper. By contrast, the pier-scour depths taken from the discharge measurements were limited to one side of the bridge and were not solely obtained on the downstream side of the bridge. The pier-scour depths were determined using an approximation of concurrent ambient bed level as described by Blodgett (1989) and Landers and Mueller (1993). Concurrent ambient bed level is representative of the typical bed elevation adjacent to the scour hole at the time of the measurement. Therefore, it is the elevation representing the streambed at the pier location without any pier scour. Each pier-scour measurement was assigned an approximate accuracy based on measuring conditions at a site. Assigned accuracy ranged from 0.5 ft for a fathometer for favorable conditions to 3 ft for a sounding weight under less favorable conditions. Measurement accuracy was adversely affected by sounding weight drift due to flow, turbulence of the flow, presence of debris piles, and the determination of concurrent ambient bed level.

With inclusion of the selected historical discharge measurements, the recurrence intervals of the measured discharges ranged from less than 2 to about 500 years. Recurrence intervals of the measured discharges were determined using procedures and information described by Landers and Wilson (1991) and Wilson and Landers (1991).

The majority of the pier-scour data presented in this paper have been entered in the National Bridge Scour Data Management System (BSDMS). The BSDMS is being developed by the USGS in cooperation with the FHWA to support preparation, compilation, and analysis of bridge-scour measurement data, and the primary functions of the BSDMS are data archival and retrieval (Landers, 1992).

Pier-scour data were collected during high flows at selected bridge sites in Mississippi representing various hydraulic, bed-material and pier-geometry characteristics. Measured pier-scour depths (Y_s) ranged from 0.6 to 20.4 ft. Scour-hole top width, where determined, ranged from 8 to 180 ft. Approach-flow depth (Y_1) ranged from 2.3 to 36.6 ft, approach-flow velocity (V_1) ranged from 1.3 to 10.4 ft/s, and approach-flow skew ranged from 0 to 46 degrees. Median bed-material size (D_{50}) ranged from 0.00092 to 0.02464 ft, and the geometric standard deviation of the bed-material sizes or the gradation coefficient

$$\sigma_g = \sqrt{\frac{D_{84}}{D_{16}}} \quad (1)$$

ranged from 1.3 to 8.3. In this equation, D_{84} is bed-material size where 84 percent is finer, and D_{16} is bed-material size where 16 percent is finer. If σ_g is equal to 1, the material is considered uniform in size, and as σ_g increases, the material is less uniform.

The pier geometry was determined from field observations and MDOT bridge plans. The pier type was classified as either a single or a group. A single refers to one pier or column supporting the entire bridge width; whereas, a group refers to spaced columns or piles. The pier shape refers to the upstream part of the pier and was classified as either cylinder, round, square, or sharp. The pier width (a) and the pier length (L) are depth-weighted averages for each respective measurement. The normal pier width (a') is the pier width adjusted for skew. If skew is zero, then a is equal to a' ; otherwise, a' will be larger than a , depending on the degree of skew. For the approach flow skews ranging from 0 to 46 degrees, measured a and a' ranged from 1.3 to 23 ft and 1.8 to 23 ft, respectively.

PIER-SCOUR DATA ANALYSIS

Jones (1984) compared many pier-scour equations by plotting measured pier-scour depth divided by pier width (Y_s/a) with approach depth divided by pier width (Y_1/a) for various Froude numbers. However, in this paper, pier-scour

depth (Y_s) was divided by normal pier width (a'). Only 12 (6 percent) of the 190 measurements are plotted above $Y_s/a' = 1.1$ (fig. 2). The envelope-curve equation developed for these data (fig. 2) is:

$$\frac{Y_s}{a'} = 0.9 \left(\frac{Y_1}{a'} \right)^{0.4} \quad (2)$$

where

- Y_s is pier-scour depth, in feet;
- a' is normal pier width, in feet; and
- Y_1 is approach flow depth, in feet.

Measurement 179 at site 22 was the only measurement that plotted significantly above the envelope curve (fig. 2). Measurement 179 was affected by a jetty and stream bank deflecting flow toward the pier and possibly debris, which was not noted during the measurement. Using techniques described by Lagasse and others (1991) for estimating scour off the downstream end of the jetty, the jetty could have caused about 9 ft of scour off its downstream end, suggesting some of the measured pier scour could have been caused by the jetty. Equation 2 predicts 14.2 ft of pier scour, which is 6.2 ft less than the measured pier scour of 20.4 ft, suggesting about 6 ft of scour not caused by the pier.

Pier-scour depths predicted by the pier-scour equation currently (1995) recommended by FHWA in HEC-18 (Richardson and others, 1993) and by equation 2 were compared to measured pier-scour depths, which ranged from 0.6 to 20.4 ft. The HEC-18 equation predicted pier-scour depths ranging from 3.9 to 25.7 ft with residuals (measured pier scour minus predicted pier scour) ranging from -21.7 to 0.2 ft. Equation 2 predicted pier-scour depths ranging from 2.2 to 19.7 ft with residuals ranging from -16.8 to 6.2 ft. The residual of 6.2 ft was for measurement 179, where some of the measured pier scour could have been caused by a jetty and stream bank, as previously described. Excluding measurement 179, residuals ranged from -16.8 to 0.5 ft. Equation 2 could be used for reasonable verifications of the HEC-18 pier-scour predictions, which are currently required in the design and maintenance of bridges in Mississippi.

Measured pier-scour depths have been shown not to exceed a certain multiple of the pier width. F.M. Chang noted that there were no pier-scour depths greater than 2.3 times the pier width for all the pier-scour data he studied (Richardson and others, 1993). Melville and Sutherland (1988) reported from laboratory data there were no pier-scour depths greater than 2.4 times the pier width for cylindrical piers. All of the Mississippi pier-scour depths were within 2.3 times the normal pier width, which agreed with previous research (fig. 3). Measured pier-scour depths were as much as 2.24 times a normal pier width of 3.3 ft. However, for normal pier widths greater than about 4 ft, measured pier-scour depths were significantly less than 2.3 times the normal pier width (fig. 3).

SUMMARY

This paper briefly summarizes pier-scour data collected during 1942-94 at 22 selected bridge sites in Mississippi. The drainage area of the bridge-scour sites ranged from 60.8 to 5,720 mi². At most sites, the bed material consisted of sand or gravel, and in some cases, the sand or gravel was underlain by a clay stratum, which is thought to affect the measured scour depths. Recurrence intervals of measured discharges ranged from less than 2 to about 500 years.

Pier-scour data were collected during high flows at sites representing various hydraulic, bed-material, and pier-geometry characteristics. Measured pier-scour depth ranged from 0.6 to 20.4 ft, with scour-hole top width, when determined, ranging from 8 to 180 ft. Approach-flow depth ranged from 2.3 to 36.6 ft, approach-flow velocity ranged from 1.3 to 10.4 ft/s, and approach-flow skew ranged from 0 to 46 degrees. Median bed-material size ranged from 0.00092 to 0.02464 ft, and the geometric standard deviation of the bed-material sizes or the gradation coefficient ranged from 1.3 to 8.3. Only 12 (6 percent) of the 190 pier-scour depths were greater than 1.1 times the normal pier width. An envelope-curve equation for the Mississippi pier-scour data was developed by relating pier-scour depth divided by normal pier width to approach-flow depth divided by normal pier width.

All of the Mississippi pier-scour depths were within 2.3 times the normal pier width, which agreed with previous research. Measured pier-scour depths were as much as 2.24 times a normal pier width of 3.3 ft. However, for pier

widths greater than about 4 ft, measured pier-scour depths were significantly less than 2.3 times the normal pier width.

Pier-scour depths predicted by the pier-scour equation currently (1995) recommended in the Federal Highway Administration Hydraulic Engineering Circular No. 18 (HEC-18) and by the envelope-curve equation developed for Mississippi pier-scour data during this study were compared to measured pier-scour depths. The HEC-18 equation predicted pier-scour depths ranging from 3.9 to 25.7 ft with residuals (measured pier-scour depth minus predicted pier-scour depth) ranging from -21.7 to 0.2 ft. The envelope-curve equation developed during this study predicted pier-scour depths ranging from 2.2 to 19.7 ft with residuals ranging from -16.8 to 6.2 ft. The residual of 6.2 ft for the envelope-curve equation developed during this study was at a site where some of the measured pier scour could have been caused by a jetty and stream bank. Excluding this measurement, residuals ranged from -16.8 to 0.5 ft. The envelope-curve equation predictions could be used for reasonable verifications of the HEC-18 pier-scour predictions, which currently are required in the design and maintenance of bridges in Mississippi.

REFERENCES

- Blodgett, J.C., 1989, Monitoring scour at the State Route 32 bridge across the Sacramento River at Hamilton City, California: Proceedings of the Bridge Scour Symposium, October 17-19, 1989, Federal Highway Administration Report No. FHWA-RD-90-035, p. 211-226.
- Highway Research Board, 1970, Scour at bridge waterways: Synthesis of Highway Practice 5, National Cooperative Research Program, 37 p.
- Hopkins, G.R., Vance, R.W., and Kasraie, B., 1975, Scour around bridge piers: Federal Highway Administration Report No. FHWA-RD-75-56, 205 p.
- 1980, Scour around bridge piers, Federal Highway Administration Report No. FHWA-RD-79-103, 141 p.
- Jones, J.S., 1984, Comparison of prediction equations for bridge pier and abutment scour: Transportation Research Record 950, p. 202-208.
- Lagasse, P.F., Schall, J.D., Johnson, F., Richardson, E.V., Richardson, J.R., and Chang, F., 1991, Stream stability at highway structures: Federal Highway Administration Hydraulic Engineering Circular No.20 (HEC-20), Publication No. FHWA-IP-90-014, February 1991, 195 p.
- Laursen, E.M., 1984, Assessing vulnerability of bridges to floods: Transportation Research Record 950, p. 222-229.
- Landers, M.N., 1992, Bridge scour data management: Proceedings of Environmental Engineering Sessions Water Forum, American Society of Civil Engineers, 1992, p. 1094-1099.
- Landers, M.N., and Mueller, D.S., 1993, Reference surfaces for bridge scour depths: Proceedings of the 1993 National Conference on Hydraulic Engineering, American Society of Civil Engineers, v. 2, p. 2075-2080.
- Landers, M.N., and Wilson, K.V., Jr., 1991, Flood characteristics of Mississippi streams: U.S. Geological Survey Water-Resources Investigations Report 91-4037, 82 p.
- Melville, B.W., and Sutherland, A.J., 1988, Design method for local scour at bridge piers: Journal of Hydraulic Engineering, American Society of Civil Engineers, v. 114, no. 10, p. 1210-1226.
- Murillo, J.A., 1987, The scourge of scour: Civil Engineering, v. 57, no. 7, p. 66-69.
- Rantz, S.E., and others, 1982, Measurement and computation of streamflow--v. 1, Measurement of stage and discharge: U.S. Geological Survey Water-Supply Paper 2175, 284 p.
- Richardson, E.V., Harrison, L.J., Richardson, J.R., and Davis, S.R., 1993, Evaluating scour at bridges: Federal Highway Administration Hydraulic Engineering Circular No. 18 (HEC-18), Publication No. FHWA-IP-90-017, 132 p.
- Wilson, K.V., Jr., and Landers, M.N., 1991, Annual peak stages and discharges for streamflow-gaging stations in Mississippi: U.S. Geological Survey Water-Resources Investigations Report 91-4098, 705 p.
- Wilson, K.V., Jr., 1995, Scour at selected bridge sites in Mississippi: U.S. Geological Survey Water-Resources Investigations Report 94-4241, 44 p.

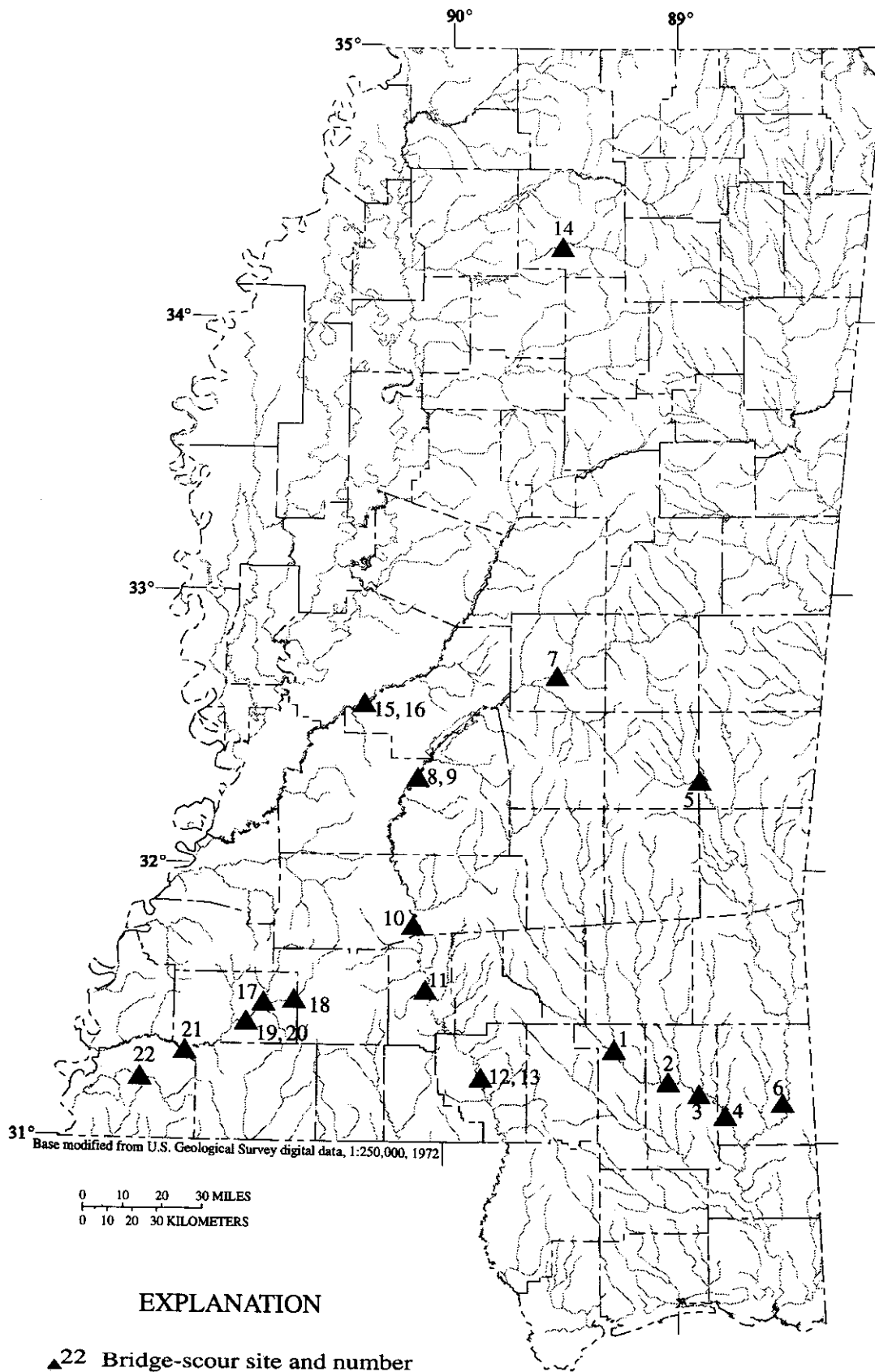


Figure 1. Location of bridge-scour sites in Mississippi.

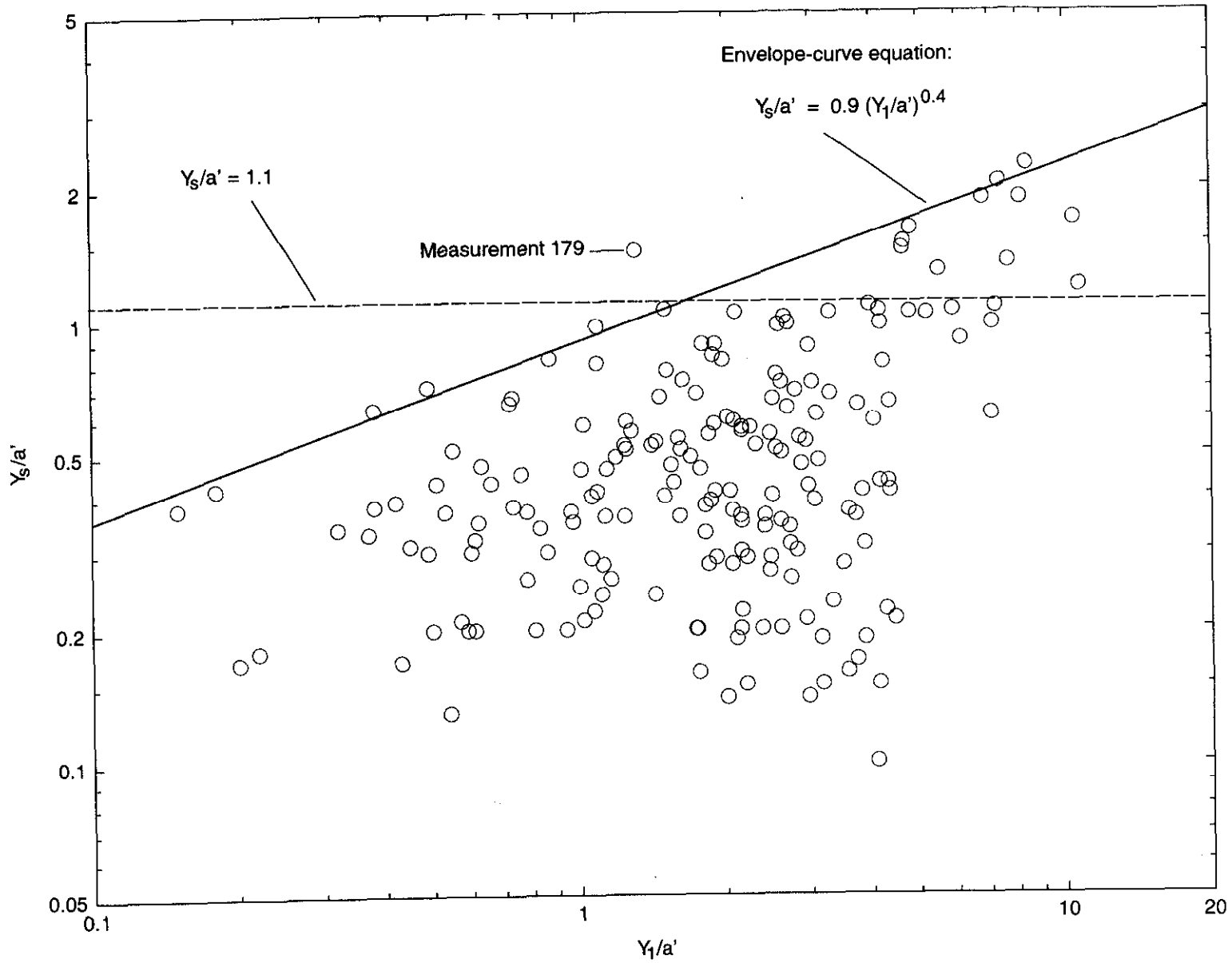


Figure 2. Relation between measured pier-scour depth divided by normal pier width (Y_s/a') and measured approach-flow depth divided by normal pier width (Y_1/a') for selected bridge sites in Mississippi.

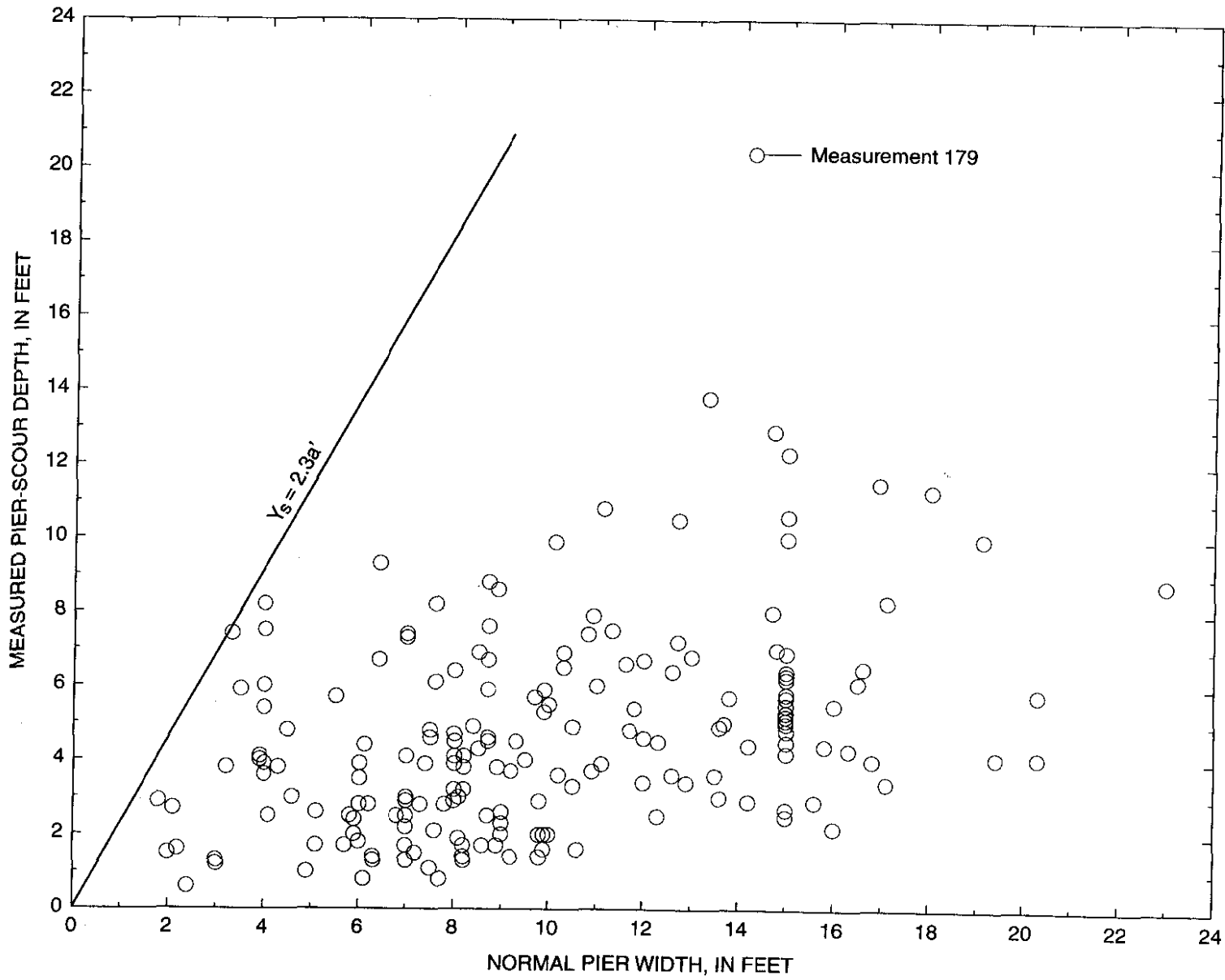


Figure 3. Relation between measured pier-scour depth (Y_s) and normal pier width (a') for selected bridge sites in Mississippi.

MODELING ALLUVIAL-RIVER EVOLUTION BY CHARACTERISTICS METHOD

By Keh-Chia Yeh, Assoc. Prof., Dept. of Civil Engrg., Nat'l Chiao Tung Univ., Hsinchu, Taiwan, R.O.C.; Wen-Lin Chen and Chen-Hua Chen, Res. Asst., Dept. of Civil Engrg., Nat'l Chiao Tung Univ., Hsinchu, Taiwan, R.O.C.; Chian-Min Wu, Chairman, Water Resour. Planning Comm., Ministry of Econ. Affairs, Taiwan, R.O.C.

Abstract: This paper extends a numerical model proposed by Yeh et al. (1995), based on a multimode characteristics method for fully coupled simulations of water and sediment movement in mobile-bed alluvial channels with non-uniform bed materials. After some modifications of the model, it was applied to simulate the bed evolution of a lower segment of the Tseng-Wen River in Taiwan during the period of 1973 - 1990. Simulated results shows that the bed variation can be reasonably predicted, whereas the observed median particle size of the bed is much finer than the computed.

INTRODUCTION

Natural river with mobile boundary constantly changes its geometry, in the form of deposition or scouring, during the passage of water flows. This phenomenon is resulted from the unequal sediment transport rate at each cross-section of the river due to the variation of flow velocity, depth, and composition of bed material at each cross-section. To predict the alluvial-channel bed evolution, one can resort to physical or numerical modeling. In general, the former is time-consuming and expensive, and the latter, on the other hand, is economical in time and money. Hence, the pursuit or further improvement of numerical techniques to simulate river-bed evolution still receives significant attention by researchers and practicing engineers.

The method of characteristics (MOC), among the existing numerical techniques, was originally developed for calculating the water-wave celerities associated with pipe flows or flows with the free surface. If the problem under consideration is simple enough, the analytical solution can be obtained using the MOC. Later on, the MOC was extended to solve the problem of alluvial mobile-bed evolution in that added to a wave celerity related to the bed deformation for uniform sand is the other two water-wave celerities (e.g., de Vriend, 1973; Wu, 1973). Because of the large difference in magnitude between the bed-deformation celerity and the two water-wave celerities, Lai (1991) proposed a so-called multimode MOC model to increase the numerical accuracy by allowing the characteristics curve associated with the disturbance of bed deformation to reach back several time steps from the current time step.

Knowing the fact that natural rivers are composed of non-uniform sediment and the previous three-characteristics MOC model for solving the uniform-sediment bed evolution has its limited practical value, Yeh et al. (1995) proposed a NMMOC model being able to account for the case of river bed composed of non-uniform sediment. In the model, several assumptions were made to allow the problem tractable and to reveal some meaningful insight of the problem in a more direct way. These assumptions include: prismatic channel with rectangular shape, no buffer reach at the upstream end of the channel, constant mixing-layer thickness, no armoring effect, and no spatial-delay effect due to non-equilibrium sediment transport. In this paper, the first two assumptions were removed to consider an alluvial river having arbitrary boundary geometry and the bed material composition at the upstream end of the river being changeable due to different sediment transport rates at that section at different times. The modified model then was applied to simulate the bed evolution in the downstream reach of the Tseng-Wen River, located in the southern Taiwan.

GOVERNING EQUATIONS

Given the assumptions of (a) constant mixing-layer thickness in the bed, (b) no armoring phenomenon during persistent degradation, and (c) no spatial-delay effect of non-equilibrium sediment transport rate, the governing one-dimensional unsteady equations for sediment-laden flow in a non-uniform-sediment alluvial channel, without lateral inflows, can be written as

$$\frac{\partial z}{\partial t} + \frac{\partial h}{\partial t} + u \frac{\partial h}{\partial x} + \frac{A}{B} \frac{\partial u}{\partial x} + \frac{u}{B} \frac{\partial A}{\partial x} \Big|_h = 0 \quad (1)$$

$$\frac{\partial u}{\partial t} + u \frac{\partial u}{\partial x} + g \frac{\partial h}{\partial x} + g \frac{\partial z}{\partial x} = -gS_f \quad (2)$$

$$\frac{\partial z}{\partial t} + \frac{1}{(1-p_r)B} \frac{\partial(q_s B)}{\partial x} = 0 \quad (3)$$

$$\frac{\partial P_{bi}}{\partial t} = -\frac{1}{a(1-p_r)B} \left[\frac{\partial(q_{si} B)}{\partial x} - F_b \frac{\partial(q_s B)}{\partial x} \right] \quad i = 1, \dots, N \quad (4)$$

where z = bed elevation; h = flow depth; t = time; x = distance; u = flow velocity; A = flow area; B = channel width; $\partial A/\partial x|_h$ = the rate of change of A with respect to x when h is held constant; g = gravitational acceleration; S_f = friction slope; p_r = sediment porosity; q_s = sediment discharge in volume per unit width; P_{bi} = fraction of sediment in the i -th size range, d_{si} , in the active layer; q_{si} = sediment discharge of i -th size range per unit width; a = thickness of mixing layer; $F_b = P_{bi}$ in case of bed aggradation; $F_b = P_{bio}$ in case of bed degradation with P_{bio} = fraction of sediment in the i -th size range of the parent bed; and N = number of different particle sizes. Sediment transport relation in Eq. (4) can be stated as

$$q_s = \sum_{i=1}^N q_{si} = \sum_{i=1}^N P_{bi} f_i(u, h, d_{si}, \dots) \quad (5)$$

where f_i denotes transport capacity of d_{si} , which is a function of flow intensity and sediment properties. In this study, Engelund-Hansen formula is adopted. Note that Engelund-Hansen formula is used for calculating the total bed material load using the median particle size, d_{50} , as the representative sediment size. To obtain the respective sediment discharge of each particle size d_{si} , Engelund-Hansen formula is used to calculate the sediment discharge capacity f_i by replacing d_{50} with d_{si} . A correction factor then is required to let the sum of the sediment discharge rates for each particle be the same as the sediment discharge rate computed by using d_{50} .

TRANSFORMATION OF GOVERNING EQUATIONS

Using the notations $z_t = \partial z/\partial t$, $u_x = \partial u/\partial x$, ..., $P_{bit} = \partial P_{bi}/\partial t$, etc., Eqs. (1) - (4) can be expressed as

$$J_i = P_{bit} + f_i P_{bix} - \delta_i \sum_{j=1}^N f_j P_{bjx} + \bar{\psi}_i h_x + \bar{\omega}_i u_x + \gamma_i = 0 \quad i = 1, \dots, N \quad (6)$$

$$J_{N+1} = z_t + h_t + u h_x + \frac{A}{B} u_x + \alpha = 0 \quad (7)$$

$$J_{N+2} = u_t + u u_x + g h_x + g S_f = 0 \quad (8)$$

$$J_{N+3} = z_t + a \sum_{j=1}^N f_j P_{bjx} + \frac{1}{p'} \psi h_x + \frac{1}{p'} \omega u_x + \beta = 0 \quad (9)$$

where $\psi = \partial q_s / \partial h$; $\omega = \partial q_s / \partial u$; $\psi_i = \partial q_{si} / \partial h$; $\omega_i = \partial q_{si} / \partial u$; $p' = 1 - p_r$; $f_j = f_j / (ap')$; $\delta_i = F_b / (ap')$; $\bar{\psi}_i = (\psi_i - F_b \psi) / (ap')$; $\bar{\omega}_i = (\omega_i - F_b \omega) / (ap')$; $\gamma_i = (q_{si} - F_b q_s) B_x / (ap' B)$; $\alpha = u / B (\partial A / \partial x) |_h$; and $\beta = q_s B_x / (p' B)$.

Combining Eqs. (6) - (9) linearly with the constants a_1, \dots, a_{N+3} yields

$$JS = a_1 J_1 + \dots + a_N J_N + a_{N+1} J_{N+1} + a_{N+2} J_{N+2} + a_{N+3} J_{N+3} = 0 \quad (10)$$

After collecting related terms, Eq. (10) reduces to

$$JS = a_1 \frac{DP_{b1}}{Dt} + \dots + a_N \frac{DP_{bN}}{Dt} + a_{N+1} \frac{Dh}{Dt} + a_{N+2} \frac{Du}{Dt} + (a_{N+1} + a_{N+3}) \frac{Dz}{Dt} + G = 0 \quad (11)$$

where the total derivative $D()/Dt = \partial()/\partial t + [\partial()/\partial x] dx/dt$, represents the differentiation in a given characteristic direction under the condition

$$\begin{aligned} \lambda = \frac{dx}{dt} &= \frac{a_{N+3} f_i' a + a_i f_i' - f_i \sum_{j=1}^N a_j \delta_j}{a_i} & i = 1, \dots, N \\ &= \frac{\sum_{j=1}^N a_j \bar{\psi}_j + a_{N+1} u + a_{N+2} g + a_{N+3} \frac{\psi}{p'}}{a_{N+1}} \\ &= \frac{\sum_{j=1}^N a_j \bar{\omega}_j + a_{N+1} \frac{A}{B} + a_{N+2} u + a_{N+3} \frac{\omega}{p'}}{a_{N+2}} \\ &= \frac{a_{N+2} g}{a_{N+1} + a_{N+3}} \end{aligned} \quad (12)$$

with $\lambda =$ characteristic value or eigenvalue; and

$$G = a_1 \gamma_1 + \dots + a_N \gamma_N + a_{N+1} \alpha + a_{N+2} g S_f + a_{N+3} \beta \quad (13)$$

Eqs. (12) and (11) are the characteristic and the compatibility equations corresponding to the original partial differential equations. Rearranging Eq. (12) yields a homogeneous system of $(N+3)$ linear equations. By the row operation, the problem of solving the system of equations reduces to a problem of finding eigenvalues. According to Cramer's theorem, it has a nontrivial solution of unknown column vector $[a_1, \dots, a_{N+3}]^T$ (called eigenvector) if and only if the

corresponding determinant of the coefficient matrix is zero. This leads to a polynomial of (N+3)th degree in eigenvalue λ . Hence, the (N+3) eigenvalues can be obtained from the polynomial. From the definition in Eq. (12), the eigenvalues represent the celerities of the (N+3) waves associated with water and solid particle disturbances in a channel. Given the eigenvalues, integration of Eq. (12) yields (N+3) trajectories of disturbances associated with water and sediment. These trajectories are called the characteristics. Two of the (N+3) characteristics are related to water-surface disturbances, and the remaining characteristics correspond to disturbances of bed deformation and composition variation in the mixing layer.

ALGORITHM OF NMMOC MODEL

Consider an x-t rectangular grid system in a plane, whose time intervals Δt are set equal, and distance intervals Δx_j are not necessarily equal (Fig. 1). At any interior grid point p at (x_j, t_{k+1}) , there are (N+3) characteristic curves passing through it. To solve for the (N+3) unknown variables, i.e., $P_{b1}, P_{b2}, \dots, P_{bN}, h, u,$ and z , at point p, Eqs. (11) and (12) are discretized as

$$x_p - x_i = \lambda_{ip}(t_p - t_i) \quad i = 1, \dots, N+3 \quad (14)$$

$$a_{1,ip}(P_{b1p} - P_{b1i}) + \dots + a_{N,ip}(P_{bNp} - P_{bNi}) + a_{N+1,ip}(h_p - h_i) + a_{N+2,ip}(u_p - u_i) \\ + (a_{N+1,ip} + a_{N+3,ip})(z_p - z_i) + G_{ip}(t_p - t_i) = 0 \quad i = 1, \dots, N+3 \quad (15)$$

where single or triple subscript = a grid or interception point; and double subscript = a curve segment of a given characteristic. Let ϕ_{ip} be a general representation of quantities $\lambda_{ip}, a_{1,ip}, \dots, a_{N+3,ip}$, and G_{ip} , which are functions of (N+3) variables at points p and i. Then ϕ_{ip} can be approximated as follows:

$$\phi_{ip} = \theta \phi_i + (1 - \theta) \phi_p \quad (16)$$

where θ is the weighting factor, which can be determined if λ_{ip} is known (see Fig. 1). Substituting Eq. (16) into Eq. (15) yields

$$F_i(\phi_{j-1}^{k+1}, \phi_j^{k+1}, \phi_{j+1}^{k+1}) = 0 \quad i = 1, \dots, N+3 \quad (17)$$

Besides the requirement of the initial steady-state condition for the entire domain, boundary conditions, which are related to characteristics or eigenvalues, are also needed in the model. One characteristic (upstream propagating water-surface disturbance wave) and (N+2) characteristics (one for the downstream propagating water-surface disturbance wave and the rest for the bed deformation and fraction variation waves) at upstream and downstream boundaries, respectively, are available for the subcritical flow condition. Therefore, (N+3) boundary conditions are required to solve the problem under the subcritical flow condition. The required boundary conditions can be stated as

$$F_i(\phi_b^{k+1}) = 0 \quad i = 1, \dots, N+3 \quad (18)$$

where the subscript "b" denotes upstream or downstream boundary of a channel. It is usually difficult to have the data on the temporal variation of bed elevation, $z(t)$, at the upstream boundary of the channel. Instead, the sediment discharge, $Q_s(t)$, is used to estimate $z(t)$ at the upstream end. To avoid the calculated $z(t)$ being affected by the choice of Δx , the concept of buffer reach (Cunge et al., 1980) was adopted. The sediment continuity equation for the buffer reach is

$$[\theta_B (\bar{Q}_s^{k+1} - Q_s^{k+1}) + (1 - \theta_B)(\bar{Q}_s^k - Q_s^k)] \Delta t = \phi \Delta x (1 - p) B (z_B^{k+1} - z_B^k) \quad (19)$$

where θ_B = weighting factor; \bar{Q}_s^k, Q_s^k = upstream imposed inflow sediment discharge and sediment discharge of the buffer reach, respectively, at time $k\Delta t$; $\phi \Delta x$ = length of the buffer reach; and z_B = bed elevation of the buffer reach. The factor ϕ can be estimated through the celerity of bed-deformation wave by the following form

$$\phi = \lambda_z \frac{\Delta t}{\Delta x} \quad (20)$$

The fraction of each sediment class, $P_{bi}(t)$, in the buffer reach can be obtained in the similar way, which is also served as one of the upstream boundary condition.

For an alluvial channel consisting of L subreaches, there are $(L+1)(N+3)$ unknowns to be solved at any time step. Combining Eqs. (17) and (18) yields a set of $(L+1)(N+3)$ linear equations with $(L+1)(N+3)$ unknowns, which can be expressed as a block-diagonal matrix system. The system can be solved using Thomas algorithm together with the LU decomposition technique. Because the coefficient matrix is nonsingular and the column vector of constants is non-zero, the solution is unique and nontrivial (Chen, 1994; Lai, 1994).

APPLICATION AND DISCUSSION

The total length of the Tseng-Wen River is 138.5 km, and the basin area is 1,176 km². It has two large tributaries: Hou-Ku Creek and Tsai-Liao Creek. The bed slope above the junction of Tseng-Wen River and Tsai-Liao Creek is over 0.0015, and is about 0.0003 below the junction. Tseng-Wen Dam was completed in 1973, which is 82 km upstream from the estuary. The reach considered here as an application example is from section no. 38 (one section downstream of Hsi-Kang Bridge) to section no. 21 (Kuo-Sheng Bridge), which are 16.6 km and 9.2 km upstream of the estuary, respectively.

Few measured data related to the bed-material composition and channel geometry of the Tseng-Wen River are available. Two bed-material composition and cross-sectional geometry data in 1973 and 1990 were used in the study. Measured bed-material composition ($d_{50} = 0.155$ mm, $\sigma_g = 1.7$) at section no. 21 (Fig. 2) in 1973 was used as the initial condition for the entire reach because of no other data available in the reach. Five representative sediment classes were used. The mixing-layer thickness was assumed to be 60 cm and Manning's roughness was estimated as 0.03. For simplicity, the highly irregular cross-sectional shapes were modified as rectangular compound ones. Figure 3, as an example, shows the original (1973) and the modified cross-sectional shapes at section no. 30.

Five large floods during 1973 - 1990 were assumed to dominate the bed evolution in that period. These five floods were resulted from a storm, and typhoons Billie, Thelma, Amy and Agnes. The regulated floods through Tseng-Wen Reservoir at Hsi-Kang Bridge were recorded. Combination of these floods in series served as the upstream inflow discharges of the considered reach. Figure 4 represents the largest flood hydrograph at Hsi-Kang Bridge due to typhoon Agnes.

Figure 5 shows the comparison of computed bed variation against the measured one. Note that the origin of the abscissa locates at the upstream boundary of the reach. The overall tendency of degradation of the river bed can be qualitatively simulated by the model. The predicted variation of d_{50} along the channel is shown in Fig. 6. It can be seen that the bed material is a little coarser in the upper reach and slightly finer in the lower reach when compared with the original composition. However, the measured d_{50} at section no. 21 in 1990 is much finer than the computed. This discrepancy may come from several factors, e.g., assumptions made in the governing equations, simplification of the channel geometry, negligence of small floods, and sand mining in the field. Figures 7 and 8, as an example, represent the temporal evolutions of simulated bed elevation and d_{50} , respectively, at section no. 28. Insignificant variation of the simulated results can be found from these figures.

CONCLUSIONS

Two assumptions of the NMMOC model proposed by Yeh et al. (1995) was relaxed in this study. The modified model was successfully applied to simulate the bed evolution of a short downstream reach of the Tseng-Wen River in Taiwan. The simulated bed variation is correct in the tendency as compared with the measured data. However, the significant fining of the bed material cannot be well predicted at the present stage due to several reasons. More field data and further refinement of the model will be equally important in the future study.

ACKNOWLEDGMENT

This research is supported by the National Science Council of the Republic of China, under grant No. NSC83-0410-E009-8.

REFERENCES

- Chen, W.L., 1994, A study on channel aggradation using multimode characteristics method. Master Thesis, Nat'l Chiao Tung Univ., Hsinchu, Taiwan, R.O.C. (in Chinese)
- Cunge, J.A., et al., 1980, User's manual of CHAR-2 program. SOGREAH Report No. 36-1328, Grenoble, France.
- De Vriend, M., 1973, River Bed Variations - Aggradation and Degradation. Delft Hydr. Lab. Publication No. 107, The Netherlands.
- Lai, C., 1991, Modeling alluvial-channel flow by multimode characteristics method. J. Engrg. Mech., ASCE, 117(1), 32-53.
- Lai, C., 1994, Multicomponent-flow analyses by multimode method of characteristics. J. Hydr. Engrg., ASCE, 120(3), 378-395.
- Wu, C.M., 1973, Unsteady flow in open channel with movable bed. Proc., Int. Symp. on River Mechanics, IAHR, Bangkok, Thailand, 3, 447-488.
- Yeh, K.C., Li, S.J., and Chen, W.L., 1995, Modeling non-uniform-sediment fluvial process by characteristics method. J. Hydr. Engrg., ASCE, 121(2), 159-170.

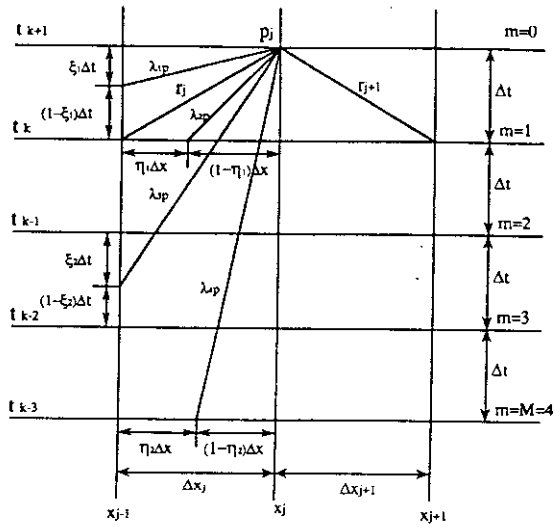


Fig. 1. Schematic Sketch of NMMOC

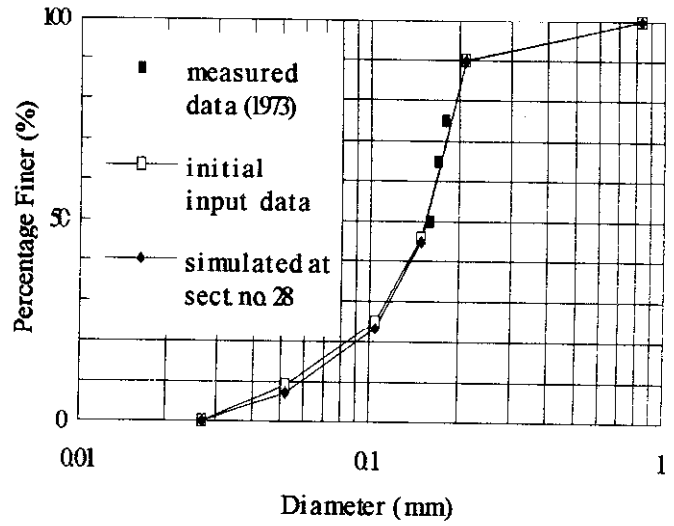


Fig. 2. Bed-Material gradation curves

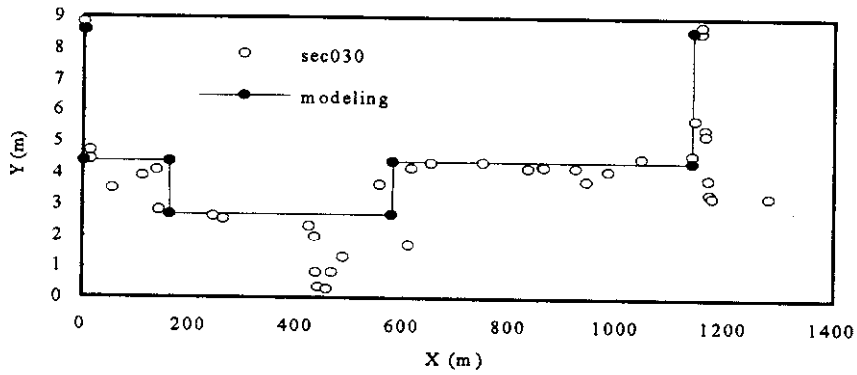


Fig. 3. Original and modified cross-sectional geometrics

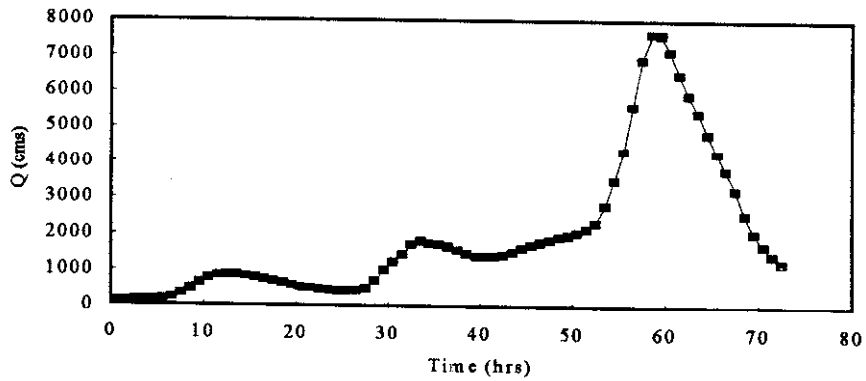


Fig. 4. Flood hydrograph by typhoon Agnes

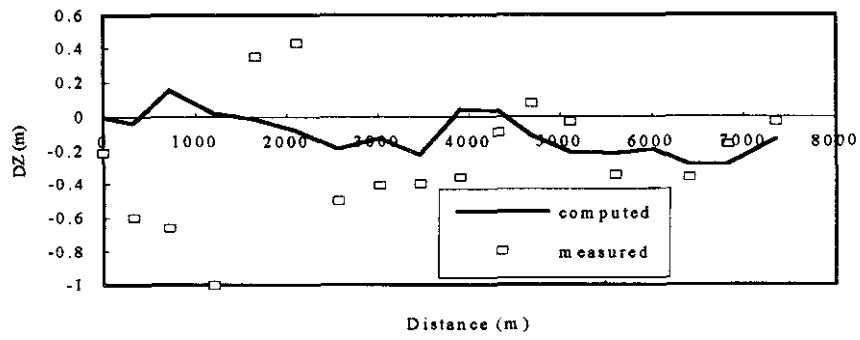


Fig. 5. Comparison of computed and measured bed variations

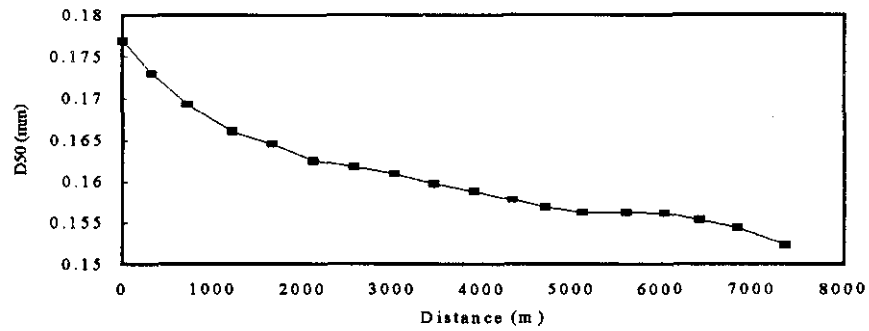


Fig. 6. Simulated variation of d_{50}

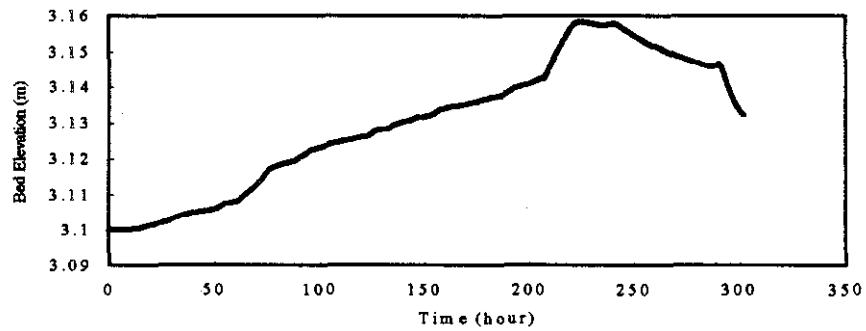


Fig. 7. Temporal evolution of bed level at Sect. 28

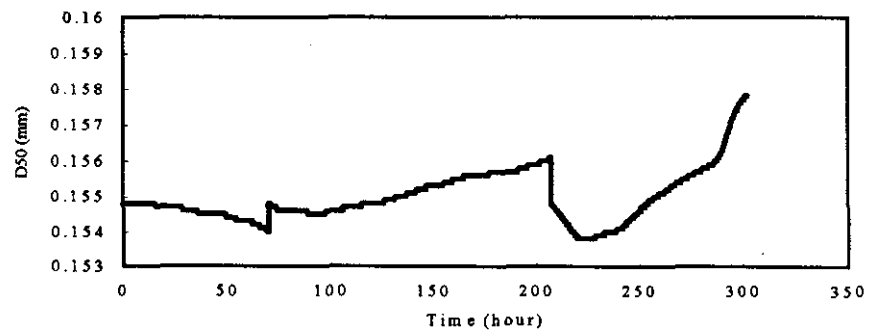


Fig. 8. Temporal evolution of d_{50} at Sect. 28

GLOBAL APPROACH FOR SENSITIVITY AND UNCERTAINTY ANALYSIS OF A SEDIMENT TRANSPORT MODEL

By Jinn-Chuang Yang, Professor, Dept. of Civil Engrg., National Chiao Tung Univ. ; Che-Hao Chang, Researcher, Energy & Resources Labs., Industrial Technology Research Institute, Hsinchu, Chian-Ming Wu, Director, Water Resources Planning Commission, Ministry of Economic Affairs, Taipei, Taiwan, ROC

Abstract: The commonly used first-order method for sensitivity and uncertainty analyses is to approximate a model by linear expansion at a selected point. Conclusions from the first-order method could be of limited use if the model responses drastically vary at different points in parameter space. To obtain the global sensitivity and uncertainty features of a sediment transport model over larger input parameter space, the Latin hypercubic sampling technique along with regression procedures were employed. For the purpose of illustrating the methodologies, the computer model HEC2-SR was selected in this study. Through an example application, the results about the parameters sensitivity and uncertainty of sediment discharge were discussed.

INTRODUCTION

Sensitivity Analysis: The sensitivity of a input parameter indicates its influence on a model output. Drastic alteration of an output with an equivalent parameters regulation rate is accomplished by a higher sensitivity coefficient. This fact indicates where data collection will best improve the confidence in model results and offers controlling insight of model behavior on which a modeler or user should give more attention (Thomson and Sykes, 1990).

Consider that the output Y of a sediment transport model is related to n stochastic input parameters $X = [X_1, X_2, \dots, X_n]^T$, with superscript 'T' being the transpose of a vector, as

$$Y = f(X) \quad (1)$$

in which $f(X)$ is a general expression for the model. A commonly used measure of sensitivity of the output with respect to the input parameters at a selected point x^* in parameter space is the gradient vector shown as

$$\nabla f(x^*) = \left[\frac{\partial Y}{\partial X_1}, \frac{\partial Y}{\partial X_2}, \dots, \frac{\partial Y}{\partial X_n} \right]_{x^*}^T \quad (2)$$

Each term of the first-order partial derivative indicates the change in the output due to one unit change in the input parameter in the neighborhood of the selected point.

Uncertainty Analysis: In a sediment transport model, basic hydraulic and sediment transport theories are for the most part included. However, the natural processes involving interactions in flow and erodible channel beds are too complicated to be described completely by the current state-of-knowledge. In other words, the uncertainty could attribute to our lack of perfect understanding about the physical phenomena and processes under consideration. All the uncertainties may contribute to the stochasticity of the input parameters to a sediment transport model which, in turn, result in the output uncertainty. Basically, the purpose of uncertainty analysis is to determine the uncertainty features of a model output as affected by stochastic input parameters.

Referring to Eq.(1), the uncertainty in a model output, by the first-order approximation, can be estimated as

$$Var(Y) \approx \nabla f(x^*)^T C_x \nabla f(x^*) \quad (3)$$

where C_x is the covariance matrix of the stochastic input parameters X . Eq. (3) points out that uncertainty of a

model output is affected by both the stochasticity and sensitivity of input parameters.

Sensitivity and uncertainty analyses are closely related but different in concept. The former is used to analyze the internal mathematical responses of model outputs as affected by changes in model input parameters, whereas the latter is used to analyze the stochasticity of the model through these internal relationships. Therefore, the important parameters identified by these two analysis might not be identical. In general, the task of uncertainty analysis involves sensitivity analysis.

A Global View of Sensitivity and Uncertainty Analysis: Sensitivity and uncertainty analyses of model behaviors could be performed from a local or global viewpoint. Local sensitivity analysis is concerned with the model output variability due to the differential changes in input parameters at a selected point in parameter space. The selected point often locates on the nominal values of the input parameters. The gradient vectors described in Eq.(2) are measures of local sensitivity. For a model whose sensitivity feature varies from one region of the parameter space to another, the local sensitivity measures evaluated at a selected point would not shed much light in understanding the sensitivity behavior of the model over the entire domain of parameter space. This argument is equally valid for using local measures, such as Eq.(3), to address the global uncertainty feature of a model output.

Analyses from a global viewpoint, on the other hand, focus on the general model behaviors over defined parameter space. Global sensitivity analysis is concerned with the pattern of change in model output due to change in input parameters over the parameter space. In general, global sensitivity analysis can be accomplished with less computation. The lack of resolution could limit its usefulness, especially when the effect of an input on an output is drastically different in various parts of the parameter space (Yeh and Tung, 1993). However, if such global analysis is performed properly, the results could be much more valuable and useful than those from local analysis.

In this paper, a practical methodological framework for global sensitivity and uncertainty analyses of a computerized sediment transport model is described. In the uncertainty analysis, the sediment transport model under consideration is treated as error-free whereas its input parameters could be subject to uncertainty. The framework employs a simple statistical sampling technique, called Latin hypercubic sampling (LHS), along with the well-known regression analysis. Among various sediment transport models, HEC2-SR (Li, 1989) is adopted for the purpose of demonstrating the methodological framework. In the following sections, the methodology for global sensitivity and uncertainty analyses are described. Then, through an application example, some results about parameter sensitivity and uncertainty of water surface, bed elevation and sediment discharge are presented.

METHOD FOR GLOBAL SENSITIVITY AND UNCERTAINTY ANALYSIS

To assess global features of model sensitivity and uncertainty, the stochastic input parameters under predefined parameter space are generated. Specifically, the LHS technique is adopted in this study. Furthermore, based on the generated input sets and the corresponding model outputs, regression analysis can be used to establish a representative input-output relationship for the model. Interpretations of statistical information from the regression analysis allow the assessments of the model sensitivity and uncertainty.

Latin Hypercubic Sampling (LHS) Technique: The basic idea of the LHS technique is to select random samples for each stochastic input parameter over its range in a stratified manner such that the overall uncertainty of a model output could be reasonably described by finite samples. Its procedure can be summarized as the following:

- (1) Consider K sets of n stochastic input parameters to be generated from which the corresponding model outputs are computed.
- (2) The plausible range of the stochastic input parameter is divided into K equal probability intervals.
- (3) Randomly draw a sample value for the stochastic input parameter under consideration from each interval resulting in K random samples for the stochastic input parameter.
- (4) Randomly permute the K samples for the stochastic input parameter.
- (5) Repeat steps 2 to 4 for all stochastic input parameters resulting in K input sets.
- (6) Apply the K input sets to the model and obtain the K outputs of interest.

The above description of the LHS assumes that the n model input parameters are uncorrelated. In the case that the stochastic input parameters are correlated, the joint probability density functions of the inputs are required.

Regression Analysis: To identify the relative importance of involved stochastic input parameters, a simple, yet representative relationship between the outputs and inputs for a model under investigation is established as

$$Y = \hat{f}(X) \quad (4)$$

in which $f(X)$ is the established surrogate model for the original model. The basic requirement for using $f(X)$ in global sensitivity and uncertainty analyses is that $f(X)$ is a sufficiently accurate approximation of the original model, $f(X)$, at least within the parameter space considered in the analyses. Such relationships can be developed using regression analysis in which the model output of interest is treated as a dependent variable while the stochastic input parameters are independent variables. Once an appropriate regression equation for the model output and input parameters is established, statistical information can be utilized to identify the relative importance of the stochastic input parameters involved. Applications of these methods to uncertainty analysis of hydraulic models can be found in Yeh and Tung (1993) and Chang et al. (1992).

It should be kept in mind that the approximated model, $f(X)$, is only a working tool for allowing easier assessment of overall model behaviors for the parameter space considered. When properly established, the approximated model can be used as a substitute for the original model within the parameter space it is derived. However, for a more general application, use of the original model is the only way.

EXAMPLE APPLICATION

To demonstrate the utility of this methodological framework for sensitivity and uncertainty analyses, a project done by Simons, Li & Associates, Inc. (SLA) was selected as the example (SLA, 1986). A 2.9-mile-long section of the Santa Cruz River adjacent to Green Valley, Arizona, U.S.A., is the study reach for hydraulic and geomorphic analysis. The project goal is to establish the design parameters associated with installation of approximately 4,500 linear feet of soil-cement pipe protection, and approximately 3,700 linear feet of soil-cement bank protection. In this paper, the procedure of sediment routing with HEC2-SR is the major concern.

Uncertainty of Model Input Parameters: Input data for a sediment-routing procedure consists of hydraulic condition in each reach including channel geometry, river and watershed information, and tributary sediment loading. Initial channel geometry can be obtained from field measurement and was assumed free from uncertainty in the study. Watershed information contains reach definition, surface and subsurface bed-material size distribution for each reach and inflow hydrograph. No tributary was considered in this study. Thus, for this application example, the uncertainty of a model output is recognized as a function of the input uncertainty in hydraulic condition and bed-material distribution. The stochastic input parameters considered include Manning's roughness coefficients at left and right banks and channel (N_l , N_r , N_c), contraction and expansion coefficients (C_c , C_e), porosity (POR), eight grain sizes (P1-P8), and surface layer thickness (SLT). The nominal values of these 15 stochastic input parameters used in the analysis were those specified in the HEC2-SR original data and all were assumed to have uniform distributions without correlations among them. The plausible ranges of variation were set at 15% for upper and lower bounds. The stochastic features of the input parameters were listed in Table 1. The percentage of the grain sizes used in analysis were kept constant and listed in Table 1. Using the LHS technique, 30 data sets for the 15 stochastic model input parameters were generated from which the corresponding outputs were computed.

Model Outputs Considered: Sediment discharge, one of the model outputs, at four spatial locations and three time points, were examined for their sensitivity and uncertainty. The four locations were cross-sections 1, 5, 7 and 9 from downstream end of the system. The three time points were at $T=2, 6$ and 9 , each representing before peak, during peak and after peak of the inflow hydrograph as shown in Fig. 1. An examination of model output variability at different times and locations allows one to assess temporal and spatial variations of model outputs. Since one output at 3 time points and 4 locations were to be analyzed, a total of 12 regression equations were established by using the statistical package MINITAB (Ryan, Joiner, and Ryan, 1985).

RESULTS AND DISCUSSIONS

In this particular study case, using a simple linear regression function as Eq.(8) has resulted in the values of R^2 exceeding 95% for the majority of the 12 cases. This fact indicates that, within the parameter space considered, the sediment transport model is well described by the 12 linear functions which can be used to perform the global sensitivity and uncertainty analyses with good confidence at the specific time steps and locations.

Results of Sensitivity Analysis: The dependence of the temporal and spatial variations in the sediment discharge on parameters sensitivities do not reveal clear pattern in this study. Due to the similar responses at different locations, the regression coefficients and t-values for the model output only at cross-sections 1 are presented in Figs.2-4 to illustrate the input parameters' sensitivity. Note that a comparison of the regression coefficients and the associated t-values among stochastic model input parameters could identify which parameters are the ones controlling the model behavior. Generally, a parameter with higher sensitivity coefficient is statistically significant. In case that a sensitivity coefficient is significant, its magnitude indicates the intensity of the sensitivity.

Two of the most significant parameters affecting the sediment discharge are the N_c and the particle size P_3 in the sensitivity analysis. The sensitivity coefficient of N_c and associated t-value, indicated by Fig. 2, shows that a negatively correlated relationship exists between the sediment discharge and the N_c . It is reasonable that the sediment transport capacity increases with the flow velocity which is inversely affected by the N_c . Referring to Table 1, the P_4 is the principle constituent in sediment composition of surface and subsurface layers. However, the result of sensitivity analysis indicates that the P_3 , rather than the P_4 , has the largest sediment transport rate in the considered flow condition according to the model computation. This can be explained by the fact that sediment transport is presented as the balance of flow condition and erodible bed. Sediment composition alone could not dominate the outcome of sediment discharge.

From a model calibration aspect, it is efficient to first consider the regulation of a model output with sensitive input parameters. Then, detail parameters tuning is applied to obtain the best agreement with observations. The generation of such sensitivity information would benefit one's realization to deterministic behavior of model computation so as to improve calibration procedure.

Results of Uncertainty Analysis: In the uncertainty analysis, the bias and standard deviation of the sediment discharge were shown in Fig. 3. The bias is the differences between the mean value of the model output computed from the input sets generated by the LHS technique and the model output obtained by using the mean values of the input parameters. The standard deviations of the model outputs were obtained from the thirty model outputs which were computed from the input sets generated by the LHS technique.

The results indicate that the uncertainty of the sediment discharge increases with the flow rate. Since sediment discharge is concerned with transport capacity which depends closely on flow condition, it is expected from Fig. 3 that the uncertainty is dominated only by the discharge.

In this study, consideration is given to the fact that model output uncertainty arises only from the uncertainty of input parameters. Namely, type II uncertainty is considered in which the model is assumed correct but contains uncertain input. One major concern of uncertainty analysis is the identification of important input parameters. The relative importance of a input parameter in uncertainty analysis is measured by its contribution to the overall uncertainty of a model output. The PCCs shown in Fig. 4 were the indicators for the relative importance of the parameter with regard to their contribution to the model output uncertainty. Compared to the sensitivity coefficients or t-values acquired from the sensitivity analysis, the N_c , POR, SLT, and P_3 are still the main contributors. But the other input parameters like the contraction and expansion coefficients have different ranks from the sensitivity analysis.

As stated previously, two major components affect the uncertainty contribution of a stochastic input parameter: the sensitivity coefficient and the variance of the parameter. The ranks of important parameters from uncertainty analysis could not, in general, be identical to the results of sensitivity analysis for the reason that the uncertainty

of input parameters is involved. Due to the assumption of uncorrelated parameters and the standardized procedure in this study, the results from both the analyses would be close.

SUMMARY AND CONCLUSION

This paper demonstrates the framework of sensitivity and uncertainty analysis of a selected sediment transport model from a global viewpoint. The framework consists of using the LHS technique and the linear regression procedure to examine the model behavior within predefined input parameters space. For the model and example application considered herein, the Manning's roughness coefficient in channel is the most important parameter due to the high sensitivity coefficient and large uncertainty contribution. The parameters for an erodible bed including the porosity, surface layer thickness, and particle size P_3 , are also the important parameters to the sediment discharge.

Uncertainty analysis provides not only useful insight with regard to model performance but also offers essential information for engineering design and decision-making. For example, in this study, the standard deviation of water surface or bed elevation could be used to calculate the proper safety factor of a bank protection design. Further study such as reliability analysis can be followed to offer more concrete measures as needed for engineering application since the stochastic nature of a model forecast is obtained from the uncertainty analysis.

Stochastic analysis allows an engineer to obtain possible variations of model outputs. Information as such is essential for effective design and/or evaluation of hydraulic structures because wide spectrum of possible model responses is available for decision-making. Results from a uncertainty analysis could help analysts identify important stochastic parameters that contribute most of the overall uncertainty of model outputs. This would allow effective design of data collection program for reducing model output uncertainty.

This study considered that all stochastic input parameters of the HEC2-SR are uncorrelated random variables with uniform distributions. In reality, the input parameters of a sediment transport model could be non-normally distributed and correlated. Comparing with the variety of the random number generation for univariate variable, multivariate random number generation is much more restricted to a few joint distributions such as multivariate normal, multivariate lognormal, and multivariate gamma (Johnson, 1987). It would be desirable that algorithms could be developed that would allow generating synthetic model input parameters which have mixture of non-normal distributions and correlated.

ACKNOWLEDGMENT

The authors wish to express their gratitude to Water Resources Planning Commission, MOEA, Republic of China for the financial support of this study.

REFERENCES

- Johnson, M. E. 1987: *Multivariate Statistical Simulation*, John Wiley and Sons, Inc., New York.
- Li, R. M., 1989: *Sediment-Routing Model HEC2-SR*. United States Department of The Interior Geological Survey.
- Simons, Li & Associates, Inc. 1986: *Hydraulic and Geomorphic Analysis of The Santa Cruz River in The Vicinity of The Wastewater Treatment Plant Green Valley, Arizona*. Prepared for Pima County Wastewater Management Department, Tucson, Arizona.
- McKay, M. D. 1988: "Sensitivity And Uncertainty Analysis Using A Statistical Sample of Input Values." *Uncertainty Analysis*, ed. by Ronen, Y., CRC Press, Inc., Boca Raton, FL, 145-186.
- Ryan, B. F., Joiner, B. L., and Ryan, T. A. Jr. 1985: *Minitab Handbook Second Edition*, Duxbury Press, Boston.
- Thomson, N. R., and Sykes, J. F. 1990: "Sensitivity And Uncertainty Analysis of A Short-term Sea Ice Motion Model." *Journal of Geophysical Research*, Vol. 95, NO. C2, 1713-1739.
- U.S. Army Corps of Engineers Water Resources Support Center, 1982: *HEC2 Water Surface Profiles Users Manual*, The Hydrologic Engineering Center, Davis, California.
- Yeh, K. C., and Tung, Y. K. 1993: "Uncertainty and sensitivity of a pit migration model." *Journal of Hydraulic Engineering*, ASCE. 119(2):262-283.

Table 1. The stochasticity of input parameters

Name	Description	L.B.*	U.B*	Mean	Stdev.	COV*
Nl	Manning's roughness coefficient at left bank	0.02975	0.0402 5	0.035 0	0.003031	0.0866
Nr	Manning's roughness coefficient at right bank	0.02975	0.0402 5	0.035 0	0.003031	0.0866
Nc	Manning's roughness coefficient at channel	0.02550	0.0345 0	0.030 0	0.002598	0.0866
Cc	Contraction coefficient	0.08500	0.1150 0	0.100 0	0.008660	0.0866
Ce	Expansion coefficient	0.25500	0.3450 0	0.300 0	0.025980	0.0866
Por	Porosity	0.34000	0.4600 0	0.400 0	0.034600	0.0866
P1	Grain size 1 S= 2% B= 2%	0.05185	0.0701 5	0.061 0	0.005283	0.0866
P2	Grain size 2 S= 2% B= 6%	0.08925	0.1207 5	0.105 0	0.009093	0.0866
P3	Grain size 3 S=25% B=17%	0.21420	0.2898 0	0.252 0	0.021820	0.0866
P4	Grain size 4 S=30% B=29%	0.50490	0.6831 0	0.594 0	0.051440	0.0866
P5	Grain size 5 S=25% B=24%	1.09480	1.4812 0	1.128 8	0.111500	0.0866
P6	Grain size 6 S= 9% B=17%	2.60610	3.5259 0	3.066 0	0.265500	0.0866
P7	Grain size 7 S= 3% B= 3%	5.68735	7.6946 5	6.691 0	0.579500	0.0866
P8	Grain size 8 S= 4% B= 2%	11.4495	15.490 5	13.47 0	1.167000	0.0866
SLT	Surface layer thickness	518.500	701.50 0	610.0 0	52.83000	0.0866

L.B. - Lower bound;

U.B. - Upper bound;

COV - Coefficient of variation;

S - Percentage of grain size interval for the surface layer;

B - Percentage of grain size interval for the subsurface layer.

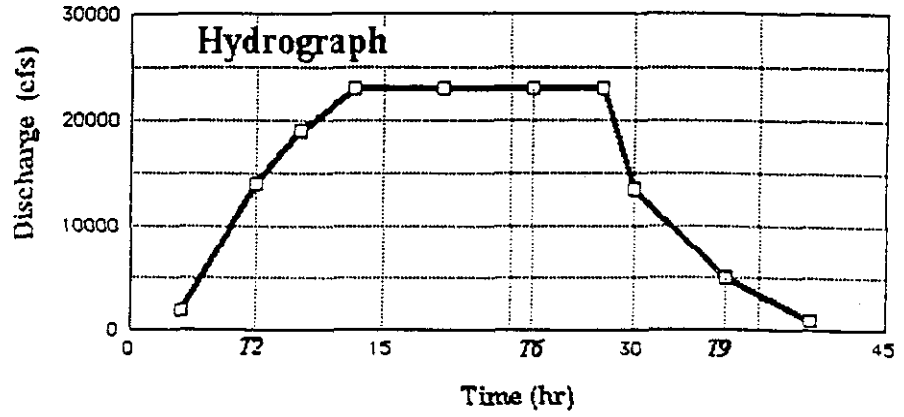


Fig. 1 Input hydrograph for example application

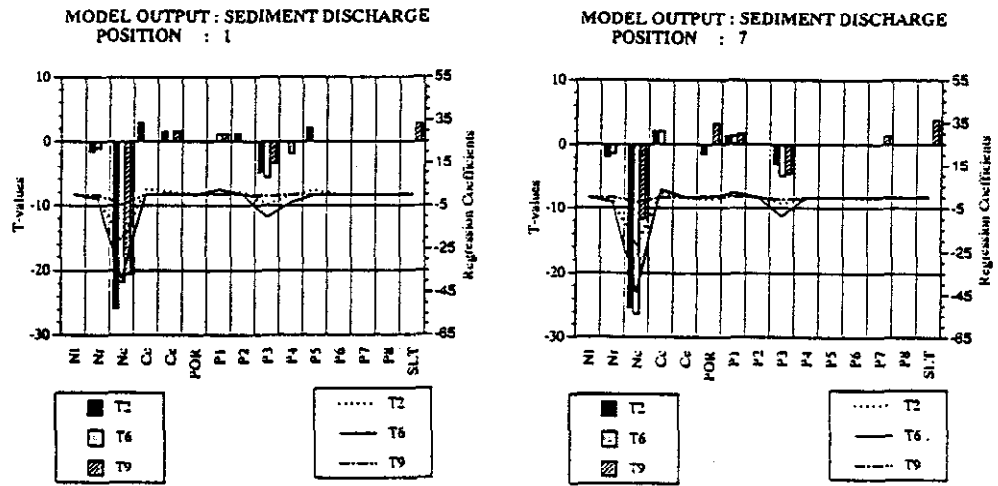


Fig. 2 Results of sensitivity analysis for sediment discharge at section 1 and section 7

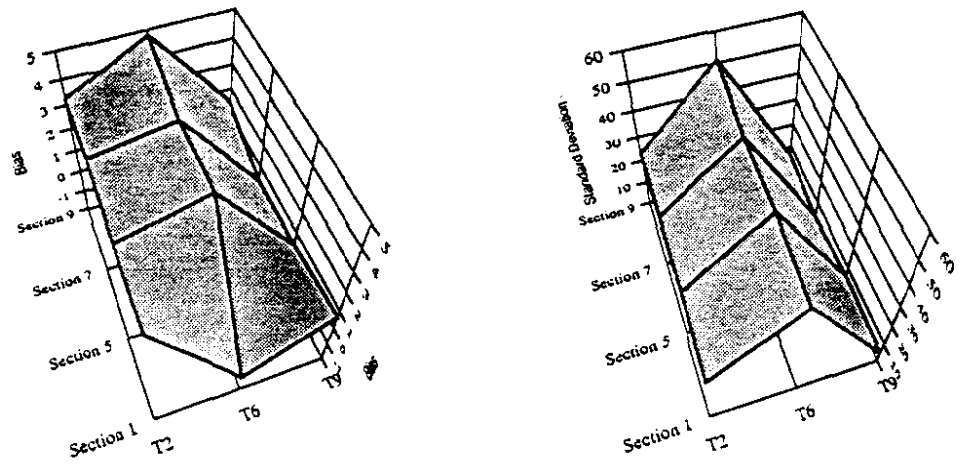


Fig. 3 Biases and standard deviations of sediment discharge at different time steps and positions

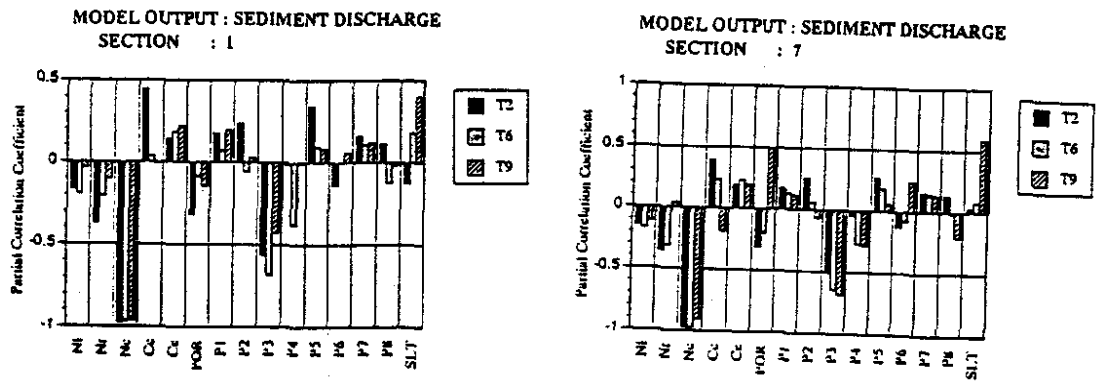


Fig. 4 Partial correlation coefficients of input parameters for sediment discharge at section 1 and section 7

TIDAL MARSH SEDIMENTATION

By Guang-dou Gordon Hu¹, Consultant in Hydraulic and Environmental Engineering
Northwest Hydraulic Consultants Inc., Sacramento, California

Abstract: An equation for tidal marsh accretion is described. The equation, as well as a chart and a table developed on basis of the equation, can be used to estimate sedimentation rate in a tidal marsh. When actual tidal records are available, the same concept can be applied to calculate sedimentation rate by numerical integration. As indicated by the analysis, the sedimentation rate decreases rapidly when marsh plain elevation rises. The averaged marsh growth rate based on long-term marsh elevation changes may be much lower than the growth rate at the early stage of the accretion process when marsh plain is lower than the mean tide level.

INTRODUCTION

A tidal marsh is a unique land form. Marshes form as a result of the combined effects of the tides, rising sea level, sediment transport, and marsh plants. Accumulation of sediment and plant material raises the elevation of a marsh surface. The rate of upward growth depends on the frequency and duration of tidal inundation, the concentration of suspended sediments in the tidal waters, the rate of plant growth, the rate of subsidence, and compaction or desiccation of the marsh soil (Allen, et al, 1988; Allen, 1990; French, 1993). Suspended sediment deposition is usually the major factor in marsh accretion (Krone, 1982; Hu, 1994).

The first numerical model for marsh accretion was developed by R. B. Krone (1985, 1987). The method of calculation includes calculation of material that deposits during each period of inundation by a high tide and summing the amount of deposit over the period of simulation. The author pointed out that the uniformity of a natural marsh surface elevation indicates that a calculation of the mean elevation would be useful, so the computation is limited to the vertical dimension. His model describes changes of suspended sediment concentration over tidal cycles. As water leaves a channel and flows onto the marsh surface during a rising tide, the suspended sediment concentration, C , diminishes as aggregates settle to the land surface. As new sediment-laden water from the channel mixes with the previously flooding water, however, the added sediment increases the concentration. This process continues until the tide reaches its maximum elevation, after which only deposition occurs while the water drains from the marsh. A mass balance of this process leads to

$$(y_w - y_m) \frac{dC}{dt} + W_s C - (C^* - C) \frac{dy_w}{dt} = 0 \quad (1)$$

where y_w and y_m are the elevations of the water surface and marsh surface relative to a selected datum. W_s is the settling velocity of the suspended aggregates, and t is time. $C^* = C_0$ during a

¹ Northwest Hydraulic Consultants Inc., 3950 Industrial Boulevard, Suite 100c, West Sacramento, CA 95691-3430.
Phone (916) 371-7400. Fax (916) 371-7475

rising tide where C_0 is the concentration of suspended soils in the flooding waters, and $C_s = C$ during a falling tide.

Laboratory tests on San Francisco Bay mud showed that when aggregation has progressed to the point where the average time between collision is long, the median settling velocity by weight of the suspended aggregates is described by

$$W_s = a C^{4/3} \quad (2)$$

where a was found to be 110 for W_s in centimeters per second and C in grams per cubic centimeter.

The deposition during a period of flooding by a high tide is

$$\Delta y_m = \int_t W_s C dt / C_s \quad (3)$$

where C_s is the grams of mineral solids per cubic centimeter of marsh soil.

The actual value of C_0 varies from hour to hour, depending on the wave heights and the water depth over the mud flats adjacent to the marsh. It is not feasible to include such variations in the calculation. The marsh surface elevation changes very slowly, by comparison, and is the integral of years of deposition. The use of a measured marsh elevation to calculate an effective C_0 for recent years of deposition provides a means for obtaining a useful value for this sensitive parameter.

ANALYTICAL SOLUTION

Tidal height can be written as a function of time $h(t)$. Assuming that the tidal marsh surface is at elevation H_0 , the water depth over marsh plain at time t is

$$\begin{cases} d(t) = h(t) - H_0 & (h(t) > H_0) \\ d(t) = 0 & (h(t) \leq H_0) \end{cases} \quad (4)$$

where $h(t) \leq H_0$ indicates that tidal elevation is lower than marsh plain and therefore the water depth is zero.

With $d(t)$ defined in Eqn (4), the amount of suspended sediment in the water column over a unit area of marsh plain will be

$$g(t) = c(t) d(t) \quad (5)$$

in which $c(t)$ is the concentration of suspended sediment in the tidal water. Both g and c are written as functions of time.

For convenience of analysis, we approximate tidal heights with a cosine function of time t . Assuming two equal high and low tides for each lunar day with tidal range $2\Delta H$, then tidal height will be

$$h(t) = \Delta H(1 + \cos(\pi t/6)) + H_{MLW} \quad (6)$$

in which t is time in hours, H_{MLW} is the elevation of mean low water.

For purpose of general applications, now we define non-dimensional tidal elevation as

$$h'(t) = (h(t) - H_{MLW})/\Delta H = 1 + \cos(\pi t/6) \quad (7)$$

which is plotted in *Figure 1*.

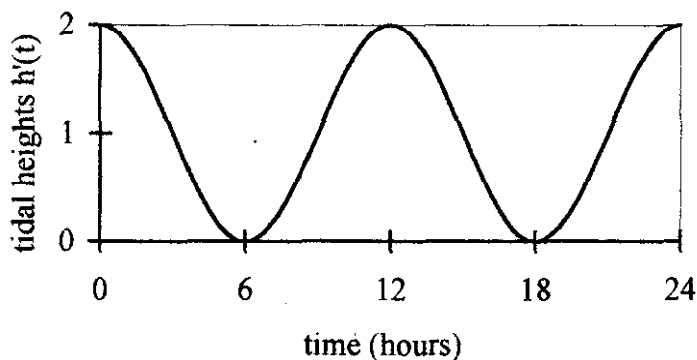


Figure 1. Non-dimensional tidal heights $h'(t)$

If we write the elevation of tidal march as $H_0 = H_{MLW} + \alpha\Delta H$ in which $\alpha < 2$, the water depth over marsh surface at time t will be

$$\begin{cases} d(t) = h(t) - H_0 = \Delta H(1 + \cos(\pi t/6) - \alpha) & (1 + \cos(\pi t/6) > \alpha) \\ d(t) = 0 & (1 + \cos(\pi t/6) \leq \alpha) \end{cases} \quad (8)$$

in where α can be considered a non-dimensional parameter of marsh elevation.

Similar with *Eqn (7)*, now we write non-dimensional water depth as

$$d'(t) = d(t)/\Delta H \quad (9)$$

which is the vertical distance between tidal height and marsh elevation α .

Substitute (8) into (5), the amount of suspended sediment in the water column over a unit area of marsh plain would be

$$g(t) = c(t) d(t) = c(t)\Delta H (1 + \text{COS}(\pi t/6) - \alpha) \quad (10)$$

when marsh plain is inundated, that is when $1 + \text{COS}(\pi t/6) > \alpha$. The discussions in the following sections will refer to the same condition if inundation is not mentioned.

Now we assume that the amount of sediment deposited over marsh surface within a certain time period is a fraction of the total amount of suspended sediment in the over laying water column, the deposition amount of the period will be

$$w(t) = f(t) g(t) = f(t) c(t) d(t) = f(t) c(t)\Delta H (1 + \text{COS}(\pi t/6) - \alpha) \quad (0 \leq f(t) \leq 1) \quad (11)$$

in which $f(t)$ is the settling rate of suspended sediment in a certain time period.

The amount of sediment deposited at marsh surface over a period Δt can be obtained by integration of Eqn (11):

$$W_{\Delta t} = \int_{\Delta t} w(t) dt = \int_{\Delta t} f(t) c(t)\Delta H (1 + \text{COS}(\pi t / 6) - \alpha) dt \quad (12)$$

In which the time unit of $f(t)$ has to be consistent with t . Take the average of suspended sediment concentration and settling rate over Δt as

$$F_{\Delta t} = \frac{1}{\Delta t} \int_{\Delta t} f(t) dt \quad (13)$$

and

$$C_{\Delta t} = \frac{1}{\Delta t} \int_{\Delta t} c(t) dt \quad (14)$$

Then Eqn(12) becomes

$$W_{\Delta t} = \Delta H F_{\Delta t} C_{\Delta t} \int_{\Delta t} (1 + \text{COS}(\pi t / 6) - \alpha) dt \quad (15)$$

Eqn (15) has an analytical solution. Integration of (15) for $\Delta t = 24$ hours is

$$W_{24} = 4.0 \Delta H F_{24} C_{24} \left\{ (1 - \alpha) \text{COS}^{-1}(\alpha - 1) + \sqrt{1 - (\alpha - 1)^2} \right\} \quad (16)$$

where subscripts 24 of F and C indicates that they are the average for a 24-hour period. Since hour is used as the unit of t for integration, the unit of F_{24} should be hourly settling rate.

To generalize the result in Eqn (16), let 24-hour non-dimensional deposition amount be

$$W'_{24} = \frac{W_{24}}{\Delta H F_{24} C_{24}} = 4.0(1-\alpha) \cos^{-1}(\alpha-1) + \sqrt{1-(\alpha-1)^2} \quad (17)$$

Table 1 lists W' for $\Delta t = 24$ hours with α from 0 to 2. The results in Table 1 is plotted in Figure 2. It is obvious that deposition amount depends on the elevation of marsh plain. The higher the elevation is, the shorter the period of inundation is. Water depth at higher elevation is also less during inundation. All these contribute to less amount of deposition at higher elevation. In marsh accretion process, the growth rate is never a constant. It decreases rapidly when marsh elevation grows.

Table 1. 24-hour non-dimensional deposition rate W'_{24}

α	0.1	0.2	0.3	0.4	0.5	0.6	0.7	0.8	0.9	1.0
W'_{24}	11.43	10.39	9.43	8.51	7.65	6.84	6.07	5.34	4.65	4.00
α	1.1	1.2	1.3	1.4	1.5	1.6	1.7	1.8	1.9	2.0
W'_{24}	3.39	2.82	2.30	1.81	1.37	0.97	0.63	0.34	0.12	0.00

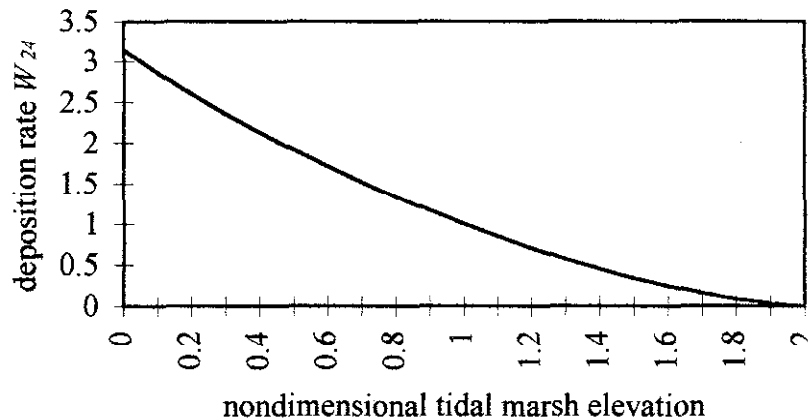


Figure 2. Nondimensional deposition rate W'_{24}

Table 1 and Figure 2 can be used for estimation of deposition rate. Firstly, calculate α based on marsh elevation, tidal range and mean low water. Then find 24-hour non-dimensional deposition rate in Table 1 or Figure 2. Finally, calculate 24-hour deposition rate by using

$$W_{24} = W'_{24} \Delta H F_{24} C_{24} \quad (18)$$

Following is an example for the application of Table 1 or Figure 2.

Example.

Tidal marsh plain at elevation -1.0 ft NGVD. Tidal range is 4.4 feet. Mean low water is -2.2 feet NGVD. Suspended sediment sampling indicates that the average suspended sediment

concentration is 0.3 gram per cubic liter. Hourly sediment settling rate is estimated as 0.8. Calculate the amount of deposition over a six month period.

$$2\Delta H = 4.4 \text{ ft, therefore } \Delta H = 2.2 \text{ ft}$$

$$\alpha = (H_0 - H_{MLW})/\Delta H = (-1 - (-2.2)) \text{ ft} / 2.2 \text{ ft} = 0.55$$

Find in Table 1 or Figure 2 that $W'_{24} = 7.25$ when $\alpha = 0.55$
 Unit conversion of C_{24} : $C_{24} = 0.3 \text{ g/l} = 8.1 \text{ g/ft}^3$

Use Eqn (18) to find the 24-hour sedimentation rate:

$$W_{24} = (7.25)(2.2 \text{ ft})(0.80)(8.1 \text{ g/ft}^3) = 103 \text{ g/ft}^2\text{-24 hour}$$

Assume that the deposition rate can be considered constant, the deposition amount in the 6-month period will be

$$(103 \text{ g/ft}^2)(30.5)(6) = 18914 \text{ g/ft}^2$$

If the density of the new deposit is 1200 g/l, this deposition amount indicates an elevation raise of about 0.6 feet in the 6-month period.

The accumulation of sediments will raise marsh plain elevation which is called marsh growth or marsh accretion. Eqn (17) as well as Table 1 and Figure 2 can be used to predict the marsh growth process.

Case Study

The analytical solution Eqn (17) used daily average tide to calculate the deposition rate by integration over a one-day period. Longer period of integration can also be used. Figure 3 is the tidal curve $h(t)$ of North San Pablo Bay near Sonoma Creek for a 14-day period which contains both spring and neap tides. Tidal characteristics are listed in Table 2.

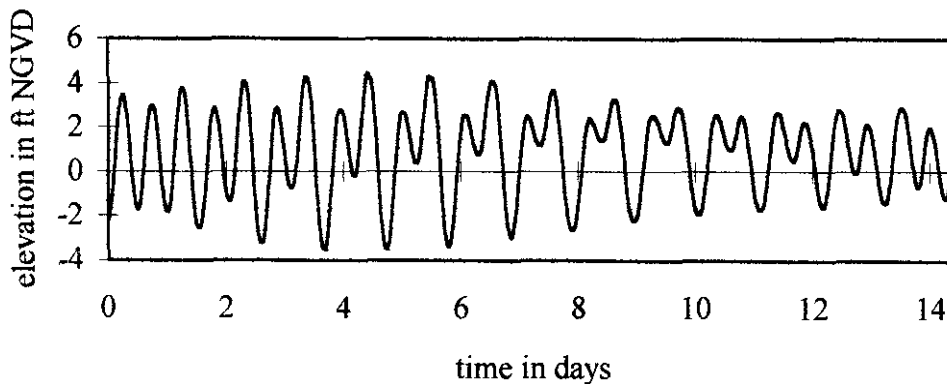


Figure 3. Neap-spring tides of north San Pablo Bay

Table 2. Tidal characteristics in North San Pablo Bay, Unit: feet NGVD

Mean Tide Level	Mean High Water	Mean Low Water	Tidal Range
0.93	3.12	-1.26	4.38

Suspended sediment concentration measurements were made in an area near Napa Marsh in San Pablo Bay (Jenkins, 1986). In the period from February to August in 1983, 176 water samples were taken to analyze the suspended sediment concentration which provided 44 suspended sediment concentration profiles during floods, high waters, ebbs, and low waters of 11 days. 44 depth-averaged concentrations were obtained and were divided into four categories: flood, high, ebb, low. The average concentrations for each are listed in Table 3.

Table 3. Measurements of suspended sediment concentration in North San Pablo Bay

Tidal Period	Flood	High	Ebb	Low	Average
Concentration (mg/l)	545.5	260.2	185.9	183.6	293.8

A salt pond intake channel in the area has been repeatedly filled by sediment and dredged. Based on the survey records of the channel bottom elevation, it is estimated that the sediment settling rate is about 50%.

Using the same concept for the analytical solution, the deposition amount in a certain time period can be obtained by integration:

$$W_{\Delta t} = F_{\Delta t} C_{\Delta t} \int_{\Delta t} (h(t) - H_0) dt \quad (19)$$

Numerical method is used to integrate Eqn (19). The results for $H_0 = -4.0 \text{ ft} \sim 4.0 \text{ ft}$ are plotted in Figure 4.

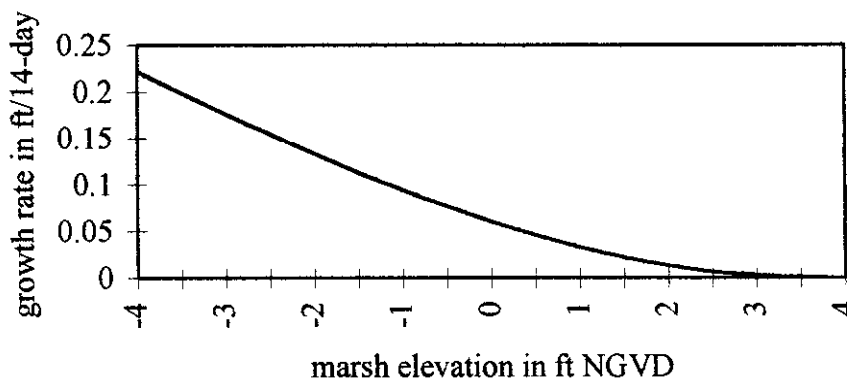


Figure 4. 14-day deposition rate

Assuming top layer density of 1200 g/l, the results in Figure 4 has been converted into depth of deposition.

The results in *Figure 4* indicate that, while the deposition rate at -4.0 feet NGVD is 0.22 ft per 14-day period, the deposition rate above 3 feet NGVD will be close to zero. The accretion process of a marsh plain at elevation -4 ft NGVD is predicted using growth rate plotted in *Figure 4*. The growth rate decreases rapidly when marsh elevation approaches mean tide level. The marsh elevation change as a function of time is plotted in *Figure 5*.

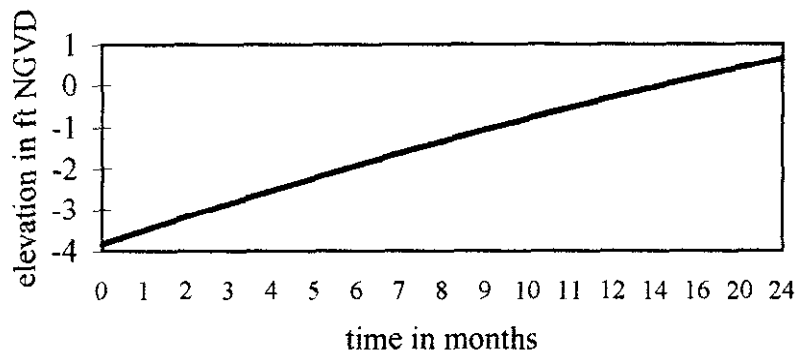


Figure 5. Predicted marsh accretion process

REFERENCES

- Allen, J.R.L., and J.E. Rae, 1988, Vertical salt-marsh accretion since the Roman Period in the Severn Estuary, southwest Britain. *Marine Geology*, 83(1988), pp. 225-235
- Allen, J.R.L., 1990, Salt-marsh growth and stratification: A numerical model with special references to the Severn Estuary, southwest Britain. *Marine Geology*, 95(1990), pp. 77-96.
- French, J.R., 1993, Numerical simulation of vertical marsh growth and adjustment to accelerated sea-level rise, North Norfolk, U.K.. *Earth Surface Processes & Landforms*, Vol. 18, 63-81.
- Ju, G., 1994, Hydraulic and Sediment Transport Models for Design of Tidal Marsh Restoration. Ph. D. dissertation, Department of Civil and Environmental Engineering, University Of California at Davis.
- Jenkins, S.A., 1986. Personal communication to John Pyles, October 3, 1986.
- Krone, R.B., 1982, Engineering Wetlands: Circulation, Sedimentation, and water quality. in M. Josselyn (ed), *Wetlands Restoration and Enhancement in California*, California Sea Grant College Program, Report No. T-CSGCP-007, December 1982. pp. 53-58.
- Krone, R.B. 1985, Simulation of marsh growth under rising sea levels. *Proceedings of the ASCE Special Conference on Hydraulics and Hydrology in the Small Computer Age*, Orlando, Florida. pp. 106 - 115.
- Krone, R.B., 1987, A method for simulating historic marsh elevations. *Proceedings of ASCE Conference, Coastal Sediments 87*, New Orleans.

Numerical Modeling of Storm-Induced Beach Erosion

S. Jarrell Smith, Hydraulic Engineer, U.S. Army Corps of Engineers, Coastal Engineering Research Center, Vicksburg, MS; Randall A. Wise, Research Hydraulic Engineer, U.S. Army Corps of Engineers, Coastal Engineering Research Center, Vicksburg, MS

Abstract: Beaches erode and accrete in response to the varying waves, water levels, and currents which characterize the nearshore zone. During storms, catastrophic beach and dune erosion can occur in a matter of hours, resulting in significant shoreline recession and damage to property and upland resources. Consequently, protection of upland resources against storm erosion, flooding, and wave attack is a primary concern in the field of coastal engineering. Beach nourishment has become a preferred method of providing such protection, and many beach fill projects have been designed and constructed in the past several years. Effective design of beach fills for shore protection requires an understanding of and an ability to predict sediment transport processes that control beach response to storms.

The Storm-induced BEACH CHange (SBEACH) numerical model was developed by the U.S. Army Corps of Engineers (USACE) for simulating two-dimensional beach and dune erosion produced by storms. The model is used in beach fill project design applications to calculate beach profile response of alternative design configurations to a statistically defined set of storms in order to estimate with- and without-project damages over the project design life. In the design process, storm erosion and damage estimates are utilized in economic analyses to compare total project costs and total project benefits (including storm damage reduction benefits) for each design alternative. Federal participation in a beach fill project occurs only if net national benefits are demonstrated for the project, and the design alternative which maximizes such benefits is typically selected. Thus, accurate prediction of beach erosion in response to storms is important in defining and optimizing both the physical performance and economic viability of a beach fill project.

INTRODUCTION

The natural beauty and serenity offered by beaches attract many visitors to America's coasts every year. This natural resource generates large revenues for local governments and residents of these areas. Not only does the beach provide a means of income, but also a means of protection from storms that attack the shoreline.

Storms are capable of causing severe damage to coastal regions (which can range from millions to billions of dollars). A healthy beach is crucial in stemming these potential damages by offering protection against storm surge and waves. The U.S. Army Corps of Engineers (USACE) is involved in assessing the level of protection that a specific beach offers. When a beach's storm protection capacity is found to be deficient, placement of sand in a beach fill is often performed to increase the beach's level of protection against coastal storms.

An essential ingredient in the assessment of a beach's level of protection is the determination of the beach profile's response to storms of varying intensity. SBEACH is designed to be used as a tool in estimating beach profile change due to erosive wave and water level conditions (accretionary processes are not modeled), and is used in determination of cost-benefit ratios for a given beach fill design.

The model was empirically founded upon sediment transport rates and profile evolution observations in large wave tank (LWT) laboratory experiments and was later verified to high-quality field data sets (Larson and Kraus 1989; Larson, Kraus, and Byrnes 1990). Since its development, the model has been continuously enhanced and now incorporates the ability to model a seawalled profile, dune overwash, and irregular waves. Primary uses of the model by the coastal engineering community are focused towards prediction of two-dimensional profile response, particularly dune and foreshore erosion for the design of effective beach fills.

SBEACH is fundamentally based upon observations that cross-shore sediment transport is proportional to the amount of incident wave energy in excess of the equilibrium energy dissipation and that sediment is conserved across the profile (Larson and Kraus 1989). The assumption that sediment is conserved across the profile during a storm limits the model's application to beaches that have negligible gradients in longshore sediment transport under storm

conditions (i.e. straight beaches with no interruptions in longshore sediment transport). SBEACH has been developed for application to beaches with median sediment diameters of 0.15 mm to 1.0 mm (in the range considered to be fine to coarse sand by the Wentworth classification system) and has been verified for grain sizes ranging from 0.2-0.42 mm (considered fine to medium sand by the Wentworth classification system).

Theory: SBEACH is based upon the assumption that profile change is caused by waves transforming and breaking across the profile. This relationship between sediment transport and wave energy dissipation across the profile requires an accurate description of the wave climate across the beach profile. SBEACH includes an internal wave model to handle this task. The internal wave model's characterization of the cross-shore wave climate is used to determine sediment transport rates and corresponding profile responses to the input wave conditions.

The wave model used in SBEACH employs linear wave theory to define wave characteristics from the seaward boundary of the model domain to the breakpoint of the incident waves. From the breakpoint shoreward, a form of the wave decay model proposed by Dally et al. (1985) is used to describe the wave height distribution across the surf zone. The random wave model currently used in SBEACH is a modified version of Dally's model designed to characterize the decay of random waves based on a Rayleigh distribution of wave heights (Larson 1995).

Upon characterization of the wave field across the beach profile, estimation of the corresponding sediment transport rates is possible. Under random waves, calculation of sediment transport across the profile is divided into three primary zones of transport. The first transport zone is located seaward of the wave breakpoint, followed by the second transport zone from the breakpoint shoreward to the swash zone, with the swash zone defined as the third zone. Figure 1 offers a schematized definition of the three zones of transport. The equations governing offshore sediment transport in these three regions are summarized as:

Zone I: Pre-Breaker Zone

$$q = q_b e^{(-\lambda_1 (x-x_b))} \quad x_b < x \quad (1)$$

Zone II: Broken Wave Zone

$$q = \begin{cases} K \left[D - D_{eq} + \frac{\epsilon}{K} \frac{dh}{dx} \right] & D > \left[D_{eq} - \frac{\epsilon}{K} \frac{dh}{dx} \right] \\ 0 & D \leq \left[D_{eq} - \frac{\epsilon}{K} \frac{dh}{dx} \right] \end{cases} \quad (2)$$

for $x_z \leq x \leq x_b$

Zone III: Swash Zone

$$q = q_z \left[\frac{x - x_r}{x_z - x_r} \right]^{\frac{3}{2}} \quad x_r < x < x_z \quad (3)$$

where

- q = net cross-shore sand transport rate, $m^3/m\text{-sec}$
- λ_1 = spatial decay coefficient in Zone I, $1/m$
- x = cross-shore coordinate directed positive offshore, m
- K = sand transport rate coefficient, m^4/N
- D = wave energy dissipation per unit water volume, $N\text{-}m/m^3\text{-sec}$
- D_{eq} = equilibrium wave energy dissipation per unit water volume, $N\text{-}m/m^3\text{-sec}$

ε = slope-related sand transport rate coefficient, m^2/sec
 h = still-water depth, m .

The subscripts b, z, and r identify quantities described at the breakpoint, seaward end of the swash zone, and the runup limit, respectively (Larson, Kraus, and Byrnes 1990). The parameters K , ε , and specification of the position of the seaward end of the swash zone are all used as calibration parameters for the model.

Data Requirements: To simulate beach erosion due to storm waves and water levels, SBEACH requires input of a fundamental set of information. Required input includes offshore wave conditions, depth at location of offshore wave input, water surface elevation, characteristic median grain diameter, and initial beach profile. This fundamental information is critical to the model and every effort must be made to obtain the most accurate data possible for model input. Additional inputs for more sophisticated simulations include incident wave angle, wind speed and direction, specification of seawall location and properties, specification of a beach fill, and measured profile (for calibration and comparison). A user interface developed for the personal computer makes the model easier to use and facilitates the organization of the input data. Description of the user interface and guidelines for the content and formatting of the model input are described in the SBEACH user's manual (Rosati et al. 1993).

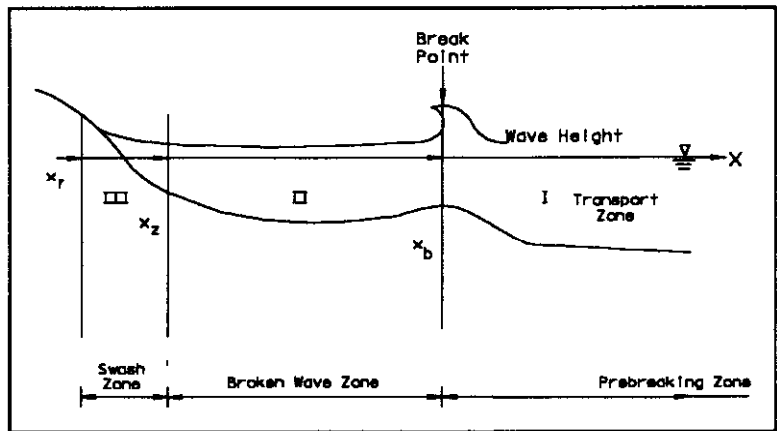


Figure 1 Principle zones of cross-shore transport

Model Output: SBEACH provides various levels of output for the user to choose from for use in project evaluation. Intermediate and final profiles are available for visual inspection, volume calculations, and further analysis. Some additional analysis is internally offered by the model and generally consists of the magnitude and location of maximum erosion, the landward-most occurrence of specified amounts of vertical erosion, and the horizontal recession of given contours. The output offered by SBEACH is designed to aid the coastal engineer in determining the response of the beach profile to a specified storm condition, and is geared towards providing useful information for economic analysis of various project alternatives.

PROJECT APPLICATION

General: As previously mentioned, the typical project evaluation using SBEACH involves simulating the beach response to a series of storms to determine the economic merits of a beach fill project. Several considerations should be made by the coastal engineer before applying the model to a given beach. First, the modeler should evaluate how well the project beach fits the assumptions made in the development of the model. Primarily, the user should consider the role of longshore transport in the evolution of the beach profile. General indicators of possible longshore transport gradients may include one or more of the following: shorelines that are not straight, nearby jetties, offshore structures that disrupt the wave field, presence of a groin field, nearby inlet, or bathymetric features that either focus or scatter wave energy.

Following the initial assessment of how well the project beach fits SBEACH's assumptions, the model should be carefully calibrated to a high-quality data set consisting of pre- and post-storm profile surveys, and wave and water-level time histories of a previous storm. As an alternative, data from a nearby, representative beach may be used. Calibration should start by running the model with the default calibration parameters and proceed by trial-and-error iteration until the best agreement between the simulated and measured post-storm data is achieved. If possible, a second data set from a different storm should be used to provide a verification of the initial calibration. In many cases, the modeler is faced with a situation in which no data sets are available for calibration. In these cases, use of the default calibration parameters is recommended.

The next step in a typical project evaluation is determination of a representative set of storms for a given area. Storms are typically characterized by maximum wave height, peak storm surge, and storm duration. Storms for a given site can be selected from historical databases or hindcasts, or synthetically generated using statistically derived frequency-of-occurrence relationships for peak storm parameters. Upon calibration of the model and selection of representative storms, the model is prepared to simulate beach profile response to these storms.

The critical evaluation of the results of a suite of simulations is perhaps the most crucial step in the project evaluation. Interpretation of the model results involves consideration of the assumptions, limitations, and tendencies of SBEACH as well as the limitations and possible variability of the input data and how the combination of these two sources of error affect the simulated results. The engineer/modeler should understand that a certain degree of error may be present due to the above factors and this error should be accounted for by design safety factors in the plan of action for the project.

Field Case (Dewey Beach, Delaware): A recent evaluation of the performance of SBEACH on a group of field cases (Wise, Smith, and Larson in preparation) involved the simulation of beach profile response to a northeaster which struck the Delaware coast on 10 December 1992. Dewey Beach, a developed beach located on the Atlantic coast of Delaware, features substantial berms backed by dunes with a typical crest elevation of +5.0 meters NGVD and a median sediment grain size of 0.33 mm. Pre- and post-storm profiles are available for the storm event and were measured on 29 October and 18 December, respectively. Wave data were collected by a wave gauge located at a depth of 9.1 m offshore of the coast of Dewey Beach and water-level data were collected by a tide gauge at Lewes, Delaware (USACE Philadelphia District 1995). A time-history plot of these wave and water surface data is presented in Figure 2. The elevated wave heights and storm surge indicated in this figure are the main influences on the erosion of the beach profiles at Dewey Beach.

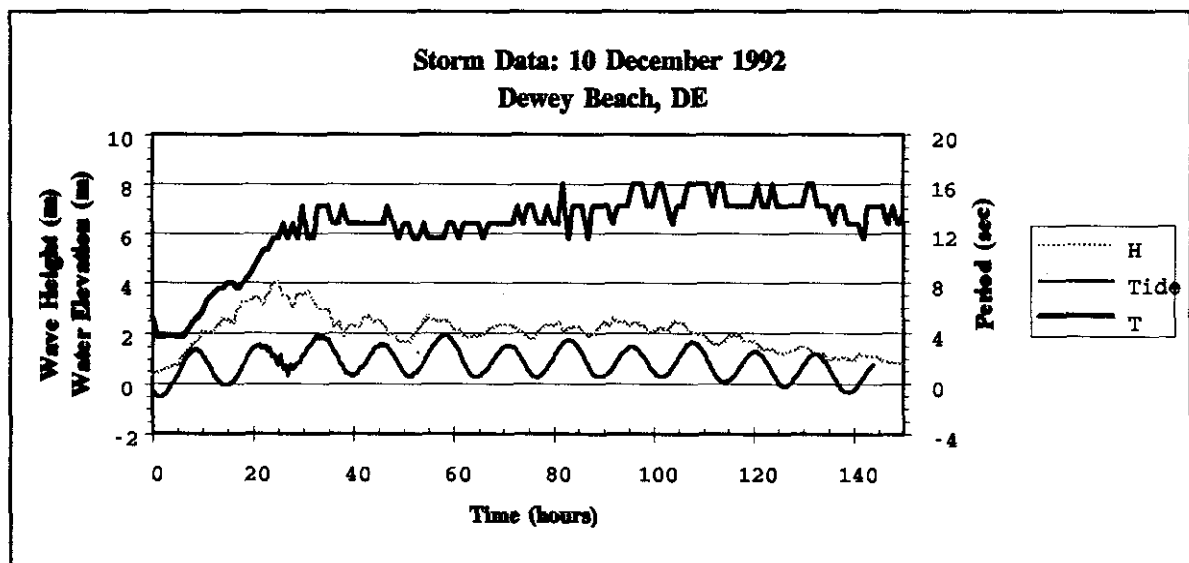


Figure 2 Storm data for the 10 December 1992 northeaster at Dewey Beach, Delaware

Profile Comparisons: The SBEACH simulations of the profile responses at Dewey Beach demonstrate some of the model's capabilities and limitations. Figures 3, 4, and 5 present the results of simulations using the default calibration parameters at Dewey profile survey lines 140, 220, and 240, respectively. These figures indicate that the model accurately simulates the erosion of the foreshore and dune which are parameters of primary concern to the USACE for beach fill design evaluation. Another significant point is that the model performed well in the simulation of overwash and erosion of the berm (Figures 3 and 5).

Also noted in the model results are the differences between the measured and simulated bars. The simulated profiles tend to have a bar which is located further offshore than the measured bar. A possible explanation of the differences in the position of the simulated and measured post-storm bar lies in the fact that there was a time lapse between the

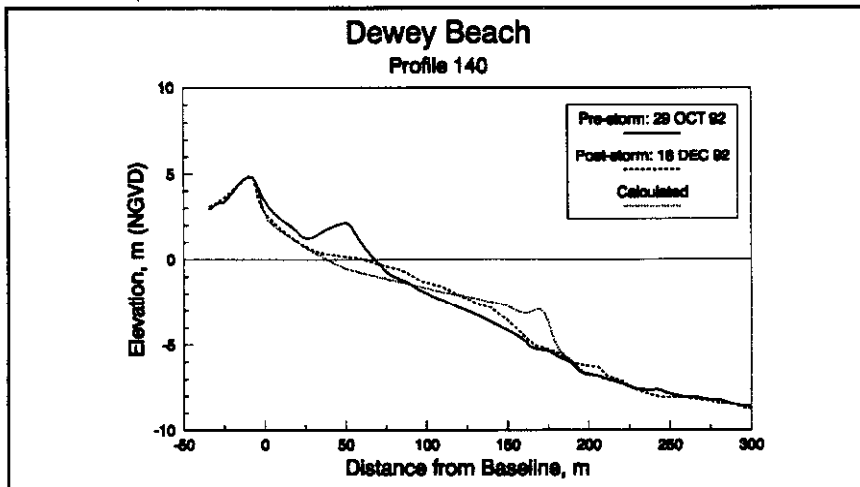


Figure 3 Result of SBEACH simulation (Profile 140, Dewey Beach, DE)

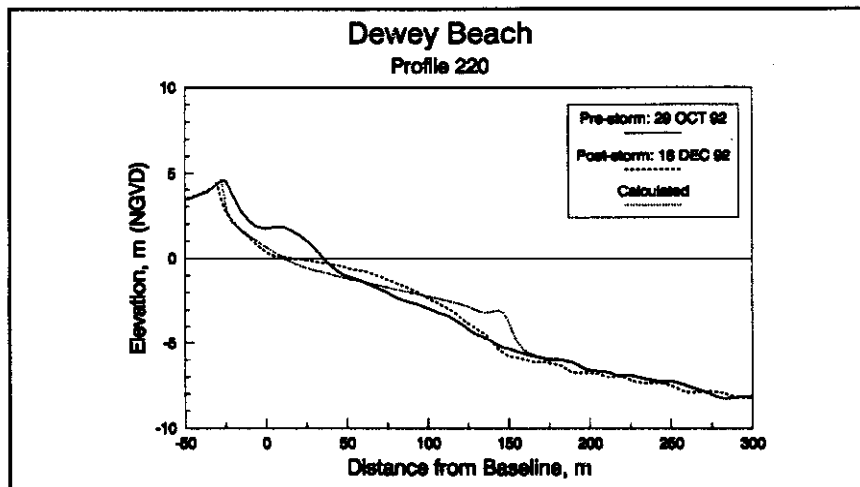


Figure 4 Result of SBEACH simulation (Profile 220, Dewey Beach, DE)

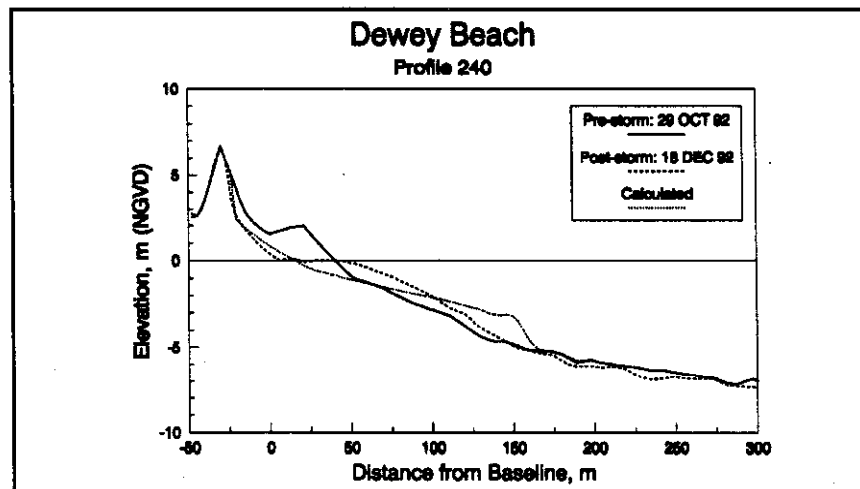


Figure 5 Result of SBEACH simulation (Profile 240, Dewey Beach, DE)

end of the storm and the measurement of the post-storm profile. During this period, the beach profile began to recover through accretionary processes. Therefore, the position of the breakpoint bar is shifted shoreward and does not allow a direct comparison to the model (at the present time SBEACH does not model accretionary processes). None-the-less, the post-storm profile surveys capture the eroded conditions of the foreshore and dune and indicate that the model provides accurate estimates of the erosion of the foreshore and dune.

Other Comparisons: Another means of evaluating model performance not as subjective as visual comparison of the profiles is comparing measures of erosion commonly used by coastal engineers in evaluating projects. Measures of erosion used in the evaluation of the model are (1) the volumetric change above the reference datum, (2) storm intrusion, and (3) the recession of a specified contour. Comparisons of the measures of erosion for the measured and simulated profiles will be presented for the entire data set at Dewey Beach, Delaware.

Volumetric change above the reference datum provides an estimate of the erosion that occurs above sea level. This measure quantifies the amount of berm and dune erosion during the storm. Figure 6 indicates that the simulated and measured volumetric change above the NGVD reference datum are quite similar.

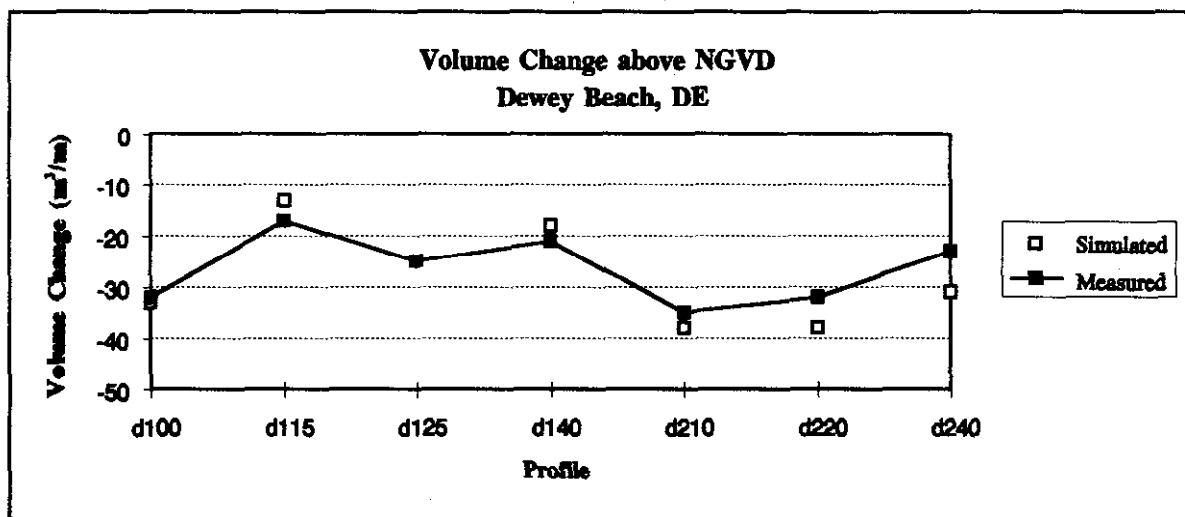


Figure 6 Comparison of measured and simulated volumetric change above the NGVD reference datum

Determination of storm intrusion offers engineers a measure of the landward extent of storm damage related to foundation undermining of coastal structures. By specifying an amount of erosion that would typically cause a foundation failure, the user can estimate losses due to foundation undermining. Figure 7 indicates close agreement between the measured and simulated landward-most occurrence of significant erosion (in this case significant erosion is defined as any amount of vertical erosion greater than or equal to 0.3 meters). All calculated results of storm intrusion are within 5% of the measured values for this data set.

The final measure of erosion is the measure of contour recession during the storm. This measure consists of defining the location of a specified contour prior to a storm, and computing the landward recession of that contour's position due to the effect of erosive wave conditions. Figure 8 shows that the +1.5 meter contour receded approximately 35-40 meters during the storm. The simulated and measured recession of the contour are in close agreement, once again with a maximum variation close to 5%.

ADDITIONAL MODEL DEVELOPMENT

Identification of Areas of Further Research: Since the initial development of SBEACH in 1986, improvements and enhancements have been added to the model. As the model continues to develop, areas of improvement are identified and recommended for further study.

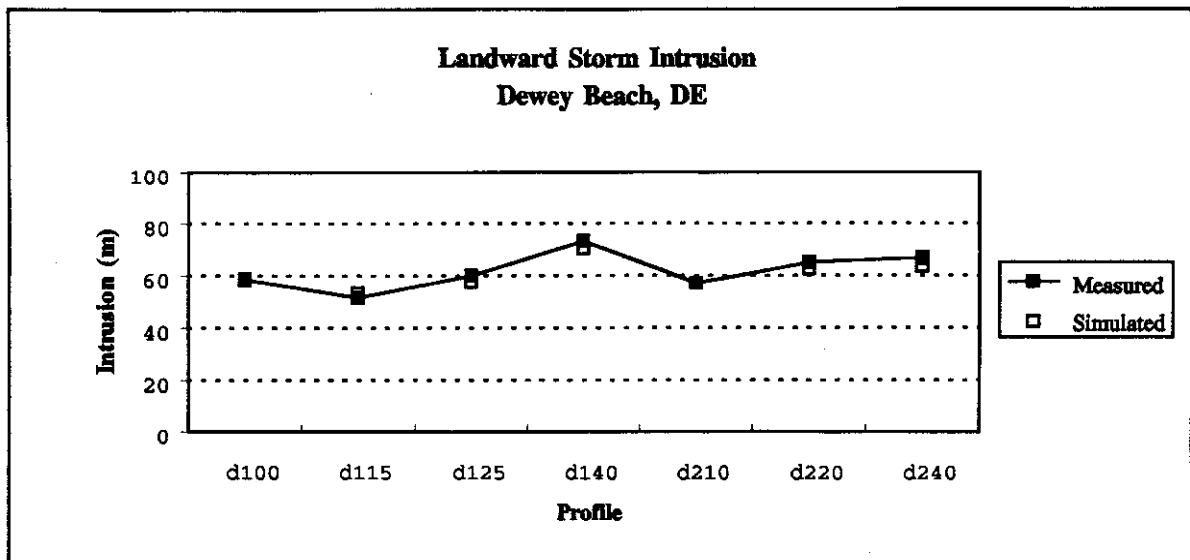


Figure 7 Comparison of measured and simulated storm intrusion. Significant erosion = 0.3 m.

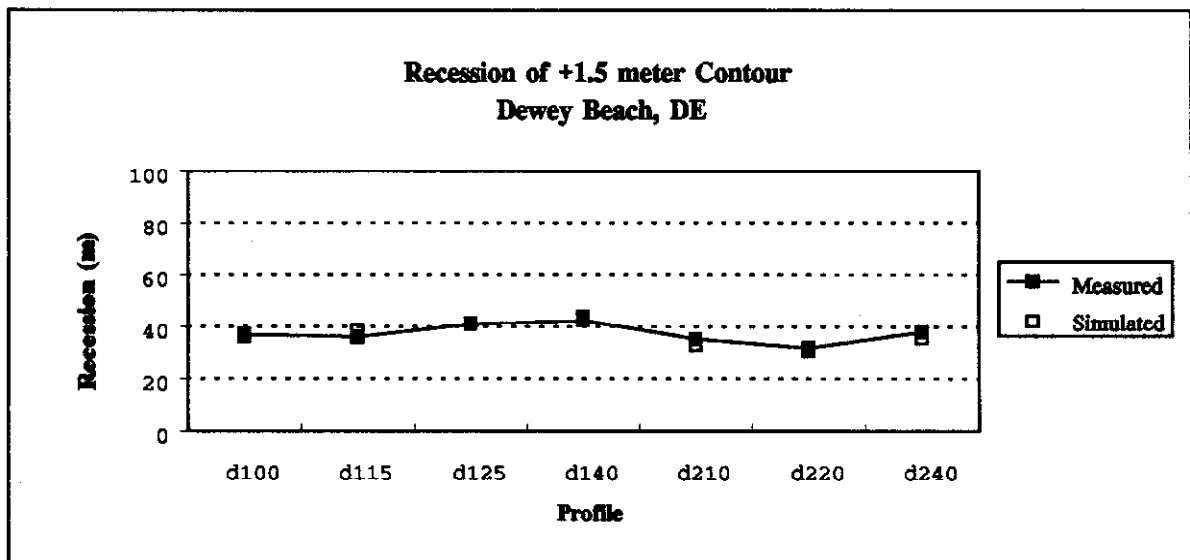


Figure 8 Comparison of measured and simulated recession of the +1.5 meter contour.

Recent enhancements to SBEACH include the addition of a dune overwashing routine. Although the routine performs well for some field cases, an improved description of foreshore sediment transport processes and dune overwash is required to better model details of beach response for a wide range of storm conditions and profile configurations.

Another issue that will potentially offer a significant improvement to SBEACH is modeling of the accretionary processes that are responsible for recovery of a beach profile after a storm. Although approximations of accretionary transport are possible with the present version of SBEACH, the accretionary transport calculations are not performed due to the qualitative nature of the results. Use of existing data sets of LWT experiments that physically model accretionary processes may allow the development of quantitative expressions for numerical modeling of accretionary transport processes.

SBEACH's requirement of a single representative grain size for the entire beach profile does not adequately describe some beach profiles. The ability to specify variable grain sizes across the beach profile would be valuable for situations in which the grain sizes of a beachfill are significantly different from the native material. In order to

accomplish this, a method of grain tracking would have to be incorporated into the model to determine the fate of grains transported along the profile.

CONCLUSION

SBEACH has proven to be a useful tool for coastal engineers in the design of beach fills and in assessment of the degree of storm protection that a given beach dune-berm configuration offers adjacent structures. The model has been demonstrated to accurately model the erosion of the dune and foreshore using a number of laboratory and field data sets (Wise, Smith, and Larson in preparation). Due to limits in both accuracy and completeness of input data combined with incomplete knowledge of foreshore and dune overwashing processes, SBEACH should not be expected to produce the same degree of accuracy exhibited in the Dewey Beach case study for all applications. Continued research into cross-shore sediment transport processes including dune overwash foreshore processes, and accretionary processes will enable continued development of SBEACH's capabilities.

ACKNOWLEDGMENTS

The work presented in this paper was performed as a part of the "Calculation of Cross-Shore Sediment Transport and Beach Profile Change" work unit of the Coastal Research Program conducted by the Coastal Engineering Research Center (CERC), U.S. Army Engineer Waterways Experiment Station. This manuscript benefitted from the reviews of Bruce A. Ebersole, Mark B. Gravens, David G. Hamilton, and Julie D. Rosati. Permission was granted by the Chief of Engineers to publish this information.

REFERENCES

- Dally, W.R., Dean, R.G., and Dalrymple, R.A., 1985, Wave Height Variation Across Beaches of Arbitrary Profile. *Geophysical Res.*, 90(6), 11917-11927.
- Larson, M., Kraus, N.C., 1989, SBEACH: Numerical Model for Simulating Storm-Induced Beach Change; Report 1: Empirical Foundation and Model Development, Technical Report CERC-89-9, Coastal Engineering Research Center, U.S. Army Engineer Waterways Experiment Station, Vicksburg, MS.
- Larson, M., Kraus, N.C., and Byrnes, M.R., 1990, SBEACH: Numerical Model for Simulating Storm-Induced Beach Change; Report 2: Numerical Formulation and Model Tests. Technical Report CERC-89-9, Coastal Engineering Research Center, U.S. Army Engineer Waterways Experiment Station, Coastal Engineering Research Center, Vicksburg, MS.
- Larson, M., 1995, Model for Decay of Random Waves in Surf Zone. *Journal of Waterway, Port, Coastal, and Ocean Engineering*, 121(1), 1-12.
- Rosati, J.D., Wise, R.A., Kraus, N.C., and Larson, M., 1993, SBEACH: Numerical Model for Simulating Storm-Induced Beach Change; Report 3: User's Manual. Technical Report CERC-89-9, Coastal Engineering Research Center, U.S. Army Engineer Waterways Experiment Station, Vicksburg, MS.
- U.S. Army Engineer District, Philadelphia, 1995, Delaware Coast from Cape Henlopen to Fenwick Island, Rehoboth Beach/Dewey Beach Interim Feasibility Study, Draft Feasibility Report and Draft Environmental Impact Statement, April.
- Wise, R.A., Smith, S.J., and Larson, M., In Preparation, SBEACH: Numerical Model for Simulating Storm-Induced Beach Change; Report 4: Cross-Shore Transport Under Random Waves and Model Validation with SUPERTANK and Field Data. Tech. Rep. CERC-89-9, Coastal Engineering Research Center, U.S. Army Engineer Waterways Experiment Station, Vicksburg, MS.

AN INQUIRY OF METHOD CALCULATING FOR TIME MEAN SEDIMENT DISCHARGE

By Niu Zhan, Senior Engineer, Bureau of Hydrology, YRCC, MWR, 2 Chengbei Road, Zhengzhou, Henan, China; Ma Qingyun, Senior Engineer, Bureau of Hydrology, YRCC, MWR, Zhengzhou, Henan, China.

Abstract: In this paper, starting from a point that discharge and sediment concentration change linearly, sediment discharge should change in quadric, we use an integral method to derive an equation calculating sediment discharge at a time interval, which has a practical significance in both theory and engineering.

Let the discharges and sediments at times t_i and t_{i+1} respectively are q_i, q_{i+1} and ρ_i, ρ_{i+1} , then the corresponding sediment discharge are $Q_{s1} = q_i \rho_i, Q_{s2} = q_{i+1} \rho_{i+1}$. If a sediment discharge is considered to change linearly as time passes, the mean sediment discharge at the time interval $t_i \sim t_{i+1}$ is given by

$$Q_{s1} = \frac{1}{2}(q_i \rho_i + q_{i+1} \rho_{i+1}) \quad (1)$$

Another way of thought is to use the product of the mean discharge $\frac{1}{2}(q_i + q_{i+1})$ and mean sediment concentration $\frac{1}{2}(\rho_i + \rho_{i+1})$ at a time interval $t_i \sim t_{i+1}$ as the mean sediment discharge at the time interval, i. e. ,

$$\begin{aligned} Q_{s2} &= \frac{1}{2}(q_i + q_{i+1}) \cdot \frac{1}{2}(\rho_i + \rho_{i+1}) \\ &= \frac{1}{4}(q_i \rho_i + q_i \rho_{i+1} + q_{i+1} \rho_i + q_{i+1} \rho_{i+1}) \end{aligned} \quad (2)$$

Factually, if the discharge and sediment concentration at the time interval $t_i \sim t_{i+1}$ are considered to change linearly, the sediment discharge should be described by a quadratic function. Let the linear changes of discharge and sediment concentration at the time interval $t_i \sim t_{i+1}$ be expressed by

$$\left. \begin{aligned} q &= q_i + k_q t \\ \rho &= \rho_i + k_\rho t \end{aligned} \right\} \quad (3)$$

in which $k_q = (q_{i+1} - q_i) / (t_{i+1} - t_i), k_\rho = (\rho_{i+1} - \rho_i) / (t_{i+1} - t_i)$.

Then the mean sediment discharge at the time interval $t_i \sim t_{i+1}$ is the ratio of time integral of $q\rho$ to the corresponding time $t_{i+1} - t_i$; For the integral, the lower limit is $t_i - t_i = 0$ and the upper limit is $t_{i+1} - t_i$, i. e. ,

$$Q_{s3} = \frac{1}{t_{i+1} - t_i} \int_{t_i - t_i}^{t_{i+1} - t_i} q \rho dt$$

By introducing equation (3) and integrating, we get

$$Q_{s3} = \frac{1}{3}(q_i \rho_i + q_{i+1} \rho_{i+1}) + \frac{1}{6}(q_i \rho_{i+1} + q_{i+1} \rho_i) \quad (4)$$

When a day is divided into n time intervals, Δt_j hours each time interval, the equations calculating a daily mean sediment discharge by using the three methods above mentioned are respectively

$$Q_{d1} = \frac{1}{24} \sum_{j=1}^n Q_{s1j} \Delta t_j = \frac{1}{48} \sum_{j=1}^n [(q_i \rho_i + q_{i+1} \rho_{i+1}) \Delta t_j] \quad (5)$$

$$Q_{d2} = \frac{1}{24} \sum_{j=1}^n Q_{s2j} \Delta t_j = \frac{1}{96} \sum_{j=1}^n [(q_i + q_{i+1})(\rho_i + \rho_{i+1}) \Delta t_j] \quad (6)$$

$$Q_{i3} = \frac{1}{24} \sum_{j=1}^3 Q_{i3j} \Delta t_j = \frac{1}{72} \sum_{j=1}^3 [(q_i \rho_i + q_{i+1} \rho_{i+1}) \Delta t_j] + \frac{1}{144} \sum_{j=1}^3 [(q_i \rho_{i+1} + q_{i+1} \rho_i) \Delta t_j] \quad (7)$$

(4) and (7) are the results we derived. Their theoretical logics are reasonable. They are very suitable for the calculation of the sediment discharge during flood of the Yellow River, in which the sediment discharge changes violently. When taking the value of (4) as a standard, for a same time interval, the calculation errors of (1), (2) are respectively

$$\Delta_{1-3} = \frac{1}{6} (q_i \rho_i + q_{i+1} \rho_{i+1} - q_i \rho_{i+1} - q_{i+1} \rho_i) \quad (8)$$

$$\Delta_{2-3} = -\frac{1}{12} (q_i \rho_i + q_{i+1} \rho_{i+1} - q_i \rho_{i+1} - q_{i+1} \rho_i) \quad (9)$$

See that the value of absolute error depends on the values of $(q_i \rho_i + q_{i+1} \rho_{i+1})$ and $(q_i \rho_{i+1} + q_{i+1} \rho_i)$. Using (3) to eliminate q_{i+1} and ρ_{i+1} yields

$$q_i \rho_i + q_{i+1} \rho_{i+1} = 2q_i \rho_i + (q_i k_{\rho_i} + \rho_i k_{q_i})(t_{i+1} - t_i) + k_{q_i} k_{\rho_i} (t_{i+1} - t_i)^2 \quad (10)$$

$$q_i \rho_{i+1} + q_{i+1} \rho_i = 2q_i \rho_i + (q_i k_{\rho_i} + \rho_i k_{q_i})(t_{i+1} - t_i) \quad (11)$$

Subtracting (10) and (11) at equations both side yields

$$(q_i \rho_i + q_{i+1} \rho_{i+1}) - (q_i \rho_{i+1} + q_{i+1} \rho_i) = k_{q_i} k_{\rho_i} (t_{i+1} - t_i)^2 \quad (12)$$

From (12), find that if K_q and K_ρ are simultaneously greater or less than zero, i. e., if discharge q and sediment concentration ρ change in the same direction, $K_q K_\rho (t_{i+1} - t_i)^2 > 0$; then the Δ_{1-3} of the (8) is positive (being to great) and the Δ_{2-3} of the (9) is negative (being to small). Factually, the processes of water and sediment almost change simultaneously, so generally, the result of (1) is great systemic, the result of (2) is small systemic. A checking computation with data from some stations has verified this point.

When computing suspended sediment, for such a time interval $t_i \sim t_{i+1}$, sometimes sediment discharge during the first half and second half of the time interval must be obtained. In the past, a simplified method was often used. After obtaining the mean sediment discharge at the time interval $t_i \sim t_{i+1}$, sediment discharge W_{sh} and W_{sh} during the first half and second half of the time interval are computed by using an equally dividing method, i. e.,

$$W_{sh} = W_{sh} = \frac{1}{2} Q_{i3} (t_{i+1} - t_i) \quad (13)$$

At the time interval $t_i \sim t_{i+1}$, when discharge q and sediment concentration ρ change linearly, the sediment discharge does not change linearly. So (13) use the equally dividing method to compute the sediment discharge during a half time interval that is not suitable, the reasonable computation should be integral method.

Suppose (3) is still suitable and the middle point of times t_i and t_{i+1} is $(t_i + t_{i+1})/2$. When taking t_i as a starting point, the mean sediment discharge Q_{i3sh} during the first half of the time interval $t_i \sim t_{i+1}$ is a ratio of the time integral of $q\rho$ to the corresponding time interval $\frac{1}{2}(t_{i+1} - t_i)$; For the integral, the lower limit is $t_i - t_i = 0$ and the upper limit is $(t_i + t_{i+1})/2 - t_i = \frac{1}{2}(t_{i+1} - t_i)$. The mean sediment discharge Q_{i3sh} during the second half time interval is the ratio of the time integral of $q\rho$ to the corresponding time interval $(t_{i+1} - t_i)/2$; For the integral, the lower limit is $(t_i + t_{i+1})/2 - t_i = (t_{i+1} - t_i)/2$ and the upper limit is $t_{i+1} - t_i$.

$$Q_{i3sh} = \frac{1}{\frac{1}{2}(t_{i+1} - t_i)} \int_{t_i - t_i}^{\frac{1}{2}(t_i + t_{i+1}) - t_i} q \rho dt$$

$$Q_{s3h} = \frac{1}{\frac{1}{2}(t_{i+1} - t_i)} \int_{\frac{1}{2}(t_i + t_{i+1}) - t_i}^{t_{i+1} - t_i} q \rho dt$$

Introducing (3) yields

$$Q_{s3q} = \frac{7}{12}q_i\rho_i + \frac{1}{6}(q_i\rho_{i+1} + q_{i+1}\rho_i) + \frac{1}{12}q_{i+1}\rho_{i+1} \quad (14)$$

$$Q_{s3h} = \frac{1}{12}q_i\rho_i + \frac{1}{6}(q_i\rho_{i+1} + q_{i+1}\rho_i) + \frac{7}{12}q_{i+1}\rho_{i+1} \quad (15)$$

Then at the time interval $t_i \sim t_{i+1}$, the mean sediment discharge during the first half and second half of the time interval are respectively

$$W_{s3q} = Q_{s3q} \left(\frac{t_i + t_{i+1}}{2} - t_i \right) = \frac{1}{2} Q_{s3q} (t_{i+1} - t_i) \quad (16)$$

$$W_{s3h} = Q_{s3h} \left(t_{i+1} - \frac{t_i + t_{i+1}}{2} \right) = \frac{1}{2} Q_{s3h} (t_{i+1} - t_i) \quad (17)$$

Clearly, $W_{s3q} + W_{s3h}$ obtained by respectively introducing (14), (15) into (16), (17) is equal to the product of Q_{s3q} of (4) and $(t_{i+1} - t_i)$, which accords with the mass-conservation principle. But, generally, W_{s3q} in (16) and W_{s3h} in (17) are not equal to the corresponding quantities in (13).

In the computation of suspended sediment, discharge and sediment concentration at a time interval are always dealt with changing linearly; So the sediment discharge at the time interval should be dealt with changing in quadric, which is the engineering significance of the study in this paper.

SEDIMENT TRANSPORT MODELING FOR THE GLEN-COLUSA IRRIGATION DISTRICT FISH SCREEN MODIFICATIONS

By Cassie Klumpp, Hydraulic Engineer, Mark Sailer, Civil Engineer, Arthur Glickman, Civil Engineer and Brent Mefford, Hydraulic Engineer, Technical Service Center, U.S. Bureau of Reclamation, Denver, Colorado

INTRODUCTION

The Glen-Colusa Irrigation District (GCID) pumping plant is located on an oxbow of the Sacramento River approximately 100 miles north of Sacramento. (Figure 1). The existing fish screen facilities do not meet current regulatory requirements and contribute to increased fish mortality. Fish in the intake channel may be subject to predation, and smaller fish may be impinged on the screens. The Bureau of Reclamation was authorized to provide feasibility and final design work for the replacement of the fish screen. The facilities designed by Reclamation will allow GCID to operate the pumping plant at or near its full capacity of 3000 ft³/s.

Sediment management issues were an important consideration in the design and location of the fish screen facilities. GCID dredges the intake channel and area in front of the existing screens following winter and spring runoff. Sediment buildup in front of the screens can exceed 3 ft annually and can exceed 9 ft. at the intake channel entrance.

Three design alternatives (A, B & D) were considered for the fish screen structures. These alternatives mainly differed in the location of the fish screens (Figure 2). Alternative A, located north of the forebay of the existing plant, consisted of multiple V screens upstream from the existing fish screens, a log boom, a pump back structure an upstream and downstream check structure, and two fish return pipelines. Alternative B consisted of multiple "V" screens located near the main river and intake channel flow split and would include a fish screen structure, a log boom, a pumpback structure and evaluation facility, and two fish return pipelines. The intake channel included an expansion of approximately 65 ft. to accommodate the screens for Alternative B. Alternative D involves extending the existing screen 660 ft. upstream with a trashrack structure and a downstream check structure, pumpback structure, and two fish return pipelines. A second version of D would allow up to 1000 ft³/s in the bypass channel and would exclude the pumpback structure and fish return pipelines. Flow through the bypass bay and pipes would be by gravity to the bypass channel.

The three alternatives were grouped into 2 options for sediment modeling based on the location of the fish screens and pumps. Alternative A and D were grouped together because they are located near the existing pump station. Alternative B was analyzed separately because it is located near the river and intake channel.



Figure 1-Location of the Glen Colusa Irrigation District Pumping Plant and Fish Screen Facilities

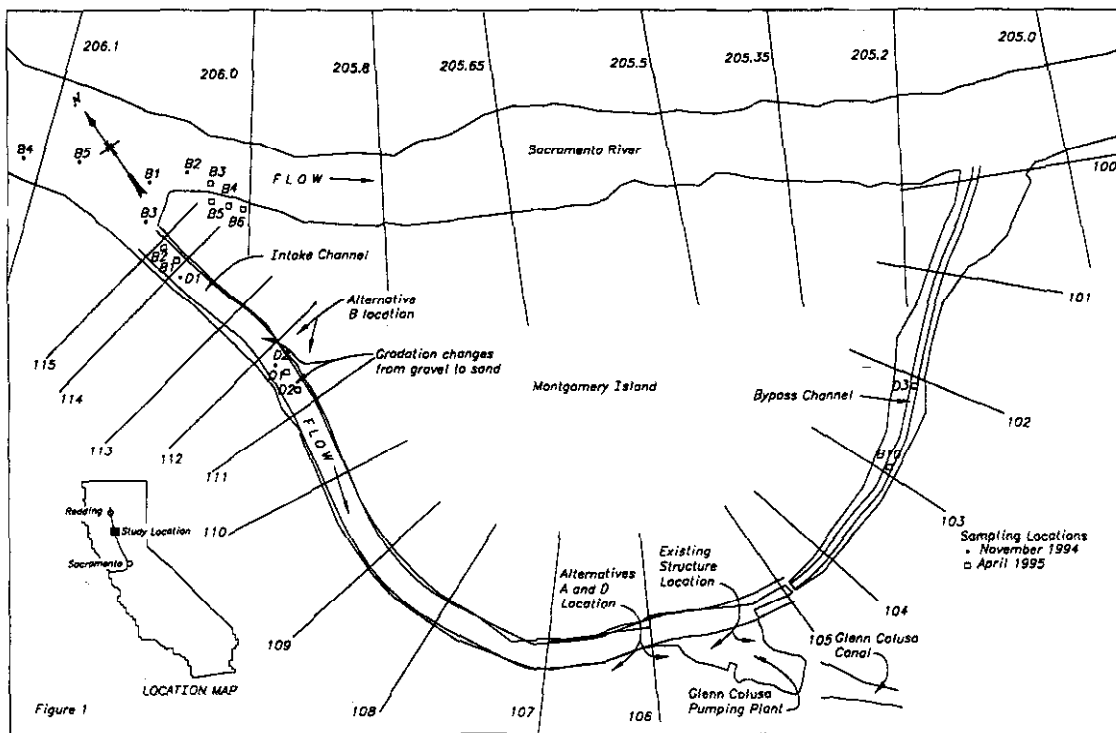


Figure 2-Location of the Alternatives and Sampling Sites

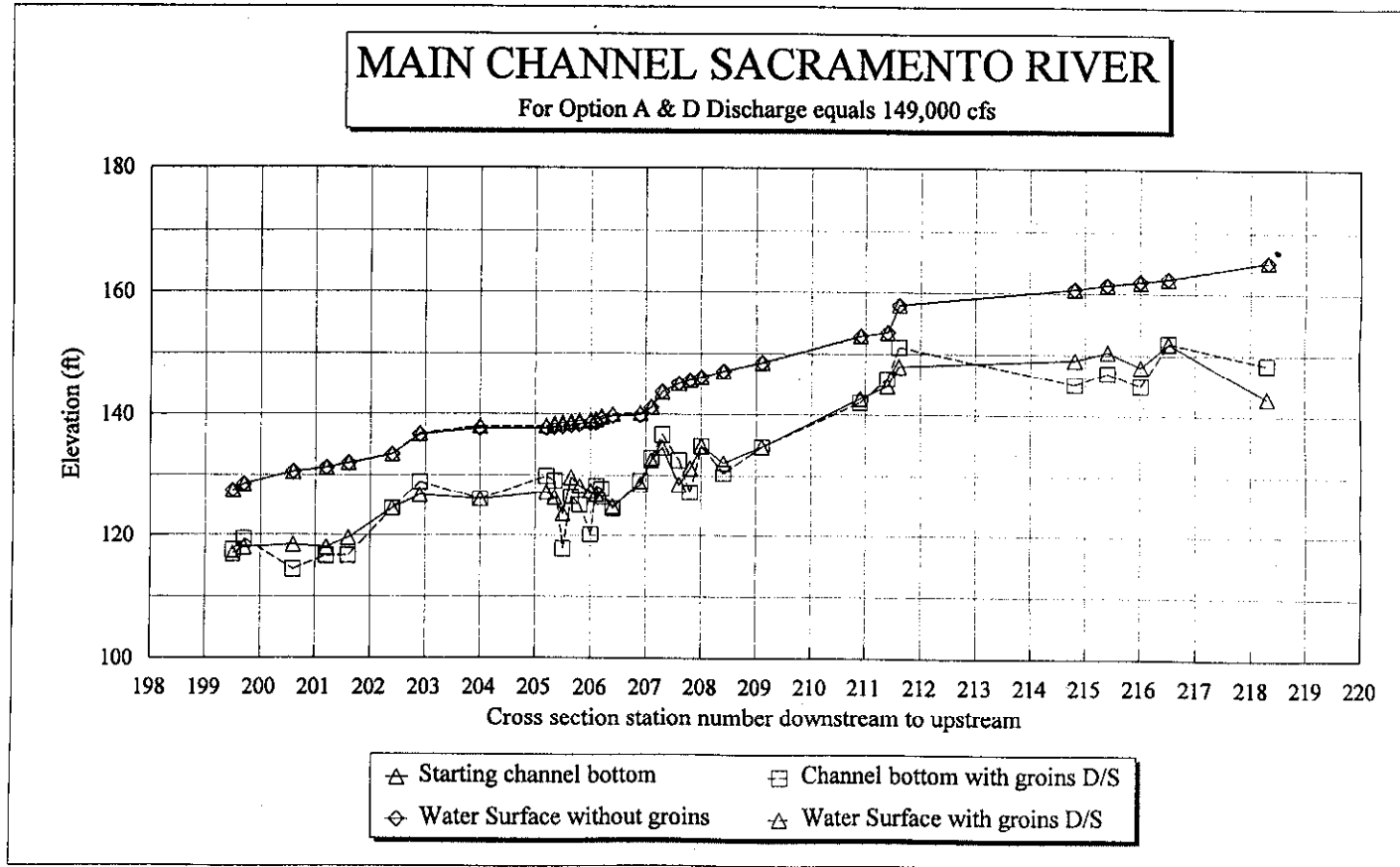


Figure 3-Changes in water surface profiles and bed elevations for the Main Channel of the Sacramento River with and without the presence of groins.

SEDIMENT MODEL

A sediment model of the Sacramento River between river miles 218.3 and 199.5 was developed for the Glen Colusa Irrigation District using a sediment model (HEC6-T) created by William A. Thomas (1994). This is a new version of HEC-6 with many enhancements. This model can handle complex flow situations including flow around islands, networks including tributary flow and diversions. This model can also simulate dredging. A variable sediment distribution coefficient can be used in the model to allow different sediment loads entering the intake and bypass channel depending on the quantity of flow in the river. Groins or spur dikes located either upstream or downstream of the intake channel were included in the sediment modeling options to see if sediment deposition in the intake channel would be reduced.

Model Calibration Estimated river cross-sections and bottom elevations were available from measured data and from previous model results of the same river reach. The U.S. Army Corps of Engineers (Corps, 1983) modeled the entire Sacramento River in 1982. Ayres Engineering previously known as Water Resources & Technology (Water Engineering and Technology, 1988a) had also modeled this reach of the river in 1989. GCID collected intake channel and bypass channel water surface and bed elevation data between 1980 and 1995. These data were used to validate that the predicted model elevations and dredge volumes were close to existing conditions for a low, normal, and flood year.

A six year hydrograph (1965, 1966, 1970, 1982, 1983 and 1984) was used in the sediment model. Peak flows varied between 70,000 ft³/s and 149,000 ft³/s. The peak flow value of 149,000 ft³/s lies between the 5 and 10 year flood. Manning's n values ranged from 0.035 to 0.045 for the main river and 0.025 to 0.055 for the intake channel and bypass channel. Overbank roughnesses varied from 0.06 to 0.12.

Upstream gradation and supply curves were originally developed by the Corps from Bend Bridge to Gianella Bridge. Ayres Engineers developed a supply curve from Woodson Bridge to Gianella Bridge (river miles 218 through 199.5) that was used in the present model. Minor modifications were made to the supply curve to reduce sediment accumulations at the first two cross-sections. The supply was extended to estimate sediment supply for flows up to 150,000 ft³/s.

Bed material gradations were measured by Water Engineering and Technology (1988b) using Wolman Counts. Additional samples were collected using the barrel sample method developed by (Milhouse et al, 1995) by the USBR in November 1994 and April 1995 in the intake channel, bypass channel and the north end of Montgomery Island. All bed gradations were close to previous samples collected on the river.

Three sediment transport equations were tested during the model calibration: Toffaleti (1966)-Schoklitsch (1930), Toffaleti-Meyer-Peter and Muller (1948) and Yang (1984) Sand and Gravel (Thomas, 1994). The Toffaleti and Schoklitsch combination was eliminated

because of the large sediment transport loads predicted by the equation causing large bed elevation fluctuations that choked off flow to the intake channel. The Toffaleti and Meyer-Peter and Muller combinations also over predicted gravel transport rates. The Yang Equation provided the most reasonable results for the conditions on the Sacramento River.

Model Results Model simulations were made for the A&D Alternative and for the B Alternatives for low, normal and high flows to show the effect on sediment deposition on the intake and bypass channel. Groins were placed either downstream or upstream of the intake channel on the main stem of the Sacramento River between river miles 205.5 and 206 for 3000 ft. Groins were set to a width of approximately one third the channel and to the approximate height of the river bank.

Additional simulations were made with the groins in place to determine if there was any reduction in sediment accumulations or dredge volumes and to see if the changes in bed elevation profiles were reduced. Figure 3 shows a comparison of water surface elevation and bed profiles for the main channel for the A&D Alternative with and without groins during a high flow year. Very little sediment is transported in the Sacramento River until flows exceed the two year flood. Consequently changes in dredge volumes and bed elevations are more apparent for the larger discharge year. Figure 4 shows a comparison of water surface elevations and bed profiles for the A&D Alternative for the Intake and Bypass Channels with and without groins for a high flow year. Bed elevations of the intake channel are reduced by approximately 1 foot with the inclusion of groins. Figure 5 shows a comparison of water surface elevations and bed profiles in the intake channel for the B Alternative with and without groins for a high flow year. Bed elevations increase by approximately 4 ft. for the B Alternative at Station 112 in comparison to the A&B Alternative because of the channel expansion to accommodate the fish screen facility.

Table 1 shows the changes in dredge volumes for low and high flow years for the A&D Alternative and the B Alternative with and without the presence of groins. During a high flow year dredge volumes are not significantly reduced with the addition of groins for the A&D Alternative. However, two things are different with the B Alternative. The volume of sediment accumulated in the intake channel increases significantly for this alternative. Secondly, groins do cause a reduction in the dredge volumes for the B Alternative during a high flow year. Dredge volumes are reduced by about 30 percent for the B Alternative with groins present in the river downstream of the intake channel.

Table 1- Sediment accumulation in the intake channel and bypass channel

	Groins present for 70,600 ft ³ /s-af	Groins not present for 70,600 ft ³ /s -af	Groins present D/S for 149,000 ft ³ /s-af	Groins not present for 149,000 ft ³ /s-af
Alternative A&D	14,200	16,300	94,100	124,200
Alternative B	20,700	19,100	111,200	143,900

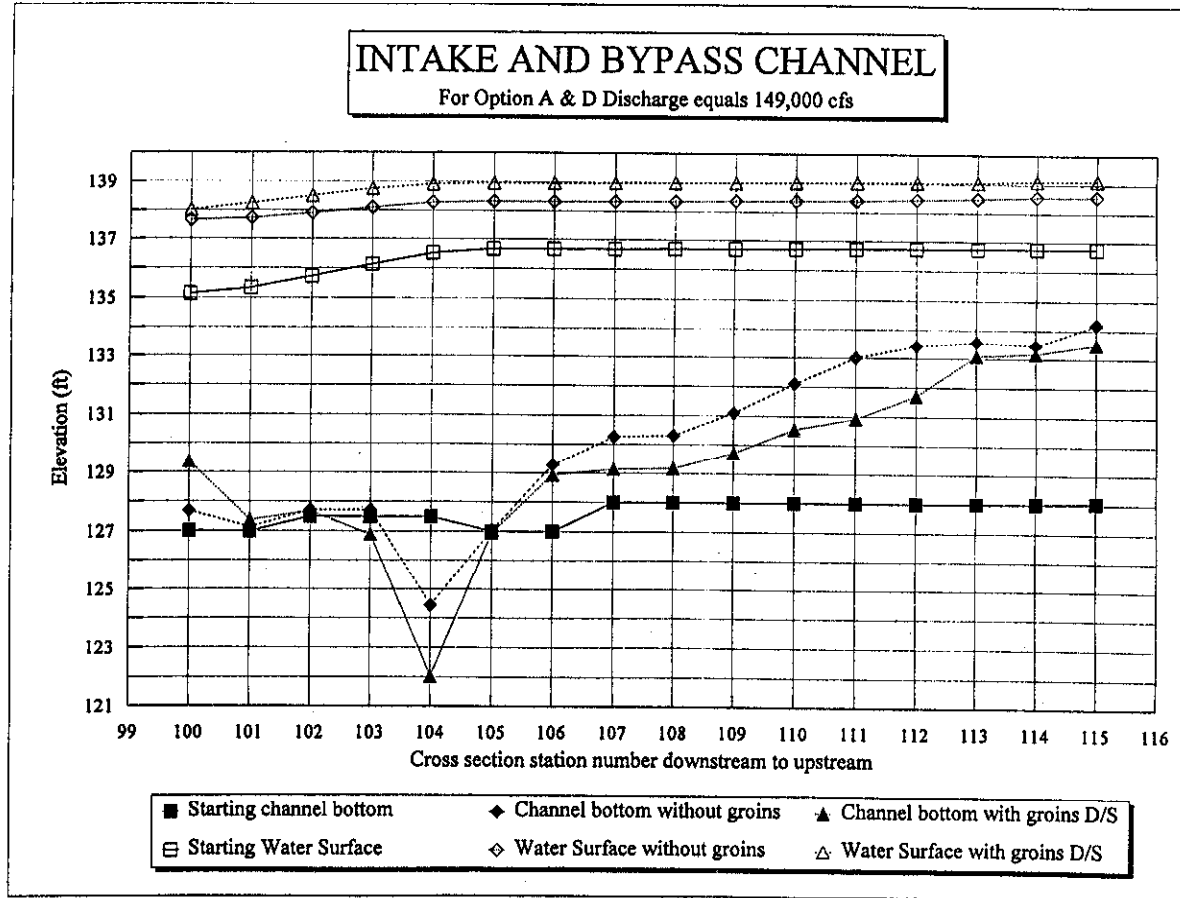


Figure 4-Changes in water surface elevations and bed elevation for the Intake and Bypass Channel, A&D Alternative, with and without the presence of groins

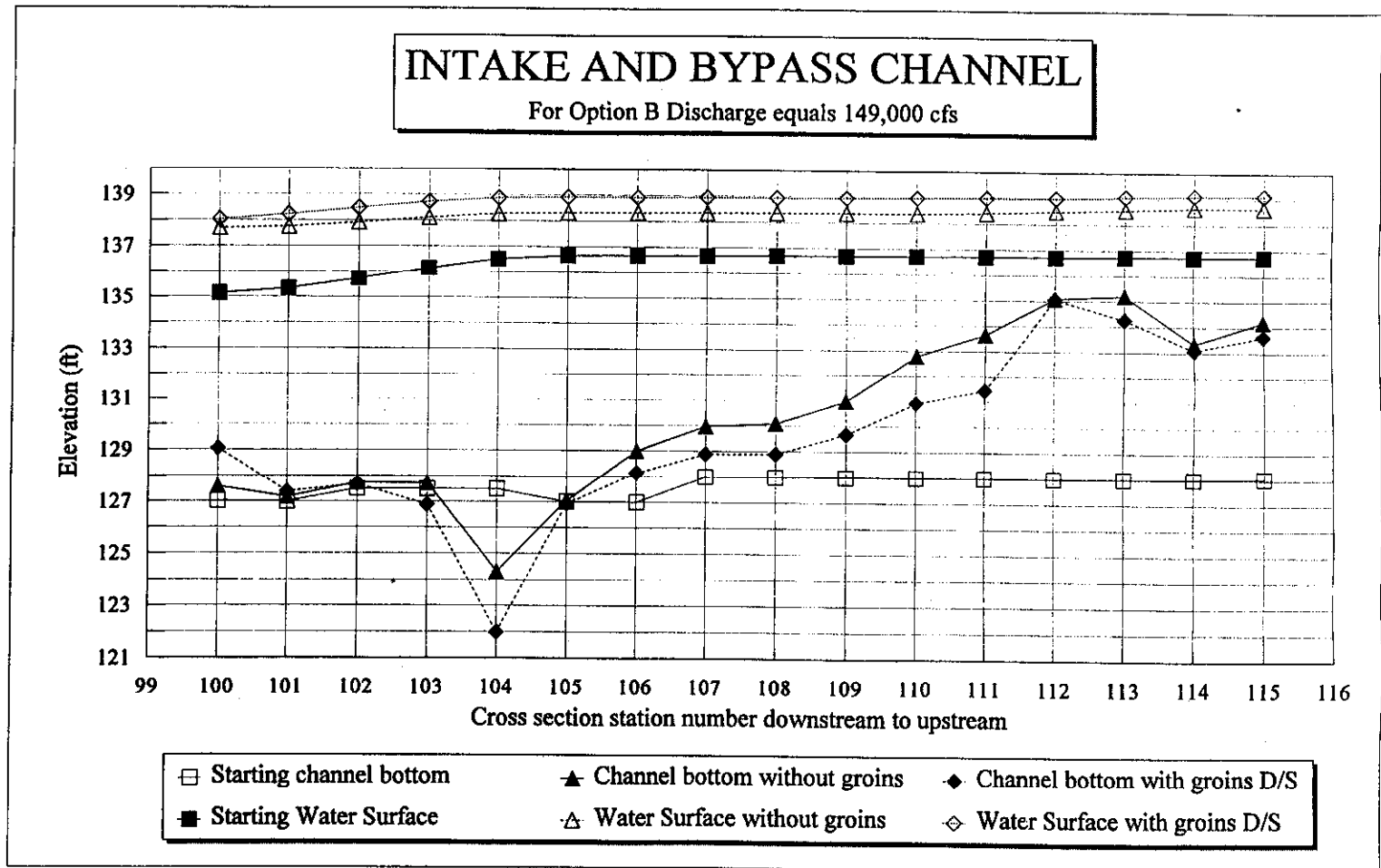


Figure 5-Changes in water surface profiles and bed elevations for the Intake Channel and Bypass Channel for the B Alternative with and without the presence of groins

CONCLUSIONS

1. With the use of the HEC6-T model, the complex flow conditions at GCID with the island flow were effectively simulated. The variable distribution of sediment was also included in the model for different discharges. Dredging was simulated with the model in a manner that is similar to field conditions. The Yang Sand and Gravel equation adequately predicted bed elevation changes.
2. Predicted bed changes for the A or D alternative in the intake channel remain the same as current bed changes for normal or high flow years. The A and D alternative would not change present dredging operations.
3. Sediment deposition in the intake channel would increase by 3 to 4 ft. for alternative B over existing conditions at the mouth of the intake channel during a high flow year. Dredge volumes would increase by at least 30 percent following a high flow period. Groins provided some reduction in sediment deposition volumes but did not prove to be viable for managing sediment for the B alternative because of fish criteria and navigation. The groins were used to decrease the bottom width of the channel so as to increase velocities to move the sediment downstream of the groins where it would be deposited. If groins were used in the main channel, the riprap size would have to be sufficient to withstand a flood of 150,000 ft³/s. Groins would have to be designed to ensure that they were not undercut by the increased channel velocity.

REFERENCES

- Meyer-Peter, E and R. Muller, 1948, "Formulas for bed-load transport," International Association of Hydraulic Research, Stockholm.
- Milhouse, R., Abt, S. R. and Watson, C. R., 1995, "Sampling River Bed Material: The Barrel Sampler," in preparation.
- Schoklitsch, 1930, Handbook der Wasserbaues, Springer, Vienna (2nd ed.), English Translation, S. Shulits, 1930.
- Thomas, William A., 1994, Sedimentation in Stream Networks, User's Manual for the HEC6-T Sediment Transport Model, Mobile Boundary Hydraulics, Vicksburg MS.
- Toffaletti, 1966, A Procedure for Computation of Total River Sand discharge and Detailed Distribution Bed to Surface, U.S.A.C.E.
- U.S. Army Corps of Engineers, 1983, Sacramento River and tributaries, bank protection and erosion control investigation: Sediment Transport Studies.
- Water Engineering and Technology (WET), 1987, Geomorphic Analysis of Sacramento River, Phase I Report, December 1987, U.S. Army Corps of Engineers, Sacramento District, Contract No. DACW05-87-0094.
- Water Engineering and Technology (WET), 1988a, Geomorphic hydraulic engineering study of Sacramento River from Hamilton City (RM 199.3) to Woodson Bridge (RM218.3): Report to Glen Colusa Irrigation District.
- Water Engineering and Technology (WET), 1988b, Geomorphic analysis of Sacramento River Phase II Draft Report, March 1988, U.S. Army Corps of Engineers, Sacramento District, Contract No. DACW05-87C-0094, 338 p.
- Yang, C. T., 1984, "Unit Stream Power for Gravel," Journal of Hydraulic Engineering, ASCE, Vol 110, #12, pp. 1783-1794.

GENERALIZED STREAM TUBE MODEL FOR ALLUVIAL RIVER SIMULATION (GSTARS-2)

By Chih Ted Yang, Manager, Sedimentation and River Hydraulics Group, Bureau of Reclamation, Denver, Colorado

Abstract: The original Generalized Stream Tube model for Alluvial River Simulation (GSTARS) was developed for a CYBER mainframe computer and released by the Bureau of Reclamation in 1985. GSTARS has been applied to several engineering projects and river morphologic studies. As a result of these projects and studies, GSTARS went through several stages of modifications and improvements. GSTARS-2 is the first major revision and enhancement of GSTARS. These revisions include a conversion of the program from CYBER to PC application, increase in the number of sediment transport functions for users to select, incorporation of channel side stability criteria to simulate the bank failure process, lateral sediment transport at a river bend, and local scour at the toe of protected surface. Examples of simulated and predicted channel geometry changes due to man-made and natural events are presented to illustrate some of the capabilities of GSTARS-2.

INTRODUCTION

Most of the sediment and water routing models, such as the HEC-6 (U.S. Army Corps of Engineers, 1993) were developed for solving one-dimensional alluvial river problems. Although there are truly two-dimensional and three-dimensional models for alluvial river simulation, they are too computationally intensive for engineering applications. The field data required for calibration and testing of these models may not be readily available. The Generalized Stream Tube model for Alluvial River Simulation (GSTARS) was developed by Molinas and Yang (1985a) to simulate the flow conditions in a semi-two-dimensional manner and the change of channel geometry in a semi-three-dimensional manner. GSTARS has been applied by different investigators for solving river engineering problems. The model was also used to simulate and predict river morphologic changes due to man-made and natural events. As a result of these applications, GSTARS has been revised and enhanced. The original GSTARS was developed for a CYBER mainframe computer. The revised and enhanced model, GSTARS-2 (Yang and Gavlick, 1995), was developed for PC applications. This paper provides a general description of GSTARS-2. Examples of simulated and predicted results based on GSTARS-2 are given to illustrate model capabilities that can be useful in solving engineering problems and river morphology studies.

GENERAL DESCRIPTION OF GSTARS-2

GSTARS-2 consists of seven main computation parts. They are: (a) channel geometry, (b) hydraulics, (c) sediment routing and armoring, (d) channel width and depth adjustments, (e) channel side stability, (f) local scour below a weir or drop structure, and (g) lateral sediment transport due to secondary current at a bend. A general description of these seven parts is given below:

a. Channel geometry: GSTARS-2 can handle irregular channel cross-sections, regardless of whether it is a single channel or it is separated by small islands and sand bars. A detailed description of channel geometry computation was given by Molinas and Yang (1985b).

b. Hydraulics: Most water and sediment routing models are based on the energy equation using the standard step method. This method limits its applications to subcritical flows. If there is a change of flow conditions from subcritical to supercritical, a critical depth is assumed. GSTARS-2 utilizes both the energy equation and the momentum equation. Consequently, it can handle both subcritical and supercritical flows, including hydraulic jumps (Molinas and Yang, 1985a,b; Yang, Molinas, and Song, 1988).

The stream tube concept is used to simulate the flow conditions in the longitudinal and lateral directions in a semi-two-dimensional manner. Based on this concept, water discharge in a given stream tube is determined by its conveyance. The discharge in each stream tube equals the total discharge divided by the number of stream tubes at a given cross-section. Although no sediment or flow can be transported across the boundary of a stream tube, the position and width of a stream tube can change after each time step of computation. This is the basis that GSTARS-2 can simulate semi-two-dimensional flow conditions even though the hydraulic computations are one-dimensional along a stream tube (Yang, Molinas, and Song, 1988).

c. Sediment Routing and Armoring: Once the hydraulic conditions are computed for each stream tube, the rate of sediment transport can be computed using one of the following methods:

1. Meyer-Peter and Müller's 1948 formula
2. Laursen's 1958 method
3. Toffaleti's 1969 method
4. Engelund and Hansen's 1972 method
5. Ackers and White's 1973 method
6. Yang's 1973 sand and 1984 gravel transport formulas
7. Yang's 1979 sand and 1984 gravel transport formulas
8. Parker's 1990 method
9. Yang's 1996 modified formula

The armoring process computations are based on the method proposed by Bennett and Nordin (1977).

d. Channel Width and Depth Adjustments: These adjustments are based on the minimum energy dissipation rate theory (Yang and Song, 1986) and its simplified version of minimum total stream power. Whether a channel will adjust its width or depth at a given computation time step depends on which condition results in less total stream power (Yang, Molinas, and Song, 1988).

e. Channel Side Stability: Channel side stability depends on the bank materials and their angle of repose. Detailed computational procedures were published by Song, Zheng, and Yang (1995).

f. Local Scour Due to Water Fall: The depth of local scour below a weir or a drop structure can be computed from the total available power per unit channel width at a given cross-section (Song, Zheng, and Yang, 1995).

g. Lateral Sediment Transport Due to Secondary Current: The stream tube concept assumes that the effect of secondary currents on flow and sediment can be neglected. A semi-empirical approach was adopted by Song, Zheng, and Yang (1995) to determine the longitudinal and lateral components of sediment transport rate computed from one of the sediment transport functions in (c) of this section.

SIMULATION RESULTS

The following application examples are used to illustrate the capabilities of GSTARS-2.

a. Lock and Dam No. 26 Replacement Project: Figure 1 shows the semi-three-dimensional cross-sectional changes at the Mississippi River Lock and Dam No. 26 replacement site near St. Louis, Missouri. The channel width was fixed by levee and coffer dam. Three stream tubes were used in these computations. The difference between computed and measured local scour depth is within 1 foot for this particular case study (Yang, Molinas, and Song, 1988).

b. Willow Creek Reservoir Emergency Spillway Erosion Study: Figure 2 shows the predicted formation and variation of a channel cross-section downstream of the emergency spillway due to overtopping of the spillway. It shows that an originally fairly straight symmetrical channel cross-section can become a non-symmetrical section typical of a meandering river at a bend. This demonstrates that GSTARS-2 has the potential to simulate and predict the channel forming process from straight to meandering in accordance with the theory of minimum energy dissipation rate (Yang, Molinas, and Song, 1988).

c. Lake Mescalero Emergency Spillway Erosion Study: Figure 3 shows a comparison of computed and eroded cross-section downstream of the Lake Mescalero emergency spillway due to a spring runoff over the emergency spillway. It is apparent that the enhanced GSTARS-2 model can more accurately simulate the erosion processes than the original GSTARS when compared with the post-flood measurement (Song, Zheng, and Yang, 1995).

SUMMARY AND CONCLUSIONS

GSTARS-2 is an improved and enhanced model of the original GSTARS computer model released by the Bureau of Reclamation in 1985. Examples of case studies indicate that GSTARS-2 can be applied for solving engineering problems and simulating river morphologic processes with accuracy. The fact that GSTARS-2 can use a one-dimensional approach along stream tubes to simulate cross-sectional changes in a semi-three-dimensional manner is especially attractive for engineering applications.

REFERENCES

- Ackers, P., and White, W. R., 1973. Sediment Transport: New Approach and Analyses, ASCE Journal of the Hydraulics Division, Vol. 99, No. HY 11, pp. 2041-2060.
- Bennett, J. P., and Nordin, C. F., 1977. Simulation of Sediment Transport and Armoring, Hydrological Science Bulletin, XXII.
- Engelund, F., and Hansen, E., 1972. A Monograph on Sediment Transport in Alluvial Streams, Teknisk Forlag, Copenhagen.
- Laursen, E. M., 1958. The Total Sediment Load of Streams, ASCE Journal of the Hydraulics Division, Vol. 84, No. 1, pp. 1530-1 - 1530-36.
- Meyer-Peter, E., and Müller, R., 1948. Formula for Bed-Load Transport, Proceedings of International Association for Hydraulic Research, 2nd Meeting, Stockholm.
- Molinas, A., and Yang, C. T., 1985a. Computer Program User's Manual for GSTARS (Generalized Stream Tube model for Alluvial River Simulation), U.S. Bureau of Reclamation, Denver, Colorado.
- Molinas, A., and Yang, C. T., 1985b. Generalized Water Surface Profile Computations, ASCE Journal of Hydraulic Engineering, Vol. III, No. 3, pp. 381-397.
- Parker, G., 1990. Surface-Based Bedload Transport Relationship for Gravel Rivers, Journal of Hydraulic Research, Vol. 28, No. 4, pp. 417-436.
- Song, C.C.S., Zheng, Y., and Yang, C. T., 1995. Modeling of River Morphologic Changes, International Journal of Sediment Research, Vol. 10, No. 2, pp. 1-20.
- Toffaletti, F. B., 1969. Definitive Computations of Sand Discharge in Rivers, ASCE Journal of the Hydraulics Division, Vol. 95, No. HY1, pp. 225-246.
- U.S. Army Corps of Engineers Hydrologic Engineering Center, 1993. HEC-6, Scour and Deposition in Rivers and Reservoirs, User's Manual, Davis, California.

- Yang, C. T., 1973. Incipient Motion and Sediment Transport, ASCE Journal of the Hydraulics Division, Vol. 99, No. HY10, pp. 1679-1704.
- Yang, C. T., 1979. Unit Stream Power Equations for Total Load, Journal of Hydrology, Vol. 40, pp. 123-138.
- Yang, C. T., 1984. Unit Stream Power Equation for Gravel, ASCE Journal of Hydraulic Engineering, Vol. 110, No. HY12, pp. 1783-1797.
- Yang, C. T., and Gavlick, S., 1995. Computer Program User's Manual for Generalized Stream Tube model for Alluvial River Simulation (GSTARS-2), U.S. Bureau of Reclamation, Technical Service Center, Denver, Colorado.
- Yang, C. T., and Song, C.C.S., 1986. Theory of Minimum Energy and Energy Dissipation Rate, Encyclopedia of Fluid Mechanics, Vol. 1, Chapter 11, Gulf Publishing Company, edited by N.P. Chermisinoff, pp. 353-399.
- Yang, C. T., Molinas, A., and Song, C.C.S., 1988. GSTARS - Generalized Stream Tube model for Alluvial River Simulation, Interagency Advisory Committee on Water Data, Subcommittee on Sedimentation Report on Twelve Selected Computer Stream Sedimentation Models Developed in the United States, edited by S. S. Fan, Federal Energy Regulatory Commission, pp. 149-178.
- Yang, C. T., Molinas, A., and Wu, B., 1995. Sediment Transport in the Yellow River, ASCE Journal of Hydraulic Engineering, Vol. 122, No. 3.

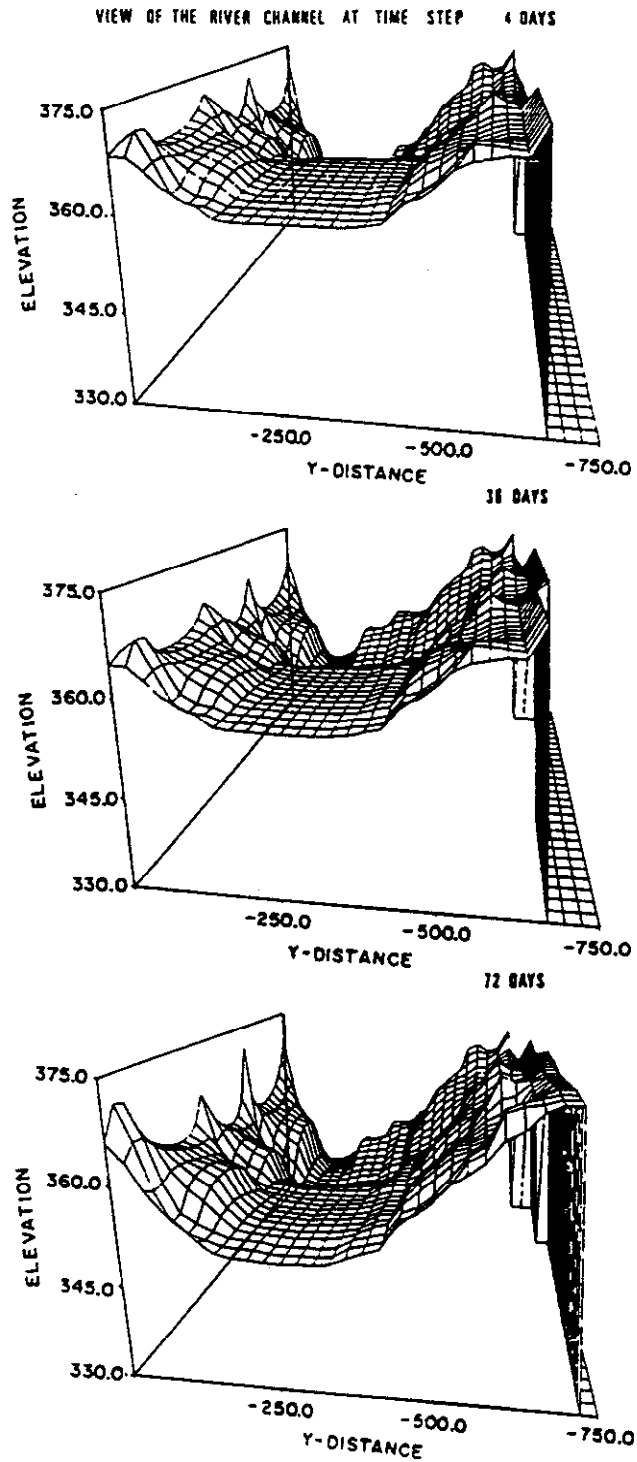


Figure 1. - Three-dimensional plot of the variation of computed scour pattern at Lock and Dam No. 26 replacement site.

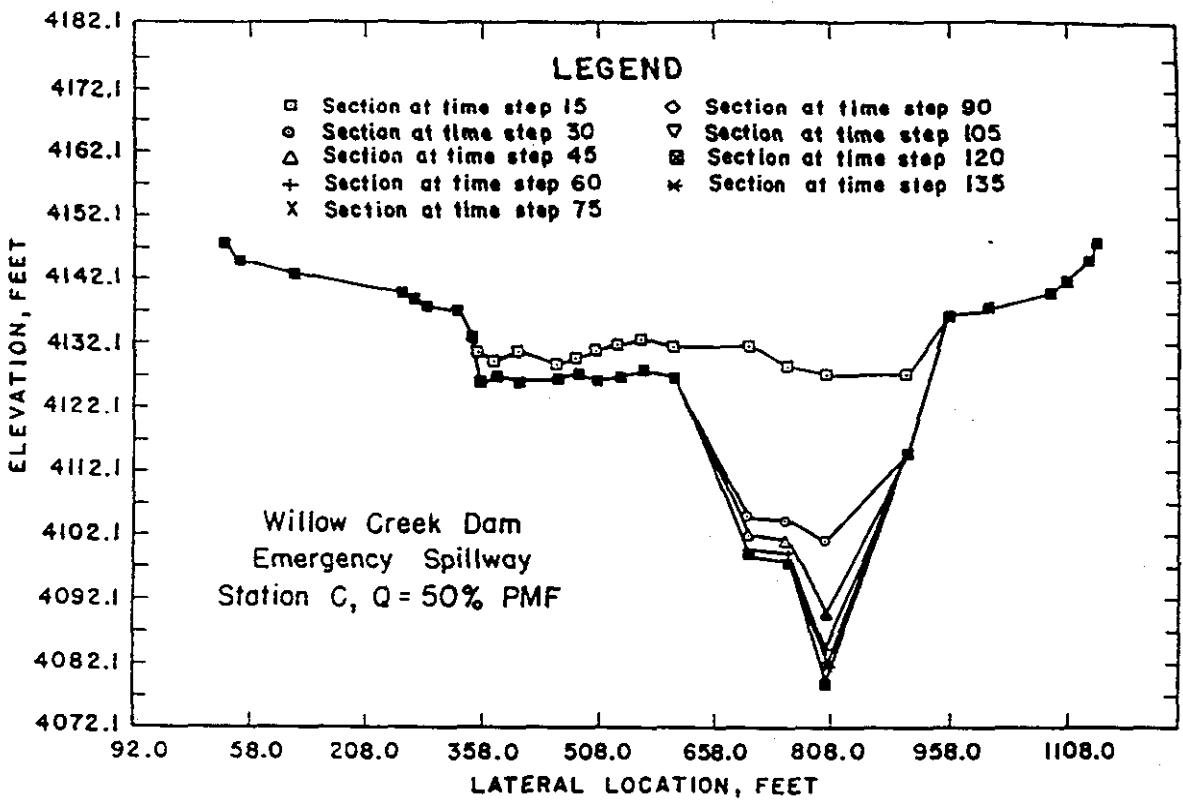


Figure 2. - Variation of channel cross-section at Station C downstream of the Willow Creek Dam emergency spillway.

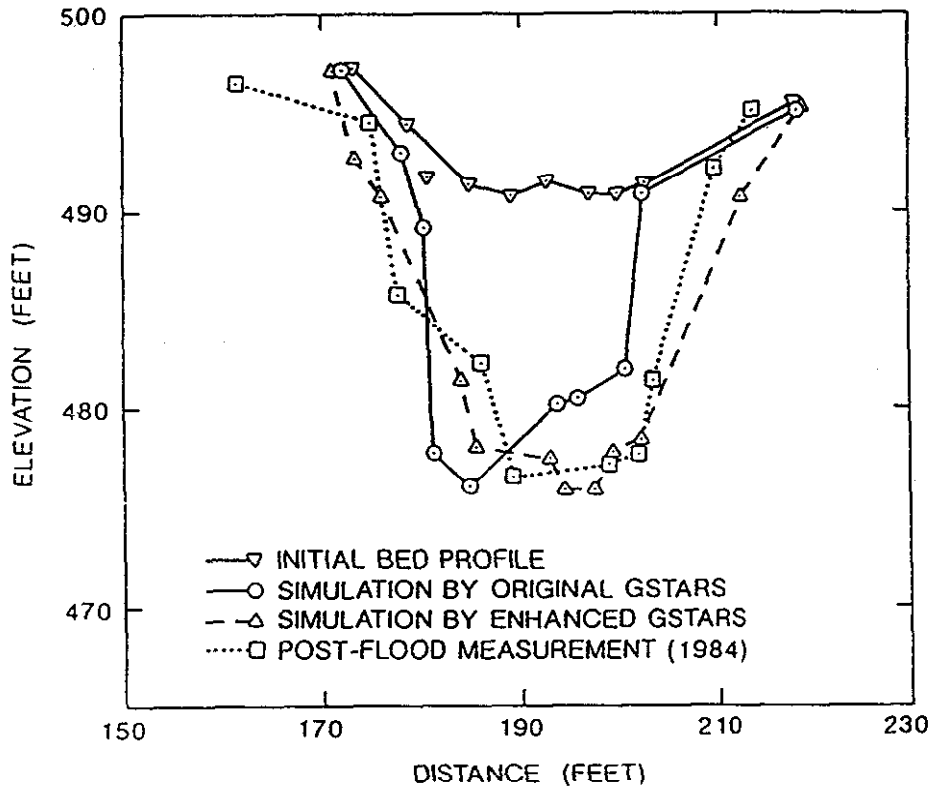


Figure 3. - Comparison among measured and predicted cross-sections at station 0+65 downstream of the Lake Mescalero emergency spillway.

Sediment Resuspension Due to Wind Generated Waves in the Shallow Navigation Pools of the Upper Mississippi River

FERRIS CHAMBERLIN

U.S. Army Corps of Engineers

St. Paul, MN

INTRODUCTION

1. After construction of the Upper Mississippi River (UMR) locks and dams, the filling of the navigation pools left the river bank levees and higher geomorphic features of the floodplain as islands. This resulted in a complex mosaic of shallow aquatic wetland and terrestrial habitats. Floods and wave action has resulted in erosion and eventual loss of many of these islands. The loss of islands along the main channel has allowed an increase of sediment-laden water through the adjacent shallow areas. The loss of islands within the shallow areas has created longer fetch lengths which has resulted in higher wind generated waves. The higher waves have more erosion potential and also cause an increase in the resuspension of bottom sediments. The increase in suspended sediment concentration reduces the amount of light penetration into the water. This in turn inhibits the growth of aquatic plants. Because aquatic plants absorb wave energy and reduce advective currents, the loss of aquatic plants allows more erosive energy to attack the shoreline.

2. To reduce the erosion of existing shallow water islands, the contributing factors to island erosion must be reduced or eliminated. The creation of islands in Pool 5 of the UMR has proved effective in breaking up wind fetch, thereby reducing wave heights which in turn reduces erosion and sediment resuspension. The reduction of sediment resuspension is key to encouraging aquatic plant growth which not only has habitat enhancing value but also attenuates wave energy and advective currents. The ability to easily predict sediment concentration levels due to wind generated waves will provide additional design guidance for island creation plans. It was the purpose of this study to,

- I. Review sediment resuspension dynamics due to wave motion.
- II. Develop a simplified mass transport balance equation for suspended solids in a water column that represents changes due to wind generated waves.
- III. Calibrate resuspension and sedimentation parameters for Pool 8 using measured values of wind speed, sediment grain size, and suspended sediment concentrations.
- IV. Assess the value of simplification and make recommendations for further study.

RESUSPENSION DYNAMICS

3. When waves are present, the motion of the wave produces an orbital motion of water particles. This motion can penetrate all the way down to the lake bottom, imparting shear stresses at the sediment-water interface. If the shear stress exceeds a certain critical value, the sediment begins to move back and forth. In the beginning when the lake bed is flat, the vertical excursions of the sediment particles are confined to a very narrow ribbon in the vicinity of the bed. As the process continues, the flat bottom gradually deforms into a steady bed form called ripples. When ripples begin to develop, the oscillatory motions of the water particles set up fluid vortices at the troughs which are convected toward the crests and are diffused upwards into the body of water a considerable distance from the bed. These vortices pick up sediment which travel with the vortices, and at the same time, settle due to the negative buoyancy. Under this

condition, the vertical excursions of the sediment particles extend to a considerable distance from the bed and the sediment is said to have come into suspension (Skafel and Krishnappen, 1984).

5. Suspended solids can take on many sizes and be made up of various substances. The inorganic particles found suspended in the UMR navigation pools include sands, silts, and clays. Critical shear velocity for sands can be easily determined by use of the Modified Shields diagram (Komar and Miller, 1975). However, a significant percentage of the bottom material is cohesive soft sediment (muds). The resuspension rate of muds is not well known.

6. The degree to which the bottom sediments are consolidated greatly impacts resuspension. Recently deposited surface material can be more easily eroded than the material farther down in the bed. During a storm event, particles are continuously deposited and brought back into suspension. The resuspended material is distributed over the lake by currents. The deposition of suspended material is dependant on settling velocity, water depth, and concentration of suspended matter.

MASS TRANSPORT BALANCE

7. Sediment transport in the UMR navigation pools is very complex. It involves (1) input and output of sediments, (2) horizontal transport by advective currents, (3) dispersion, (4) resuspension of bottom sediments, and (5) sedimentation of suspended solids. Field observations have shown very little vertical gradient in the concentration of fine suspended solids. Therefore, the first simplification to the mass transport equation was made by eliminating vertical dispersion. The mass balance for suspended solids in the water column can now be represented by the following differential equation (Blom et al., 1992):

$$\frac{\partial hC}{\partial t} + \frac{\partial huC}{\partial x} + \frac{\partial hvC}{\partial y} - \frac{\partial}{\partial x} \left(hD_x \frac{\partial C}{\partial x} \right) - \frac{\partial}{\partial y} \left(hD_y \frac{\partial C}{\partial y} \right) - R_F + S_F = 0$$

where, h = water depth

t = time

C = suspended solids concentration

R_F = resuspension flux

S_F = sedimentation flux

u = depth-averaged velocity along x-axis

v = depth-averaged velocity along y-axis

D_x = dispersion coefficient along x-axis

D_y = dispersion coefficient along y-axis

8. Advective currents are present in all navigation pools and vary from almost non-existent during drought periods to several feet per second during flood events. These currents bring sediments into the pool and transport sediments out of the pool. When the currents are of sufficient magnitude, the bottom erodes bringing sediments into suspension. While advective currents greatly impact lateral transport and provide some sediment resuspension, it was assumed for this study that the suspended sediment concentration at a given location was due primarily to wind generated waves. Therefore, the variation in suspended solids concentration with time at a specific location is dominated by resuspension and sedimentation and can be represented by:

$$dC/dt = R_F - S_F$$

9. Resuspension flux is a result of the shear force exerted on the bottom by wave motion. When shear force exceeds the critical shear necessary to initiate motion, resuspension begins. A simple empirical relationship for resuspension of sediments was developed by Parchure and Metha, 1985).

$$R_F = M (1 - \tau_{cr}/\tau_b) \quad (R \geq 0)$$

τ_{cr} = critical shear stress required to initiate motion

τ_b = shear stress applied to the bottom

M = numerical constant with units of mass per unit area time

All uncertain factors which can have an effect on resuspension are taken into account in M. The shear stress τ_b is understood to be the average over a wave period and is given as:

$$\tau_b = (\rho/2) f_w u_m^2 \quad \begin{array}{l} f_w = \text{wave friction factor} \\ u_m = \text{maximum orbital velocity on the bottom} \end{array}$$

Jonsson (1966) introduced the wave friction factor f_w as a function of the bottom roughness length and the semi-excursion length of the orbital wave at the bottom. The maximum horizontal orbital velocity on the bottom u_m is most easily determined using linear wave theory (mathematical formulation resulting if the equations of motion are *linearized*):

$$u_m = \frac{\pi H}{T \sinh\left(\frac{2\pi h}{L}\right)} \quad \begin{array}{ll} H = \text{wave height} & L = \text{wavelength} \\ T = \text{wave period} & h = \text{water depth} \end{array}$$

Simplification of this equation can be made by assuming predominately deep- or shallow-water conditions prevail. Previous studies of the UMR navigation pools (Chamberlin, 1994) has shown transitional water depths (i.e. between deep and shallow) are common. Therefore, no simplification of the equation is allowed.

10. In a study performed by Blom et al. (1992), the relationship for sediment resuspension flux was represented by:

$$R_F = K (u_m - u_{cr})$$

K = resuspension constant (mass per unit volume)

u_{cr} = critical shear velocity (velocity at which resuspension begins)

This relationship is very similar to that developed by Parchure and Metha. The basic difference being the wave friction factor incorporated with all other uncertainties in the resuspension constant. As part of their study, calibration of resuspension and sedimentation parameters for very fine materials was performed. The value of u_{cr} was calibrated to be in the range of 0.0 to 0.0048 meters per second (m/s).

11. When comparing a critical shear velocity of 0.0048 m/s to orbital wave velocities typically occurring at a depth of one-meter, the critical shear velocity seems insignificant. For example.

a wave with a height of 10-centimeters (cm) would produce an orbital wave velocity of about 0.048 m/s at a depth of 1-meter; a magnitude greater than the critical shear velocity. Because the bottom sediments in the UMR navigation pools consist of very fine material with a high moisture content, critical shear velocities are very low. It is suggested that the impact of retaining the parameter u_{cr} in the resuspension flux relationship is insignificant when computing resuspension for UMR navigation pools. Therefore, resuspension flux R_F can now be represented by:

$$R_F = K u_m$$

12. A common description of sedimentation flux S_F was given by (Sheng and Lick 1979):

$$S_F = w_s C \quad w_s = \text{sedimentation velocity}$$

The sedimentation velocity w_s can be estimated using Stokes law for sediment fall velocity which equates sediment immersed weight to the resisting drag force of a spherical particle.

$$w_s = \frac{1}{18\nu} (s-1) g d^2 \quad \begin{array}{l} d = \text{sediment diameter} \\ \nu = \text{kinematic fluid velocity} \\ s = \rho_s/\rho \quad (\rho = \text{fluid density, } \rho_s = \text{sediment density}) \end{array}$$

While Stokes law is acceptable for determining sedimentation velocities for non-cohesive particles, the physico-chemical forces binding the cohesive soils present in the UMR navigation pools will require measured data or data obtained through calibration of balancing resuspension and sedimentation to known suspended sediment concentrations.

13. The mass balance equation for change in suspended sediment concentration due to wind generated waves can now be represented by:

$$\Delta C = \frac{[K(u_m) - w_s(C_i + \Delta C)] \Delta t}{h}$$

ΔC = change in suspended sediment concentration	K = resuspension constant
C_i = initial concentration of suspended solids	w_s = sedimentation constant
Δt = change in time	h = water depth

INPUT DATA

14. Measured data was obtained at a specific site in Pool 5 of the UMR over the period of 7 April 1994 through 7 November 1994. Pool 5 is located between river miles 743 and 747 on the Mississippi River. A data platform was located in north-central portion of the pool. The water depth at the platform site was about 1-meter. An anemometer located 2-meters above the water surface was used to measure wind speed. The daily average wind speed and direction

were recorded based 2-minute samples taken hourly. Suspended sediment samples were taken every 4-hours from mid-depth. Sampling was performed such that each sample bottle contained six daily samples, thus providing the average daily suspended sediments concentration. An analysis of a grab sample taken of the bottom sediments showed the material at the data collection site to be 91-percent inorganic by weight. The inorganic material consisted of 50-percent sand ($>65\mu\text{m}$), 39-percent silt ($<65\mu\text{m}->3.9\mu\text{m}$), and 11-percent clay ($<3.9\mu\text{m}$).

15. Because wave heights were not recorded, they were estimated based on the wind speed and direction. For wave height predictions, wind speeds U must be adjusted to an elevation of 10-meters above the water surface. This was done by,

$$U_{10} = U_z \left(\frac{10}{z} \right)^{1/7} \quad U_z = \text{wind speed at elevation } z$$

The water surface roughness varies with wind speed. Therefore, the wind speed must also be adjusted for the nonconstant coefficient of drag. As shown in the Shore Protection Manual (SPM 1984), the wind speeds were adjusted for drag by,

$$U_A = 0.71 U^{1.23} \quad (U \text{ in m/s})$$

16. Wind direction was used to determine fetch length F . Fetch length is a region in which the wind speed and direction are reasonably constant. Fetch lengths were measured from shore to the platform location site along 16-compass points. The recorded average wind speed direction, which was given in degrees, was assigned the direction of the nearest compass point and hence a fetch length for that days average wind speed was determined. Fetch lengths for the platform site varied from 1,000 to 2,500 meters.

17. To simplify the determination of wave characteristics requires an assumption that either deep-water or shallow-water conditions prevail. Relative water depths in the UMR navigation pools are typically deep to transitional (Chamberlin, 1994). For transitional-water depths, the assumption of deep-water conditions over predicts wave height, wave period, and wavelength; whereas, the shallow-water assumption under predicts these wave characteristics. Because water depths are typically deep to transitional, deep-water conditions were assumed realizing a slight over prediction in wave characteristics would occur. Wave heights H and wave periods T were computed using the deep-water wave equations developed by Smith (1991).

$$H = 0.0015 g^{0.5} F^{0.5} U \quad \text{and} \quad f_p = 2.6 g^{0.72} F^{-0.28} U^{-0.44}$$

The wave period T is simply the inverse of the wave frequency f_p . Wavelength L was computed using the following deep-water relationship (SPM, 1984):

$$L = gT^2 / 2\pi$$

COMPUTED RESULTS

18. Average daily wind speeds and the corresponding fetch length associated with the average daily wind direction were placed in a spreadsheet. Daily average wave heights and wavelengths were then computed. The computed wave heights and wavelengths were then used to determine the maximum orbital wave velocity at a depth of 1-meter. An estimated sedimentation constant w_s was computed using Stokes law for a particle diameter of $3.9\text{-}\mu\text{m}$. An estimate of the resuspension constant K was made based on results of previous studies. Resuspension R and sedimentation S were then computed for a Δt of 24-hours. Because Δt is constant, it was incorporated into the resuspension and sedimentation constants producing K' and w_s' respectively.

19. Resuspension concentrations R were computed by multiplying K' by the average daily orbital wave velocity u_m . For the first day, the loss of suspended sediments S due to sedimentation was computed by multiplying w_s' by one-half the predicted resuspension concentration. Predicted suspended solids (SS) concentration for the first day was simply $R - S$. Sedimentation for the successive days was determined by combining the previous days predicted SS concentration (C) with the days predicted resuspension concentration (R), dividing by two and then multiplying by the sedimentation constant w_s' . A column showing change in concentration was then prepared by computing $R - S$. Predicted SS concentrations were computed by adding the previous days SS concentration to the change in SS concentration. When the total resulted in a negative number, zero concentration was assigned..

20. The resuspension and sedimentation constants, K' and w_s' , were adjusted to provide a best fit to the measured average daily SS concentration. The resulting values were,

$$K = 1.0 \times 10^{-2} \text{ g/m}^3 \qquad w_s = 1.2 \times 10^{-5} \text{ m/s}$$

Figures 1 and 2 show the comparison of predicted and observed suspended solids concentration over the record period of 208 consecutive days.

CONCLUSIONS

21. Considering the number of parameters involved, the large time interval, and the degree of simplification that was done to represent the complex three-dimensional mass transport that was occurring, Figures 1 and 2 show a good correlation between predicted and observed values of SS concentration. A closer fit to the observed concentrations may be accomplished by considering the bottom sediment in two fractions, accounting for changes in water depth, and adjusting sediment concentrations that occurred during high inflow periods.

22. Future studies should include data collection over shorter time periods. With a change in time of 24-hours, peak wind speeds and direction of the peak wind speeds are missed. Unless fetch length to the study area is the same in all directions, wind direction can have a major impact on the predicted wave height. Based on typical fetch lengths for the UMR navigation pools, a two-hour Δt would be preferred. This would allow for fully developed seas, provide a good wind direction for determining fetch length, and would give a much better estimate on change of SS concentration due to wind generated waves.

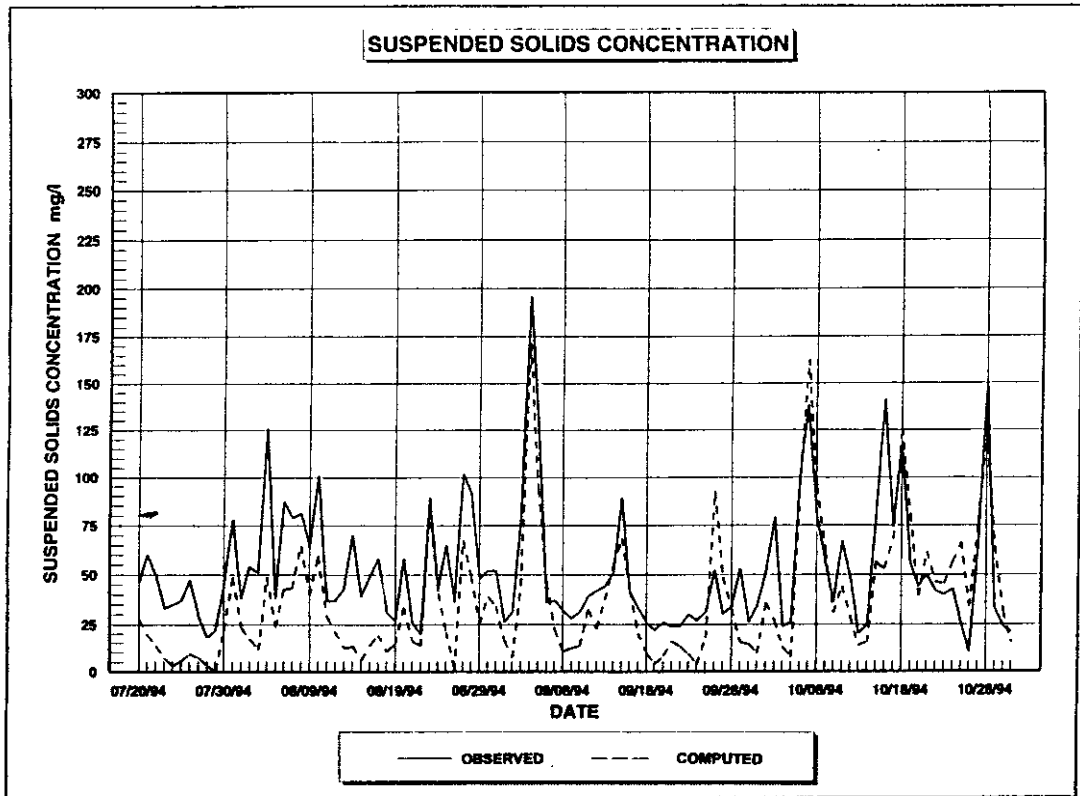


Figure 1. Mississippi River, Pool 5, Site 8A; 7 April - 19 July 1994

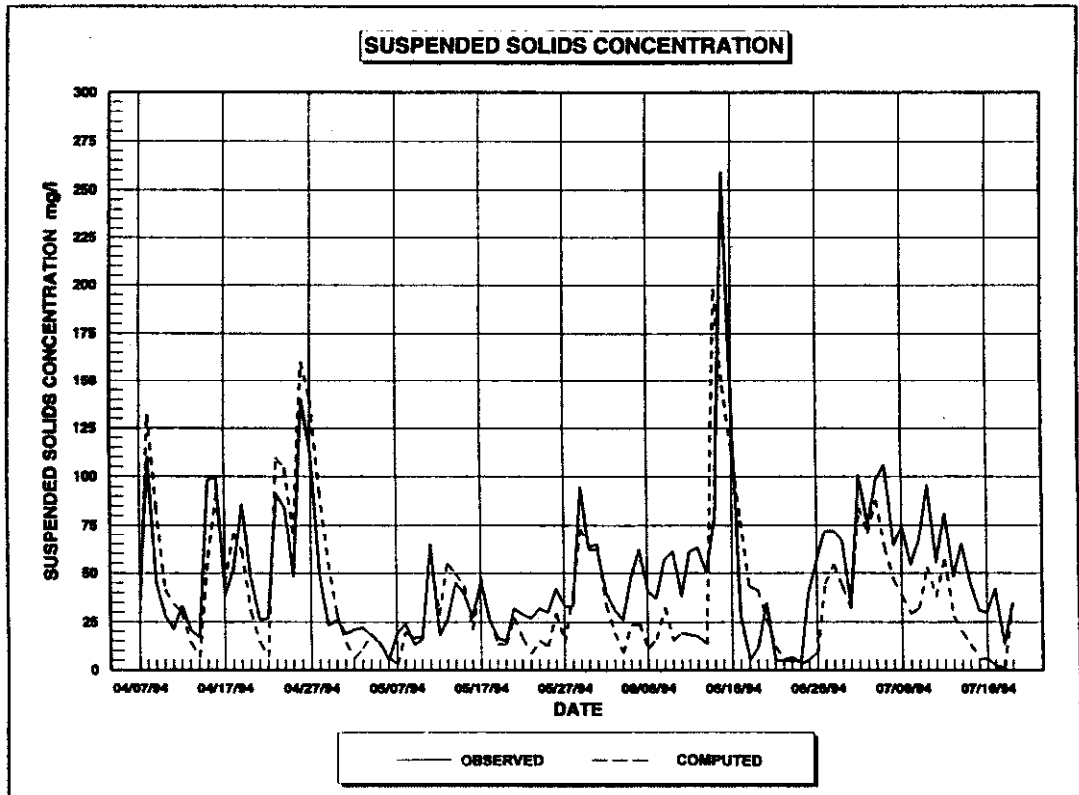


Figure 2. Mississippi River, Pool 5, Site 8A; 20 July - 7 November 1994

REFERENCES

- Blom, G., et al. 1992. "Modelling Sediment Transport in Shallow Lakes - Interactions Between Sediment Transport and Sediment Composition," *Hydrobiologia* 235/236, pp. 153-166
- Chamberlin, F. W. 1994. "Wind Generated Waves in Navigation Pools," National Biological Survey, Environmental Management Technical Center, Long Term Monitoring Program, Special Report 94-S001
- Komar, P. D. and Miller, M. C. 1975. "The Initiation of Oscillatory Ripple Marks and the Development of Plane-Bed at High Shear Stresses Under Waves," *Journal of Sedimentary Petroleum*, Volume 45, Number 3, pp. 697-703
- Parchure, T. M. and Metha, A. J. 1985. "Erosion of Soft Cohesive Deposits," *Journal of Hydraulic Engineering*, Number 10, pp. 1038-1326
- Sheng, Y. P. and Lick, W. 1979. "The Transport and Resuspension of Sediments in a Shallow Lake," *Journal of Geophysics Research*, Volume 84, pp. 1809-1826
- Skafel, M. G. and Krishnappen, B. G. 1984. "Suspended Sediment Distribution in Wave Field," *Journal of Waterways, Ports, Coastal and Ocean Engineering*, Volume 110, Number 2, May, pp. 205-230
- U.S. Army Corps of Engineers (USACE) 1984. *Shore Protection Manual*, Coastal Engineering Research Center, Waterways Experiment Station, Vicksburg, Mississippi

The k-ε TURBULENCE MODEL FOR PREDICTING SECONDARY CURRENTS IN OPEN CHANNELS

By Y.I. Hafez, Researcher, Nile Research Institute, Egypt

Abstract: Secondary currents are predicted by solving the governing equations for mean turbulent flows in open channels. A slightly modified form of the algebraic-stress model of Naot et al. (1993) is used to model the turbulent stresses appearing in the governing equations. The k-ε turbulence model is used for predicting the turbulent viscosity which is needed in that algebraic-stress model. A finite element method is used for solving the set of governing equations. The model predicts well the depression of the main velocity maximum below the free surface in the open channel with aspect ratio of 1:2. A large upper vortex and lower smaller one, predicted in one half of the channel, is in good agreement with experiments and Naot and Rodi's numerical predictions (1982). The cell vortex structure in channels with lateral periodic bed roughness and aspect ratio of 1:7.5 is well predicted while the cell structure disappears in the same channel but with uniform bed roughness.

INTRODUCTION

Secondary Currents: Secondary currents play an important part in river mechanics. For example, secondary currents affect significantly the main velocity contour lines (4,11,13), the boundary shear stress distribution (3,4,13,16), bed and suspended load distributions (6,20), and lateral bed configurations (2,5). Open Channel flows are often turbulent in which secondary currents are induced by the anisotropy of the turbulent normal stresses (4,11,13,16). Therefore, they are called "turbulence-induced secondary currents" and are discussed in this paper.

The magnitude of such secondary currents is generally less than 5 percent of the main velocity (14) which causes their measurements to become difficult (9,15). Therefore, mathematical prediction of secondary currents has been implemented by various researchers (11,12,13).

Prediction of secondary currents is accomplished by solving the mean turbulent flow governing equations which consists of the continuity equation and the Reynolds equations of motion. The turbulent stresses appearing in the Reynolds equations are modeled by an algebraic-stress model. The k-ε model is applied for predicting the turbulent viscosity appearing in the turbulent stress expressions.

So far, most models for predicting secondary currents have used the finite difference method along with tuning of some empirical constants of the model (11,12,13). In this paper, the finite element method is used for predicting secondary currents because of its popularity and ease in handling boundary conditions. The standard values for the model empirical constants are used in this paper. Besides, some modifications are introduced to the algebraic stress model of Naot et al. (1993).

The MATHEMATICAL MODEL

The Mean Turbulent Flow Equations: The governing equations for steady, uniform, and high Reynolds number mean turbulent flow are:
the continuity equation

$$\frac{\partial V}{\partial Y} + \frac{\partial W}{\partial Z} = 0 \quad (1)$$

the Reynolds equations of motion:

X direction or the longitudinal flow direction

$$V \frac{\partial U}{\partial Y} + W \frac{\partial U}{\partial Z} = -\frac{d}{dx} \left(\frac{P}{\rho} \right) + \frac{\partial}{\partial Y} \left(\frac{\tau_{yx}}{\rho} \right) + \frac{\partial}{\partial Z} \left(\frac{\tau_{zx}}{\rho} \right) + F_x \quad (2)$$

Y direction or the vertical direction

$$V \frac{\partial V}{\partial Y} + W \frac{\partial V}{\partial Z} = -\frac{\partial}{\partial Y} \left(\frac{P}{\rho} \right) + \frac{\partial}{\partial Y} \left(\frac{\tau_{yy}}{\rho} \right) + \frac{\partial}{\partial Z} \left(\frac{\tau_{zy}}{\rho} \right) + F_y \quad (3)$$

Z direction or the transverse direction

$$V \frac{\partial W}{\partial Y} + W \frac{\partial W}{\partial Z} = -\frac{\partial}{\partial Z} \left(\frac{P}{\rho} \right) + \frac{\partial}{\partial Y} \left(\frac{\tau_{yz}}{\rho} \right) + \frac{\partial}{\partial Z} \left(\frac{\tau_{zz}}{\rho} \right) + F_z \quad (4)$$

where U, V, W are the time average mean velocities in the X (longitudinal channel direction), Y (vertical direction), Z (lateral direction), respectively, P is the time average mean pressure, ρ is the fluid density, τ_{ij} are turbulent (Reynolds) normal and shear stress components, and F_i are body force components.

The Algebraic-Stress Model: The non-linear algebraic stress relations of Naot et al. (1993) are used with some modifications. Their relations take into account free surface effects by reducing the length scale and turbulent viscosity at the free surface. Besides, the free surface effects are induced in the turbulent stress expressions (τ_{yx} and τ_{zx}) using turbulent viscosity for the vertical momentum transfer which is different than that for the lateral momentum transfer (i.e., using non-isotropic turbulent viscosity) and choosing the model coefficients to reflect free surface effects. The modified turbulent stresses are expressed (4)

$$\frac{\tau_{yx}}{\rho} = \nu_{TY} \frac{\partial U}{\partial Y} \quad ; \quad \nu_{TY} = \frac{c_1^2}{(c_1 + \frac{3}{2}c_3)(c_1 + 2c_3)} \nu_T \quad ;$$

$$\nu_T = C_\mu \frac{K^2}{e} \quad (5)$$

$$\frac{\tau_{zx}}{\rho} = \nu_{TZ} \frac{\partial U}{\partial Z} \quad ; \quad \nu_{TZ} = \frac{(c_1 + \frac{5}{2}c_3)}{(c_1 + 2c_3)} \nu_T \quad (6)$$

$$\begin{aligned} \frac{\tau_{yy}}{\rho} = & -\frac{K}{(c_1 + 2c_3)} \left[\frac{2}{3} \left(\alpha - \frac{1}{2}\beta + c_1 - 1 \right) \right. \\ & \left. + \frac{\beta}{e} \left(-\frac{\tau_{yx}}{\rho} \frac{\partial U}{\partial Y} + \frac{\tau_{zx}}{\rho} \frac{\partial U}{\partial Z} \right) \right] \\ & + 2 \nu_{TY} \frac{\partial V}{\partial Y} \end{aligned} \quad (7)$$

$$\begin{aligned} \frac{\tau_{zz}}{\rho} = & -\frac{K}{C_1} \left[\frac{2}{3} \left(\alpha - \frac{1}{2} \beta + C_1 - 1 \right) \right. \\ & + \frac{\beta}{\epsilon} \left(-\frac{\tau_{zx}}{\rho} \frac{\partial U}{\partial Z} + \frac{\tau_{yx}}{\rho} \frac{\partial U}{\partial Y} \right) - C_3 \frac{\tau_{yy}}{\rho K} \left. \right] \\ & + 2 v_{TZ} \frac{\partial W}{\partial Z} \end{aligned} \quad (8)$$

$$\begin{aligned} \frac{\tau_{yz}}{\rho} = & -\frac{\beta}{\left(C_1 + \frac{3}{2} C_3 \right)} \frac{K}{\epsilon} \left(-\frac{\tau_{zx}}{\rho} \frac{\partial U}{\partial Y} - \frac{\tau_{yx}}{\rho} \frac{\partial U}{\partial Z} \right) \\ & + v_{TY} \frac{\partial W}{\partial Y} + v_{TZ} \frac{\partial V}{\partial Z} \end{aligned} \quad (9)$$

where the non-isotropic turbulent viscosities v_{TZ} and v_{TY} are used in expressions for turbulent stresses τ_{zz} , τ_{yy} , and τ_{yz} in contrast to (12,13) who used an isotropic viscosity v_T . The turbulent viscosity is expressed in Equation (5) in terms of the turbulent kinetic energy K , the rate of dissipation of the turbulent kinetic energy ϵ , and the dimensionless constant C_μ of standard value 0.09.

The model coefficients are given in terms of two functions that account for the distance from a solid wall (f_1) and the distance from an open surface (f_2) as

$$\alpha = 0.7636 - 0.06 f_1 \quad ; \quad \beta = 0.1091 + 0.06 f_1 \quad (10)$$

$$C_1 = 1.5 - 0.5 f_1 \quad ; \quad C_3 = 0.1 f_2 \quad (11)$$

Instead of using the functions f_1 and f_2 as given by (11,12,13) in which the mixing length is generally unknown, simpler functions are introduced in this paper. These functions are expressed as

$$f_1 = [1 - (N/H)]^2 \quad ; \quad f_2 = (Y/H)^2 \quad (12)$$

where N is the normal distance to the nearby wall, Y is the vertical distance from the bed wall, and H is the channel depth.

The k - ϵ turbulence model: The two quantities K and ϵ are evaluated from differential transport equations. The transport equations for steady, fully developed, and high Reynolds number flow are the turbulent kinetic energy transport equation (K):

$$\begin{aligned} v \frac{\partial K}{\partial Y} + w \frac{\partial K}{\partial Z} = & \frac{\partial}{\partial Y} \left(\frac{v_{TY}}{\sigma_K} \frac{\partial K}{\partial Y} \right) + \frac{\partial}{\partial Z} \left(\frac{v_{TZ}}{\sigma_K} \frac{\partial K}{\partial Z} \right) \\ & + v_T \left[\left(\frac{\partial U}{\partial Y} \right)^2 + \left(\frac{\partial U}{\partial Z} \right)^2 \right] - \epsilon \end{aligned} \quad (13)$$

and the dissipation rate of the turbulent kinetic energy transport equation (ϵ):

$$\begin{aligned}
 v \frac{\partial \epsilon}{\partial Y} + w \frac{\partial \epsilon}{\partial Z} = \frac{\partial}{\partial Y} \left(\frac{v_{TY}}{\sigma_\epsilon} \frac{\partial \epsilon}{\partial Y} \right) + \frac{\partial}{\partial Z} \left(\frac{v_{TZ}}{\sigma_\epsilon} \frac{\partial \epsilon}{\partial Z} \right) \\
 + C_{e1} C_\mu K \left[\left(\frac{\partial U}{\partial Y} \right)^2 + \left(\frac{\partial U}{\partial Z} \right)^2 \right] - C_{e2} \frac{\epsilon}{K}
 \end{aligned} \quad (14)$$

where σ_K , σ_ϵ , C_{e1} , and C_{e2} are dimensionless constants which have standard values (17) as 1.0, 1.3, 1.44, and 1.92, respectively. These standard values are used in this paper.

Boundary Conditions: The wall function approach of Launder and Spalding (1974) is adopted. In this approach the boundary conditions are specified at a virtual boundary located a distance from the wall outside the viscous sublayer in which the K- ϵ model is not applicable. This distance is taken as 0.04 H from the walls. According to Sill (1982) the shear stress is nearly constant within a distance 0.06 H from the wall.

The longitudinal (primary) shear stress (on virtual wall boundaries) divided by the fluid density is expressed in terms of the main velocity as by Schamber and Larock (1981) as

$$\frac{\tau_l}{\rho} = -u_* |u_*| = \frac{-\kappa^2}{\left[\ln \left(E \frac{N u_*}{\nu} \right) \right]^2} |U| U \quad (15)$$

where u_* is the shear velocity, κ is the von Karman constant (here 0.4), N is the normal distance to the nearby wall, E is taken as by Krishnappen and Lau (1986) for the entire turbulent regime, and ν is the fluid viscosity. The transverse shear (τ_t) on virtual wall boundaries is expressed in terms of the main velocity and the corresponding parallel secondary velocity (U_t) as

$$\tau_t = -\rho \left(\frac{u_*}{U} \right)^2 U_t |U_t| \quad (16)$$

The boundary conditions for K and ϵ at virtual wall boundaries are:

$$K = \frac{u_*^2}{\sqrt{C_\mu}} \quad ; \quad \epsilon = \frac{u_*^3}{\kappa y} \quad (17)$$

The normal velocity at the virtual boundaries, planes of symmetry, and the free surface is zero. Gradients of the variables at planes of symmetry and the free surface are also zero. The exception is the free surface boundary condition for ϵ which is taken as by Yacoub et al. (1992) as

$$\frac{d\epsilon}{dY} = C_{eF} \frac{\epsilon^2}{K^{3/2}} \quad (18)$$

where C_{eF} is taken as 3.5.

The equations are solved using the finite element method. Because all the cases considered herein consist of rectangular channels, use is made of the 4-node rectangular element which is simple and sufficient for representing the computational

domain, the three velocity components, K , and ϵ variables. The pressure is assumed constant over each element. The details of the numerical procedure are given in Hafez (1995).

APPLICATION OF THE MODEL

The model is applied to open channel cases where secondary currents are induced by the geometry of the channel cross section, the wall roughness conditions, and the free surface. For symmetry reasons, half of the channels are only considered.

The secondary velocities are initially set to zero at all nodes. The computer model is run on a DEC-station 5000 (UNIX environment) located at Colorado State University.

1. The Smooth Open Channel (1:2): The smooth walled channel has an aspect ratio of 1:2, a depth of 0.076 m, a slope of 0.000966, and a flow Reynolds number of 39,000. The secondary velocity structure, Figure 1a, shows two vortex structure with a larger upper vortex and a smaller lower one. This pattern of secondary currents is different from that in a quadrant of square ducts (1,9) where the two vortices are symmetrical along the duct diagonal. The free surface in the open channel enhances the growth of the upper vortex which becomes much stronger and occupies a larger area than the lower vortex.

The pattern of the secondary velocities matches well the one determined experimentally by Nezu et al. (1989) shown in Figure 2a and reported in (16), and that determined numerically by Naot and Rodi (1982) shown in Figure 2b. The maximum secondary velocity is in the transverse direction along the free surface, about 0.5 H from the side walls with a magnitude of 1.2 times the average shear velocity.

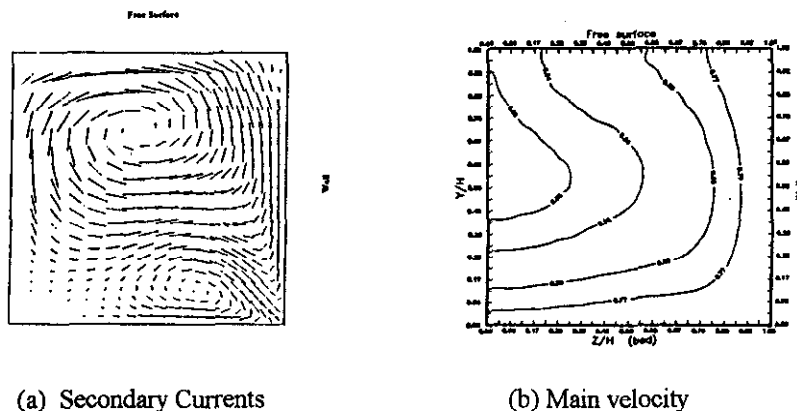


Figure 1. Present Model Velocities In the Open Channel (1:2)

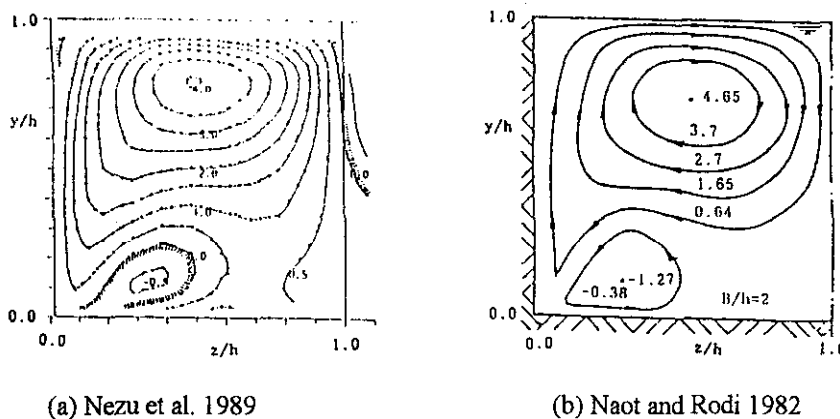


Figure 2. Secondary Currents in the Open Channel (1:2)

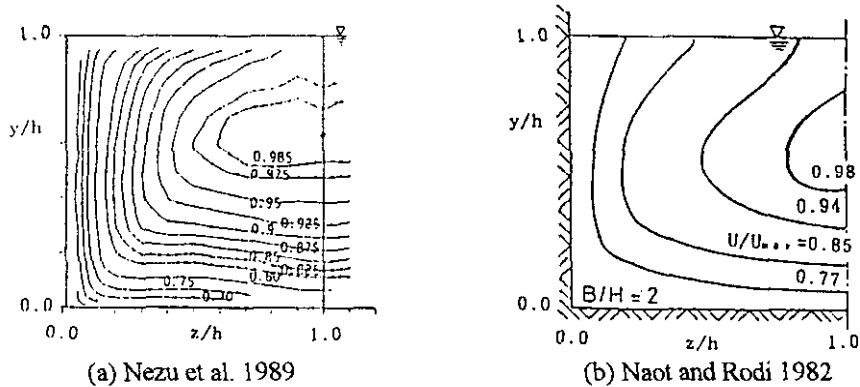


Figure 3. Main Velocity Contours in the Open Channel (1:2)

The longitudinal velocity contours predicted by the present model, Figure 2b, indicate the success of simulating the depression of the velocity maximum which occurs at 0.61 H above the bed along the channel vertical axis of symmetry. This is in agreement with the laboratory data by Nezu et al. (1989), Figure 3a, and the numerical simulation of Naot and Rodi (1982), Figure 3b. The downward vertical secondary velocity is responsible for the depression of the main velocity maximum.

2. The Rectangular Open Channel (1:7.5) with Periodic Roughness: Data from Muller and Studerus (1979) experiments on channels with lateral periodic smooth and rough stripes is used herein. The rough stripes have roughness height of 0.0025 m. The channel has a depth of 0.08 m, a slope of 0.00152, and a flow Reynolds number of 38,000.

The pattern of the secondary velocities shown in Figure 4a, consists of a cellular structure with the flow directed downward over the two central rough stripes and upward over the smooth stripes. This agrees with the numerical simulation by Naot (1984), Figure 4b and with Muller and Studerus measurements. Close to the side walls, the two vortex structure with a large upper vortex and a small lower one is observed as in the last case.

The contours of the main velocity shown in Figure 5a, are pushed by the secondary velocities downward over the central rough stripes and upward over the adjacent smooth stripes. This distribution is similar to that of Naot (1984) shown in Figure 5b.

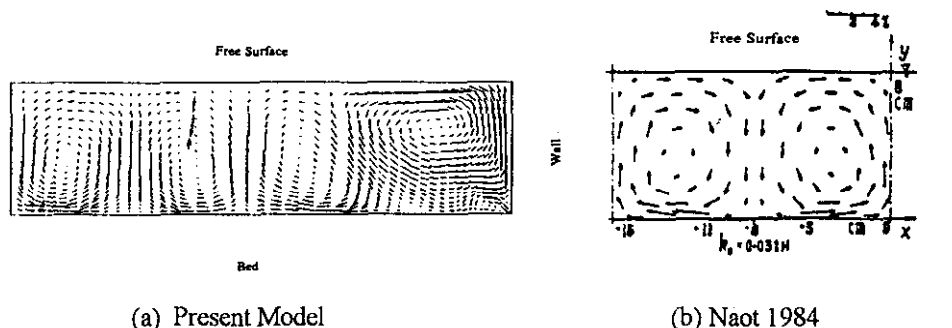


Figure 4. Secondary Currents in The Open Channel (1:7.5) with periodic roughness

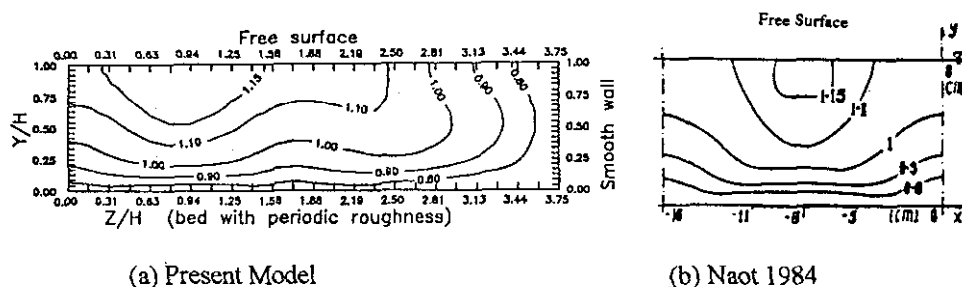
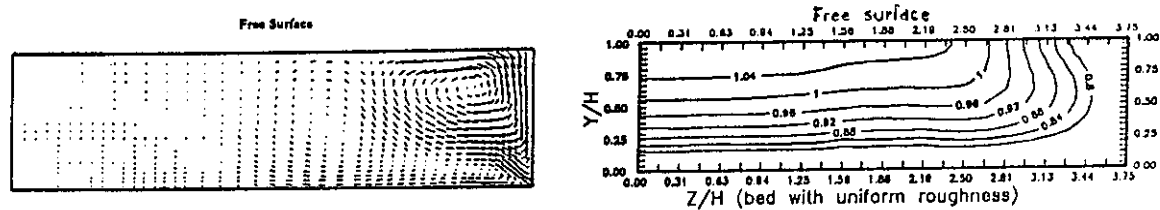


Figure 5. Main Velocity in the Open Channel (1:7.5) with Periodic Roughness

3. The Rectangular Channel (1:7.5) with Uniform Bed Roughness:

To verify that the cellular secondary structure obtained in the last case is due to the periodic variation of the roughness and not due to the channel being relatively wide, the bed roughness is taken uniform. The same rectangular channel studied by Muller and Studerus (1979) is investigated but with uniform roughness of 0.0025 m all over the channel bed while the side walls are left smooth.



(a) Secondary Currents

(b) Main Velocity Contours

Figure 6. Velocity Field In the Open Channel (1:7.5)

The secondary velocities are shown in Figure 6a. The cellular secondary structure disappears, and instead, two vortices at the side wall peculiar to rectangular channels with uniform bed roughness are observed with a large upper vortex and a small lower one. The upper vortex extends to a distance about 1.15 H from the side wall. Therefore, it is evident that the cellular secondary structure could only be predicted in channels with periodic roughness.

Very weak secondary velocities beyond the upper vortex are observed which could not affect the main velocity contour lines as seen in Figure 6b. The main velocity maximum lies on the free surface. The main velocity distribution in this part of the channel can be assumed two-dimensional where the secondary flow can be neglected.

REFERENCES

1. Brundrett, E., and Baines, W. D. (1964). The Production and Diffusion of Vorticity in Duct Flow. *Journal of Fluid Mechanics*, 19, 375-392.
2. Culbertson, J.K. (1967). Evidence of Secondary Circulation in an Alluvial Channel. U.S. Geological Survey, Prof. Paper 575-D, D 214-D 216.
3. Gosh, S., and Roy, N. (1970). Boundary Shear Distribution in Open Channel Flow. *Journal of Hydraulics Division, ASCE*, 96, 967-994.
4. Hafez, Y. (1995). A K- ϵ Turbulence Model for Predicting the Three-Dimensional Velocity Field and Boundary shear in Closed and Open Channels. Ph.D. thesis presented to Colorado State University, Colorado, USA.
5. Karcz, I. (1973). Reflections on the Origin of Source Small-scale Longitudinal Stream bed Scours. *Fluvial Geomorphology*, M. Morisawa, ed., Proceedings of the fourth annual geomorphology symposia series, 149-173.
6. Kinoshita, R. (1967). An Analysis of the Movement of Flood Waters by Aerial Photography; Concerning Characteristics of Turbulence and Surface Flow. *Photographic surveying*, 6, 1-17 (in Japanese).
7. Krishnappen, B.G., and Lau, Y.L. (1986). Turbulence Modelling of Flood Plain Flows. *Journal of Hydraulic Engineering, ASCE*, 112 (4), 251-267.
8. Launder, B. E., and Spalding, D. B. (1974). The Numerical Computation of Turbulent Flow. *Computer Methods in Applied Mechanics and Engineering*, 3, 269-289.
9. Melling, A., and Whitelaw, J.H. (1976). Turbulent Flow in a Rectangular Duct." *Journal of Fluid Mechanics*, 78, 289-315.

10. Muller, A., and Studerus, X. (1979). Secondary Flow in Open Channel. Proceedings of Congress of the IAHR, Italy, 19-24.
11. Naot, D. (1984). Response of Channel Flow to Roughness Heterogeneity. Journal of Hydraulic Engineering, ASCE, 110, 1568-1587.
12. Naot, D., and Nezu, I., and Nakagawa, H. (1993). "Hydrodynamic Behavior of Compound Rectangular Open Channels." J. Hydr. Engng., ASCE, 119, 390-408.
13. Naot, D., and Rodi, W. (1982). Calculation of Secondary Currents in Channel Flow. Journal of Hydraulic Divisions, ASCE, 108, 948-968.
14. Nezu, I., and Nakagawa, H. (1984). Cellular Secondary Currents in Straight Conduit. Journal of Hydraulic Engineering, ASCE, 110, 173-193.
15. Nezu, I., and Rodi, W. (1985). Experimental Study on Secondary Currents in Open Channel Flow. Proceedings of 21st Congress of IAHR, Melbourne, 2, 115-119.
16. Nezu, I., Tominaga, A., and Nakagawa, H. (1993). Field Measurements of Secondary Currents in Straight Rivers. Journal of Hydraulic Engineering, ASCE, 119, 598-614.
17. Rodi, W. (1984). Turbulence Models and Their Applications in Hydraulics- A State of the Art Review. IAHR publication, Delft, The Netherlands.
18. Shamber, D. R., and Larock, B. E. (1981). Numerical Analysis of Flow in Sedimentation Basins. Journal of Hydraulics Divisions, ASCE, 107(5), 575-591.
19. Sill, B.L. (1982). New Flat Plate Turbulent Velocity Profiles. Journal of Hydraulic Engineering, ASCE, 108, 1-14.
20. Vanoni, V.A. (1946). Transportation of Suspended Sediment by Water. Transactions, ASCE, 111, 67-133.
21. Yacoub, N., Moalem, M.D., and Naot, D. (1992). Towards the Numerical Simulation of the Horizontal Slug Front. International Journal of Numerical Methods in Fluids, 14, 127-146.

NOTES

☆ U.S. GOVERNMENT PRINTING OFFICE:1996-717-180/82558